AD-753 936

ON THE STATISTICAL MODELING OF RADAR TARGETS

James W. Wright, et al

Army Missile Command
Redstone Arsenal, Alabama

November 1972

AD

TECHNICAL REPORT
RE-72-19

ON THE STATISTICAL MODELING OF RADAR TARGETS

by

James W. Wright
Abraham H. Haddad

November 1972

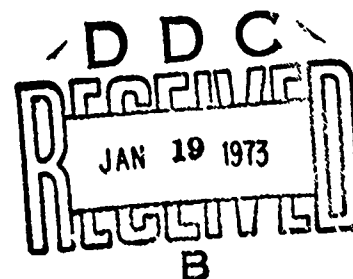Approved for public release; distribution unlimited.

U.S. ARMY MISSILE COMMAND
Redstone Arsenal, Alabama

DDC
RECEIVED
JAN 19 1973
B

DISPOSITION INSTRUCTIONS

DISCLAIMER

TRADE NAMES

ACCESSION for

FTIS	White Section	☑
D C	Buff Section	☐
USA		☐

JUSTIFICATION

BY

DISTRIBUTION/AVAILABILITY CODES

Dist.	Avail. and/or SPECIAL
A	

DOCUMENT CONTROL DATA - R & D

(Security classification of title, body of abstract and indexing annotation must be entered when the overall report is classified)

1. ORIGINATING ACTIVITY *(Corporate author)*	2a. REPORT SECURITY CLASSIFICATION
Advanced Sensors Directorate US Army Missile Res, Dev & Eng Laboratory US Army Missile Command Redstone Arsenal, Alabama 35809	UNCLASSIFIED
	2b. GROUP NA

3. REPORT TITLE

ON THE STATISTICAL MODELING OF RADAR TARGETS

4. DESCRIPTIVE NOTES *(Type of report and inclusive dates)*

Technical Report

5. AUTHOR(S) *(First name, middle initial, last name)*

James W. Wright
Abraham H. Haddad

6. REPORT DATE	7a. TOTAL NO. OF PAGES	7b. NO. OF REFS
November 1972	137	74

8a. CONTRACT OR GRANT NO.	9a. ORIGINATOR'S REPORT NUMBER(S)
b. PROJECT NO. NA	Technical Report RE-72-19
c.	9b. OTHER REPORT NO(S) *(Any other numbers that may be assigned this report)*
d.	AD_____

10. DISTRIBUTION STATEMENT

Approved for public release; distribution unlimited.

11. SUPPLEMENTARY NOTES Details of illustrations in this document may be better studied on microfiche. None.	12. SPONSORING MILITARY ACTIVITY Same as No. 1

13. ABSTRACT

The objective of this research is to develop techniques and procedures for computing the statistical characteristics of some electromagnetic scattering phenomena from radar targets. Radar measurements are perturbed by electromagnetic scattering phenomena induced by complex targets including radar cross section scintillation and glint or position error. The statistical characteristics of these phenomena may be used to evaluate radar system performance, develop optimum tracking systems, and develop stochastic models to use in system simulations.

The procedures developed use numerical integration to compute the moments of the probability density functions and the characteristic function method to compute the covariance functions. As part of the research, a deterministic model of the electromagnetic scattering from M bodies has been developed and applied to an ellipsoidal model of a common target drone. This model is used as the electromagnetic scattering input to the analytic computation of the statistical characteristics and to the simulation which is used to check the general accuracy of the analytic solutions.

The statistical characteristics are computed at three points on a typical flight path of interest for three different sets of target flight characteristics. These statistical characteristics are conditional on the flight path, i.e., they

(Continued)

DD FORM **1473** REPLACES DD FORM 1473, 1 JAN 64, WHICH IS OBSOLETE FOR ARMY USE.

I-a

14. KEY WORDS	LINK A		LINK B		LINK C	
	ROLE	WT	ROLE	WT	ROLE	WT
Radar Scattering						
Radar Cross Section						
Glint						
Statistical Modeling						
Simulation						

13. ABSTRACT (Continued)

are functions of the flight path. The agreement
between the analytic computations and simulations
is excellent. The sensitivity of the electromag-
netic scattering statistics to the flight motion
statistics is generally as expected. The data
from the simulations are very similar in nature
to dynamic measurements.

November 1972   Technical Report RE-72-19

ON THE STATISTICAL MODELING OF RADAR TARGETS

by

James W. Wright
Abraham H. Haddad

Advanced Sensors Directorate
US Army Missile Research, Deve'opment
and Engineering Laboratory
US Army Missile Command
Redstone Arsenal, Alabama 35809

$I\text{-}C$

CONTENTS

Preceding page blank

1. INTRODUCTION

1.1 Introduction to the Radar Problem

Many modern radar systems are capable of tracking targets in four dimensions: range, azimuth angle, elevation angle, and doppler frequency. There is, however, a point at which target induced effects become significant contributors to system measurement errors. Angle tracking is perturbed by an effect called glint; range tracking and other functions are perturbed by cross-section scintillation; and doppler tracking is perturbed by apparent target phase center motion not related to translational motion.

A pulse doppler radar system transmits a pulse of electromagnetic energy of known amplitude and phase at a known time. The signal reflected from a target is received by the radar, and is processed to give

    (1) The target range

    (2) The target size or radar cross-section (RCS)

    (3) The target azimuth angle

    (4) The target elevation angle

    (5) The target phase angle.

The errors involved in these measurements can be divided into two basic types. Type I errors are those caused by noise and imperfect signal and data processing. These errors exist even for a perfect target such as a sphere. Type II errors are those introduced by the

2

the target. A complex target such as an aircraft, or even two spheres, has RCS and scattering phase which are functions of the aspect angles and reflect or scatter a wavefront which is distorted or nonspherical.

The Type I errors have been investigated and extensively studied [1, 2, 3]. The Type II errors have had less development than the Type I errors. The primary reasons for this are the complexity of the problem and the dependence of the effects on the particular body under consideration. Unlike thermal noise which can readily be modeled as white noise, the target induced effects depend on the target, its aspect angles and its motion. The following is a summary of the errors of interest and an indication of the relationship of the two types of errors.

The equation for power received by a monostatic radar is given by

$$P_{rec} = \frac{P_t \, G^2 \, \lambda^2 \, S}{(4\pi)^3 \, R^4 \, L} \qquad (1.1)$$

where

P_t = transmitted power

G = antenna gain

λ = radar wavelength

R = range from radar to target

L = numerical factor to account for losses

S = target RCS.

The measurement of target range is generally limited by the signal-to-noise ratio which depends on received power. The rms range error caused by thermal noise is given by [3]:

$$e_r \approx \frac{c}{2} \sqrt{\frac{\tau}{\frac{2BE}{N_0}}} \qquad (1.2)$$

where

c = velocity of light

τ = transmitted pulse width

B = receiver bandwidth

E = received energy

N_0 = receiver noise power spectrum.

The target induced errors are manifested as changes in the received energy, E, (sometimes exceeding 50 decibels peak to peak) caused by changes in apparent target RCS; it is apparent from (1.2) that the two errors are interrelated. Similarly, the target induced errors affect the angular position measurements and the target phase angle (doppler frequency) measurements.

All angle tracking systems are essentially phase-front measuring devices and have been shown to be equivalent to each other in performance [4]. Only amplitude monopulse systems will be discussed herein since they are predominant in the modern generation of radar systems. A dual-plane monopulse radar generally has four squinted beams which are combined to give a sum channel and two angle error channels [2]. An ideal target on boresight will give zero outputs from the angle tracking channels. The target induced error is manifested as a tilt in phase front which gives an apparent target error signal. The angular error signal is inversely proportional to range. The effects of glint, then, are most significant at close ranges such as encountered in homing missile systems. The theoretical rms angular error, caused by thermal noise for a uniformly illuminated antenna, is given by [1]

4

$$e_\theta = \frac{0.628\,\theta_b}{\sqrt{\dfrac{2E}{N_0}}} \qquad (1.3)$$

where θ_b is the half-power beam width. Again the effect of variation in E should be noted.

Doppler tracking, in a pulse doppler radar, is accomplished by measuring the phase shift of the RF signal from transmission to reception, modulo 2π radians. The rms phase error caused by thermal noise is given by [3]

$$e_\varphi = \sqrt{\dfrac{\tau}{\dfrac{2BE}{N_0}}} \qquad . \qquad (1.4)$$

In addition to this error, there is an apparent target phase center motion which is aspect angle dependent. Target motion, other than purely radial, may cause a random modulation of the target phase range.

However, as outlined previously, the major interdependence of the two types of errors are caused by the change in RCS and so in the received energy, E. Therefore, it is possible to separate the two types of errors in a convenient manner. It will be assumed hereafter that the only interdependence is that induced by the RCS. Thus, modeling of the target induced effects need not consider the radar characteristics, except as delineated below, and the radar receiver model need not be modified to consider the Type II errors.

The phenomena of amplitude scintillation, glint, and doppler scintillation are different manifestations of the vector summation of the electromagnetic waves reflected and refracted by complex targets. Although basically target induced, these phenomena are affected by some of the characteristics of the observing radar such as resolution,

polarization, wavelength, tracking implementation, and type (monostatic or bistatic*). All but very few targets have RCS, glint, and phase centers which are sensitive to wavelength and polarization. These characteristics should be included in any complete model of the target phenomena, but not all are within the scope of this work.

Although bistatic radars are of some interest, especially in semi-active homing systems, the discussion and proposed research will be limited to monostatic systems. It is assumed that the range resolution is such that the entire target is always in the range resolution cell. Similarly, it will be assumed that the target is smaller than the angular resolution and is always in the angular resolution cell. The range of radar frequencies will be limited to those most commonly used for search and tracking systems, i.e., L-band through X-band ˝. GHz through 10 GHz).

It would, at first, appear to be of value to have a complete deterministic model of the particular target of interest to the radar system. Further consideration, however, indicates that this is not a very practical goal. The target appearing in the radar field of view and the target aspect angles will seldom be known, except perhaps by the ability to classify the target in general terms such as rotary wing; fixed wing, propeller driven; fixed wing, jet propelled; etc. It would not be practical to store complete target data for all targets of interest in the radar system computer even if it was possible to

---

*A monostatic radar has its transmitting and receiving antennas collocated or common whereas a bistatic radar may have its transmitting and receiving antennas separated by large distances.

generate such data. The most obvious and most practical approach is to model the problem statistically.

The objective of this research has been to develop techniques to determine important statistical properties of target induced scintillation and glint.

1.2 Review of Past Work

A brief review of the history and evolution of radar systems and the development of models will help to gather perspective on the problem and the status of work in the area. The review presented is necessarily brief and oriented toward the problem under study. References [1, 2, 3, 5, 6, 7, and 8] are general treatises on modern radar systems.

The radar systems operating at the start of World War II were used primarily for early warning and ranging since they had poor angular accuracy. The war spurred research and development on radar systems, especially radar fire control systems for antiaircraft systems. The SCR 584, introduced early in the war, was the first operational fire control system developed by the U.S. which required no assistance from optical angle trackers. It could track targets in three dimensions: azimuth angle, elevation angle, and range. Since World War II the development and evolution of radar systems have continued at an almost fantastic pace. The types of radar systems have proliferated due to differing operating requirements and constraints.

Amplitude scintillation was noted in World War II when target fading was frequently observed. It was not until angle tracking systems improved significantly that glint was first noticed. At first it was ascribed as an effect of amplitude scintillation since large values of

glint occurred only with low signal levels. Later it was determined to be a separate phenomenon. The relationships between glint and amplitude scintillation had to wait even longer before it was clearly established. It is now accepted that the three phenomena of amplitude scintillation, glint, and doppler scintillation are different manifestations of the same target induced effects.

The development of target models, both analytical and statistical, parallels the evolutionary growth in sophistication and performance of radar systems. Amplitude scintillation and its effects on target detection have been extensively treated from a statistical point of view. Marcum [9] developed the theory of detection probabilities of constant cross section targets in additive white noise for search type radars, considering the effects of pulse integration, scanning effects, etc.

Swerling [10, 11] advanced the theory by considering fluctuating targets. The four cases originally considered, which encompassed most targets, are as follows:

(1) Case 1 – The target is assumed to be constant for time-on-target for a single scan but fluctuates randomly on a scan-to-scan basis. The probability density function of the target cross section, S, is assumed to be:

$$f_S(s) = \frac{1}{\bar{s}} \exp\left(-\frac{s}{\bar{s}}\right), \quad s \geq 0 \qquad (1.5)$$

where

$$\bar{s} = E(S) \qquad \qquad .$$

8

(2) Case 2 - The target fluctuations are random on a pulse-to-pulse basis. The probability density function is the same as for Case 1.

(3) Case 3 - The target is assumed to be constant for the time-on-target of a single scan but fluctuates on a scan-to-scan basis with the cross section having a probability density function given by

$$f_S(s) = \frac{4s}{\bar{s}^2} \exp\left(-\frac{2s}{\bar{s}}\right), \quad s \geq 0 \quad . \qquad (1.6)$$

(4) Case 4 - The target fluctuations are random on a pulse-to-pulse basis with the same probability density function as Case 3.

These distributions are chi-square distributions with 2 and 4 degrees of freedom for Cases 1 and 2 and Cases 3 and 4, respectively.

Swerling's work has found wide acceptance in the field, especially since the results were presented in convenient graphical form. Swerling [12] has investigated additional fluctuating models including log-normally distributed targets. Heidbreder and Mitchell [13] have also investigated detection probabilities for log-normally distributed targets. A log-normally distributed target is one which has a cross section whose logarithm is normally distributed. The density function is given by

$$f_S(s) = \frac{1}{\sigma s \sqrt{2\pi}} \exp\left\{-\frac{(\ln s - \mu)^2}{2\sigma^2}\right\}, \quad s \geq 0$$

$$(1.7)$$

where μ and σ are the mean and variance of $\ln S$, respectively. Sponsler [14] investigated the track-while-scan problem encountered with mechanically scanned search radars. Using a first-order, two-state Markov process, Sponsler established bounds on the scan-to-scan correlation coefficient and derived the Kolomogorov differential

equations for a nonstationary, continuous parameter Markov process which could be used to simulate radar data for arbitrary flight paths. The equations are a function of the blip-to-scan ratio, i.e., time-on-target to scan time ratio.

Weinstock [15] investigated target models for missile and satellite shapes and concluded that the chi-square models give poor representation of the tails of the distributions. Weinstock also concluded that if one was constrained to using chi-square models the median rather than the mean should be specified.

The U.S. Naval Research Laboratory has been investigating glint since 1947. The efforts have been devoted primarily to understanding and explaining the underlying causes of the phenomenon. The first published work on statistical modeling of glint was by Delano [16, 17]. Considering mathematically simple arrays of point scatters, Delano computed the statistical distribution of the angular errors. For example, considering a single angle tracking channel and a linear array of scatterers of statistically independent amplitude and phase, all scatterers having approximately the same mean value, Delano derived the result that the apparent target center is outside the actual target 13.4 percent of the time. This result was of great significance and has been quoted many times, often out of context.

Muchmore [18, 19] investigated amplitude scintillation spectra using Delano's models. Although Muchmore's and Delano's work was criticized by Peters and Weimer [20, 21, 22] because of the simplicity of the models, the spectra obtained were reasonably similar to empirical results. Development of statistical glint models has not

10

progressed significantly since these two papers, probably due in part to the extreme complexity of the problem.

Meade et al. [23] investigated the two body model, often called the dumbbell model, and derived the result that the apparent target position, θ_T, is given by

$$\theta_1 = \frac{\theta_0}{2} \left(\frac{1 - k^2}{1 + k^2 + 2k \cos \varphi} \right) \qquad (1.8)$$

where

θ_0 = angular separation of the targets

k = cross section ratio of the targets

φ = relative phase angle of the response

of the targets.

Meade's results indicate that the angle error can go to infinity. Ostrovityanov [24] corrected this error by noting that the assumption $\tan \theta \approx \theta$ was implicit in Meade's derivation. Making the correction, one finds that θ is bounded by $\pm \pi/2$ which is more reasonable. Howard [25] interpreted glint as a distortion or tilt in the wavefront and demonstrated means of computing glint as a function of aspect angle for N-body targets, where N is any finite number. Gubonin [26] used Howard's interpretation of glint and derived glint statistics, arriving at essentially the same results as Delano. Gubonin did, however, avoid the implied approximation of $\tan \theta \approx \theta$ and obtained more general results.

Lindsay [27] expanded on the phase front approach and concluded that glint and amplitude and doppler scintillation can be explained by considering $\nabla \varphi$, i.e., the normal to the phase front, and its relation to the antenna beam axis. Dunn and Howard [28] concluded basically

the same fact independently, and demonstrated that the phenomena can be explained by considering the Poynting vector of the reflected or scattered wave.

Modeling of large complex radar targets such as aircraft is at best an extremely difficult and rather inexact task [29], and the techniques used are guided to some extent by the specific objective of the researcher. Little or no effort has been devoted to target modeling as proposed herein. Previous work has been devoted to investigating or modeling one or more of the phenomena such as Borison [30] in doppler scintillation; Swerling [10, 11, 12], Weinstock [15], Heidbreder and Mitchell [13], Edrington [31] and Sponsler [14] in amplitude scintillation; Muchmore [18] in scintillation spectra; Delano [16], Howard [25], Gubonin [26], Besalov and Ostrovityanov [32], D··n and Howard [29, 33], and Sims and Graff [34, 35] in glint; or in the analysis of the relationships among the phenomena such as work by Lindsay [27] and Dunn and Howard [28].

RCS modeling is the most developed area of radar target scattering. The IEEE devoted an entire issue of the Proceedings (Vol. 53, No. 8, August 1965) to radar reflectivity. Included in the papers was a rather extensive bibliography [36] of work in the field through 1964. A bibliography of more recent works may be found in [37]. Techniques in RCS modeling range from the exact solution for spheres by Mie [38] to the empirical approximations by Crispin and Maffett [39]. Three comprehensive works in the field have been published in recent years [40, 41, 42]. Some of the more interesting work in radar scattering recently include the works of Ross [43, 44], Oshiro, et al.,

12

[45, 46, 47], Moll and Seecamp [48], Ryan \49, 50], Keller [51, 52,

53], Bechtel [54], Uslenghi and Lee [55], and Pierson and Clay [56].

Electromagnetic (EM) scattering has been categorized into three

regions: Rayleigh, resonance, and optical, depending on the character-

istic dimensions of the body. The Rayleigh region is characterized by

bodies whose characteristic dimensions are less than a quarter of a

wavelength. In this region, the RCS is approximately proportional to

the volume squared and inversely proportional to the wavelength of the

fourth power, neglecting degenerate cases such as discs and wires. The

resonance region covers the region from approximately a quarter

wavelength to a few wavelengths in body dimenions. In the resonance

region body shape, orientation and specific dimensions are of

particular importance. The simplest example of resonance effects is

the variation of cross section versus frequency curve for spheres.

The optical region covers bodies whose characteristic dimensions

are large with respect to a wavelength. In the optical region many

approximation techniques such as geometric optics, physical optics,

geometrical theory of diffraction, and fringe wave theory are applied.

Modeling of glint has had less development although the subject

has remained of significant interest since the original work by the

Naval Research Laboratories. The subject of doppler scintillation has

received little attention although interest in this phenomenon has

increased in recent years because of the development of pulse doppler

radar systems and the increased resolution capabilities desired.

1.3 Statement of the Problem

The evaluation of the performance of a radar system requires a

knowledge not only of the radar system hardware and characteristics,

but also of the radar target. Radar system evaluations are generally performed using probabilistic or statistical approaches, with performance specified in terms like probability of detection, probability of false alarm, and rms tracking accuracy (in range, azimuth and elevation angles, and doppler frequency). Such an evaluation requires statistical models of the EM scattering parameters which affect system performance. The statistical characteristics of the EM scattering parameters are, as mentioned in Section 1.1, dependent on the target and its angular and translational motion. The objective of this work is to develop techniques to determine these statistics. In particular, this work is directed toward development of techniques to: (1) determine the moments of the RCS and the azimuth and elevation errors, AZER and ELER, respectively, and (2) determine the covariance functions for these three parameters.

The work is divided into two basic phases. The first phase, described in Chapter 2, is the development of a deterministic model of the EM scattering from a target. The equations for the RCS and target induced error signals are developed for an M-body target and then applied to an ellipsoidal model of a target drone. The second phase, described in Chapter 3, is the selection of important statistical characteristics of the EM scattering and development of techniques to compute these statistical characteristics. The characteristic function method of computing these statistical characteristics is derived for the discrete case and implemented on a digital computer.

A simulation was developed to provide a check on the general accuracy of the analytic solutions. A comparison of the simulations and analytic solutions is presented in Chapter 4.

14

A secondary objective of this research is to identify the areas where data or theory is inadequate to support the ultimate objective of developing stochastic models of the radar scattering for use in simulations of air defense systems. Many of these limitations are identified as they are encountered, and all identifiable problem areas are covered in the conclusions.

2. ANALYTIC MODELING OF RADAR TARGET SCATTERING PARAMETERS

2.1 General

In this section the deterministic models for the scattering

parameters of interest are derived. These parameters are the target

induced effects which cause errors in the radar system, namely the

radar cross section (RCS), the azimuth error (AZER), the elevation

error (ELER), and the target phase (PHAS). The RCS is used here in

its conventional form. Glint, for the purposes of this research, is

defined as the linear errors, in meters, in the target azimuth (AZER)

and elevation (ELER) positions, referenced to the target range. The

target phase (PHAS) is defined here as the phase of the electromagnetic

(EM) vector reflected from the target as compared to an EM vector

reflected from a point scatterer located at the target center.

The approach used assumes that the target can be divided into

M different scattering elements located at fixed points in the target

coordinate system. The EM scattering from each element is determined

as a function of the aspect angles. Then, the scattering parameters

can be determined, as functions of the aspect angles, by vector

summation of the scattering from the M scattering elements.

Two primary coordinate systems (shown in Figure 2.1) are of

interest. One is the ground fixed coordinate system with the observing

radar at its origin. The azimuth (AZ) and elevation (EL) angles

normally used by radar systems are indicated as are the conventional
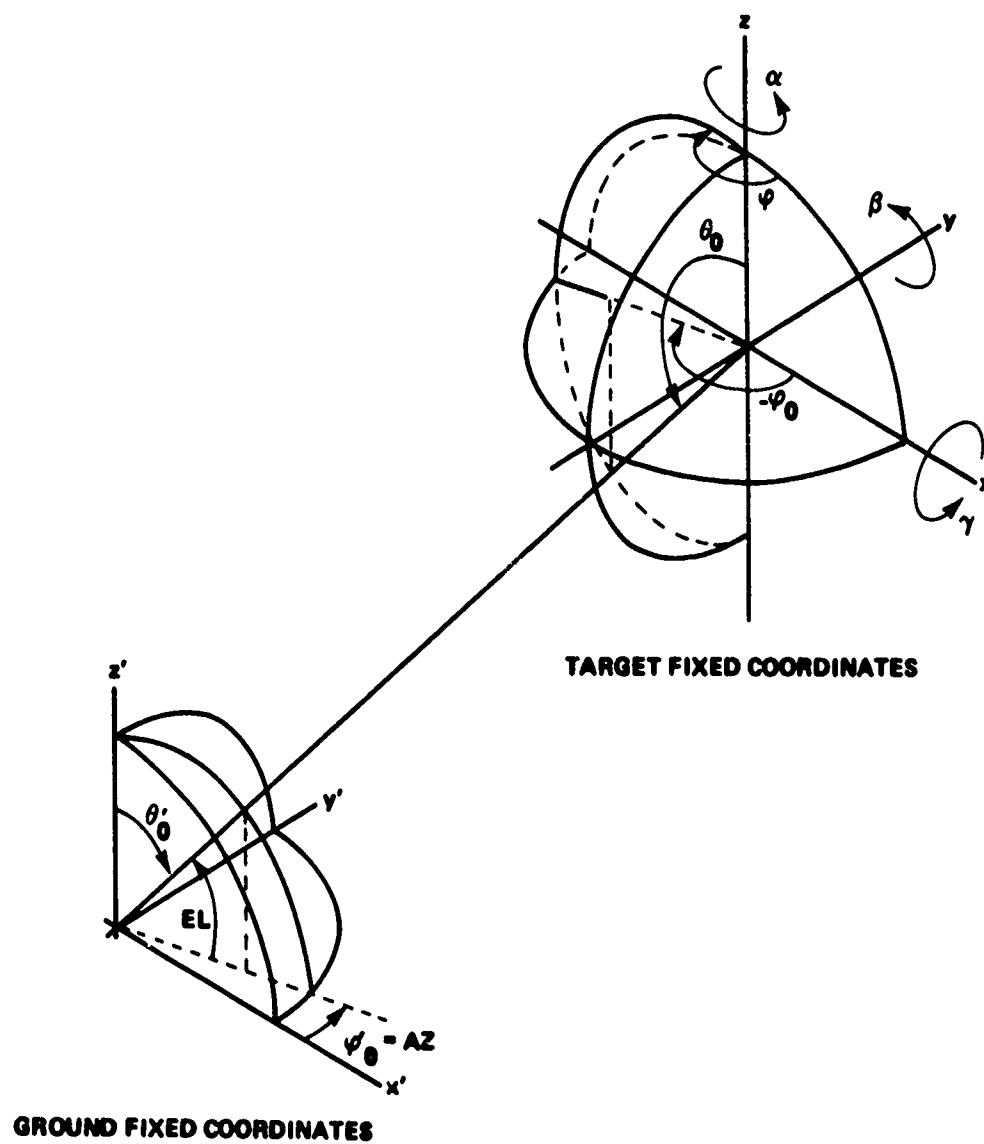
TARGET FIXED COORDINATES

GROUND FIXED COORDINATES

Figure 2.1. Coordinate Systems

polar coordinates. The x' coordinate is downrange, the y' coordinate is cross range, and the z' coordinate is altitude. The position of the target is given by (x_0, y_0, z_0) or in polar coordinates by $(R_0, \theta_0, \varphi_0)$. The other coordinate system is the target fixed coordinate system with the center of the target located at the origin. The x axis is the longitudinal axis, the positive y axis is out the left wing, and the positive z axis is up. The yaw, pitch, and roll angles, α, β, and γ, respectively, are rotations about the z, y, and x axes, respectively where α and γ are defined in a right sense and β is in a lefthanded sense. The angles θ and φ which are the polar coordinates of the radar in the target fixed coordinates system are usually referred to as the aspect angles.

The two coordinate systems are related by the following transformations:

$$\begin{bmatrix} x \\ y \\ z \end{bmatrix} = \begin{bmatrix} t_{11} & t_{12} & t_{13} \\ t_{21} & t_{22} & t_{23} \\ t_{31} & t_{32} & t_{33} \end{bmatrix} \begin{bmatrix} x' - x_0 \\ y' - y_0 \\ z' - z_0 \end{bmatrix} \qquad (2.1)$$

$$\begin{bmatrix} x' \\ y' \\ z' \end{bmatrix} = \begin{bmatrix} t_{11} & t_{21} & t_{31} \\ t_{12} & t_{22} & t_{32} \\ t_{13} & t_{23} & t_{33} \end{bmatrix} \begin{bmatrix} x \\ y \\ z \end{bmatrix} + \begin{bmatrix} x_0 \\ y_0 \\ z_0 \end{bmatrix} \qquad (2.2)$$

where

$$t_{11} = \cos \alpha \cos \beta - \sin \alpha \sin \beta \sin \gamma$$

$$t_{12} = \sin \alpha \cos \beta$$

$$t_{13} = \cos \alpha \sin \beta + \sin \alpha \cos \beta \sin \gamma$$

$$t_{21} = -\cos \alpha \sin \beta \sin \gamma - \sin \alpha \cos \beta$$

$$t_{22} = \cos \alpha \cos \gamma$$

$$t_{23} = \cos \alpha \cos \beta \sin \gamma - \sin \alpha \sin \beta$$

$$t_{31} = - \sin \beta \cos \gamma$$

$$t_{32} = - \sin \gamma$$

$$t_{33} = \cos \beta \cos \gamma. \tag{2.3}$$

2.2 Scattering Parameters of M-Bodies

The modeling approach selected is based upon the work of Dunn and Howard [28] and Ostrovityanov [24]. It is assumed that there are M scatterers on the body, each of which may be aspect angle dependent. The i-th scatterer is located at (x_i, y_i, z_i) in the target coordinate system and has RCS of S_i. Both the location and RCS of each scatterer are assumed to be aspect angle dependent, where the aspect angle dependence permits the scatterers to be shadowed or disappear from view. Each scatterer is assumed to be independent of the others, and only single reflections are considered. This admittedly ignores such phenomena as interior corners and ducts, but these are considered to be of relatively minor importance statistically. Polarization sensitivity can be included but the derivation of the scattering equations assumes polarization independence, primarily for convenience.

It has been shown by Dunn and Howard [28] that glint computed by taking the normal to the phase front is the same as the glint computed by the ratio of the nonradial and the radial components of reflected power. This is true for all currently used angle tracking systems. The approach used here utilizes the Poynting vector representation of the reflected power. The EM vector backscattered from each of the M scatterers is computed and these are summed vectorially. The Poynting vector is then calculated and decomposed into three orthogonal components. The first component is radially directed from the target

to the radar. The other two components are, for convenience, the azimuthal and elevational components in the target coordinate system. The radial component of the Poynting vector is related to the RCS and the nonradial components are related to the glint errors. The results for the scattering parameters are derived in Appendix A and are given by:

$$S = \sum_{i=1}^{M} \sum_{j=1}^{M} \sqrt{S_i S_j} \; \cos\left(\alpha_i - \alpha_j\right) \tag{2.4}$$

$$\epsilon_\varphi = \frac{1}{S} \sum_{i=1}^{M} \sum_{j=1}^{M} \sqrt{S_i S_j} \; f_{2i} \cos\left(\alpha_i - \alpha_j\right) \tag{2.5}$$

$$\epsilon_\theta = \frac{1}{S} \sum_{i=1}^{M} \sum_{j=1}^{M} \sqrt{S_i S_j} \; f_{1i} \cos\left(\alpha_i - \alpha_j\right) \tag{2.6}$$

$$PHAS = \arctan\left(\frac{\sum_{i=1}^{M} \sqrt{S_i} \sin \alpha_i}{\sum_{j=1}^{M} \sqrt{S_j} \cos \alpha_j}\right) \tag{2.7}$$

where ϵ_θ and ϵ_φ are the errors in the target coordinate system, θ and φ are the target aspect angles, and

$$\alpha_i = \frac{4\pi}{\lambda} \left(-x_i \sin \theta \cos \varphi - y_i \sin \theta \sin \varphi - z_i \cos \theta\right) \tag{2.8}$$

$$f_{1i} = -x_i \cos \theta \cos \varphi - y_i \cos \theta \sin \varphi - z_i \sin \theta \tag{2.9}$$

$$f_{2i} = -x_i \sin \varphi + y_i \cos \varphi \qquad . \tag{2.10}$$

The ϵ_φ and ϵ_θ errors given in (2.5) and (2.6) must be transformed to azimuth and elevation errors, AZER and ELER respectively, in radar coordinates to account for the orientation of the target. Let

$$[D(\theta,\varphi)] = \begin{bmatrix} \sin\theta\,\cos\varphi & \sin\theta\,\sin\varphi & \cos\theta \\ \cos\theta\,\cos\varphi & \cos\theta\,\sin\varphi & -\sin\theta \\ -\sin\varphi & \cos\varphi & 0 \end{bmatrix} \qquad (2.11)$$

Then, the azimuth and elevation errors are obtained from

$$\begin{bmatrix} \epsilon \\ ELER \\ AZER \end{bmatrix} \approx \left[D\left(\theta_0,\ \varphi_0\right) \right]\left[\overline{T^{-1}}\right]\left[D^{-1}(\theta,\ \varphi)\right]\begin{bmatrix} 0 \\ \epsilon_\theta \\ \epsilon_\varphi \end{bmatrix} \qquad (2.12)$$

ϵ is a dummy variable, and $[\overline{T^{-1}}]$ is $[T^{-1}]$ with the mean values of α, β, and γ substituted for α, β, and γ. For straight and level flight where the mean pitch and roll angles are zero

$$\left[D\left(\theta_0,\ \varphi_0\right)\right]\left[\overline{T^{-1}}\right]\left[D^{-1}(\theta,\ \varphi)\right] = \begin{bmatrix} 1 & 0 & 0 \\ 0 & 1 & 0 \\ 0 & 0 & 1 \end{bmatrix}$$

and (2.12) yields

$$AZER \approx \epsilon_\varphi$$

$$ELER \approx \epsilon_\theta \qquad\qquad . \qquad (2.13)$$

In order to derive the S_i and $(x_i,\ y_i,\ z_i)$ of each scattering element, the target is modeled by M ellipsoids.

2.3 Ellipsoidal Surface Model

It is assumed that the surfaces of the target can be approximated by ellipsoids, as depicted in Figures 2.2 and 2.3 for a target drone BQM-34A. Ellipsoids were chosen because of the relative ease with which one can find and describe the scattering from the specular point. Each ellipsoid is described by its conjugate radii and its position and orientation in the target fixed coordinate system. An associated
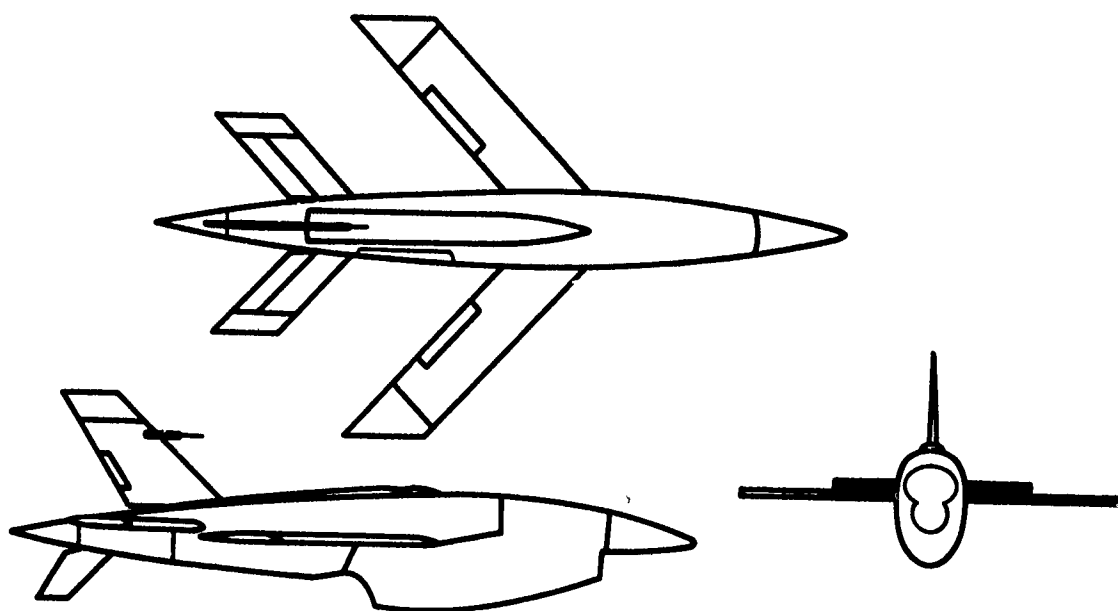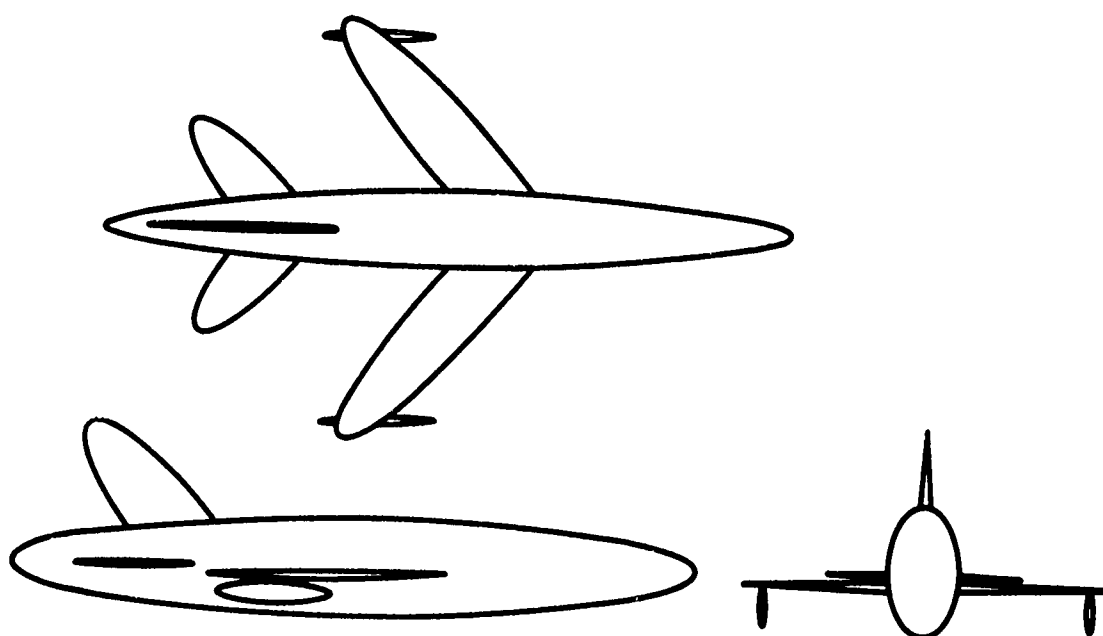
Figure 2.2. The BQM-34A Target Drone

Figure 2.3. Ellipsoidal Model of BQM-34A Target Drone

modulating function is defined for each ellipsoid which truncates the ellipsoid, approximates the shadowing by the other surfaces, and provides a relatively smooth transition into the field of view. It may also be used to provide an empirical method of improving the fit of calculated to empirical data. Each ellipsoid may be considered as a point scatterer with RCS, S_i, and location (x_i, y_i, z_i), determined by the specular point [41, 42].

First a single ellipsoid located at the origin with its principal axes oriented along the Cartesian coordinate axes is considered. The RCS of such an ellipsoid is given approximately by

$$S \approx \pi\, R_1\, R_2 \qquad (2.14)$$

where R_1 and R_2 are the principal radii of curvature at the specular point [41]. The specular point is found by finding the point on the surface of the ellipsoid having the same direction cosines as the lines of sight.

Let

$$F(x,\ y,\ z) = \frac{x^2}{a^2} + \frac{y^2}{b^2} + \frac{z^2}{c^2} - 1 = 0 \qquad (2.15)$$

be the equation of an ellipsoid. Then the normal to the ellipsoid at $(x,\ y,\ z)$ is given by

$$\vec{N} = \frac{2x}{a^2}\,\vec{i} + \frac{2y}{b^2}\,\vec{j} + \frac{2z}{c^2}\,\vec{k} \qquad (2.16)$$

so that the direction cosines of the normal are given by

$$\cos \delta_x = \frac{x}{a^2 r}$$

$$\cos \delta_y = \frac{y}{b^2 r}$$

$$\cos \delta_z = \frac{z}{c^2 r}$$

$$r = \sqrt{\frac{x^2}{a^4} + \frac{y^2}{b^4} + \frac{z^2}{c^4}} \qquad . \qquad (2.17)$$

However, the direction cosines for the line of sight are given by

$$\cos \delta_x = \sin \theta \cos \varphi$$

$$\cos \delta_y = \sin \theta \sin \varphi$$

$$\cos \delta_z = \cos \theta \qquad\qquad (2.18)$$

where θ and φ are the aspect angles of the ellipsoid given in its own (local) coordinate system. The ambiguity of the normal can be resolved by noting that the outward normal must be in the same octant as the line-of-sight. Thus from (2.17) and (2.18) the parametric angular coordinates, u_s and v_s, of the specular point are obtained as

$$v_s = \arctan\left\{\frac{b}{a} \tan \varphi\right\}$$

$$u_s = \arctan\left\{\frac{1}{c} \tan \theta \sqrt{a^2 \cos^2 \varphi + b^2 \sin^2 \varphi}\right\} \qquad . \qquad (2.19)$$

The product of the principal radii of curvature, $R_1 \times R_2$, is derived as in [41] by

$$R_1 R_2 = \frac{\left[\left(\frac{\partial F}{\partial x}\right)^2 + \left(\frac{\partial F}{\partial y}\right)^2 + \left(\frac{\partial F}{\partial z}\right)^2\right]^2}{\Delta} \Bigg|_{\substack{\text{specular} \\ \text{point}}} \qquad (2.20)$$

where

24

$$\Delta = \begin{vmatrix} \dfrac{\partial^2 F}{\partial x^2} & \dfrac{\partial^2 F}{\partial x \partial y} & \dfrac{\partial^2 F}{\partial x z} & \dfrac{\partial F}{\partial x} \\[3mm] \dfrac{\partial^2 F}{\partial x \partial y} & \dfrac{\partial^2 F}{\partial y^2} & \dfrac{\partial^2 F}{\partial y \partial z} & \dfrac{\partial F}{\partial y} \\[3mm] \dfrac{\partial^2 F}{\partial x \partial z} & \dfrac{\partial^2 F}{\partial y \partial z} & \dfrac{\partial^2 F}{\partial z^2} & \dfrac{\partial F}{\partial z} \\[3mm] \dfrac{\partial F}{\partial x} & \dfrac{\partial F}{\partial y} & \dfrac{\partial F}{\partial z} & 0 \end{vmatrix} \qquad (2.21)$$

The application of (2.20) to the ellipsoid (2.15) results in the expression

$$R_1 R_2 = a^2 b^2 c^2 \left(\frac{x_s^2}{a^4} + \frac{y_s^2}{b^4} + \frac{z_s^2}{c^4} \right)^2 \qquad (2.22)$$

where (x_s, y_s, z_s) are the coordinates of the specular point and are given from (2.16) by:

$$x_s = a \sin u_s \cos v_s = \frac{a^2}{p} \sin \theta \cos \varphi$$

$$y_s = b \sin u_s \sin v_s = \frac{b^2}{p} \sin \theta \sin \varphi$$

$$z_s = c \cos u_s = \frac{c^2}{p} \cos \theta \qquad (2.23)$$

where

$$p = \sqrt{a^2 \sin^2 \theta \cos^2 \varphi + b^2 \sin^2 \theta \sin^2 \varphi + c^2 \cos^2 \theta} \qquad .$$

Consequently, the RCS of the ellipsoid may be found from (2.14) and (2.22) to be given explicitly by

$$S = \pi R_1 R_2 = \frac{\pi a^2 b^2 c^2}{p^4} \qquad . \qquad (2.24)$$

The results given in (2.23) and (2.24) for a single ellipsoid may now be applied to each of the M ellipsoids, after the proper coordinate transformations.

Consider now an ellipsoid which has its center located at (x_{ti}, y_{ti}, z_{ti}) in the target coordinate system. A local coordinate system for the ellipsoid is defined, with the origin located at the center of the ellipsoid and with the coordinate axes coincident with the principal axes of the ellipsoid. Under these conditions the ellipsoid is given by (2.15). The angular rotations from the target coordinate system to the local coordinate system are defined as θ_t and φ_t, where φ_t is taken first about the z axis and then θ_t is taken about the new y axis.

Let x, y, and z be the coordinates of a point in the target fixed coordinate system, and let x', y', and z' be the coordinates of the point in the local coordinate system. Then the coordinates of the point are related by the following transformation:

$$
\begin{bmatrix} x' \\ y' \\ z' \end{bmatrix} = [T] \begin{bmatrix} x - x_{ti} \\ y - y_{ti} \\ z - z_{ti} \end{bmatrix}
\tag{2.25}
$$

where

$$
[T] = \begin{bmatrix} \cos \varphi_t \cos \theta_t & \sin \varphi_t \cos \theta_t & -\sin \theta_t \\ -\sin \varphi_t & \cos \varphi_t & 0 \\ \cos \varphi_t \sin \theta_t & \sin \varphi_t \sin \theta_t & \cos \theta_t \end{bmatrix} .
$$

Let θ and φ be the aspect angles of the target and (x_0, y_0, z_0) be the coordinates of the point on the unit sphere with these angular coordinates, then

$$\begin{bmatrix} x_0 \\ y_0 \\ z_0 \end{bmatrix} = \begin{bmatrix} \sin\theta\cos\varphi \\ \sin\theta\sin\varphi \\ \cos\theta \end{bmatrix} \qquad (2.26)$$

If r, s, and t are the coordinates of this point in the local coordinate system of the ellipsoid, then

$$\begin{bmatrix} r \\ s \\ t \end{bmatrix} = [T] \begin{bmatrix} \sin\theta\cos\varphi \\ \sin\theta\sin\varphi \\ \cos\theta \end{bmatrix} \qquad (2.27)$$

hence the local aspect angles can be found from

$$\varphi_i = \arctan\left(\frac{s}{r}\right)$$

$$\theta_i = \arctan\left(\frac{1}{t}\sqrt{r^2 + s^2}\right) \qquad (2.28)$$

The octant in which the angles are located must be determined by consideration of the signs of r, s, and t.

2.4 Computational Procedure

Let θ and φ be the target aspect angles; θ_i and φ_i be the local aspect angles of the i-th ellipsoid; θ_{ti} and φ_{ti} be the angular translations from the target coordinate system to the local coordinate system for the i-th ellipsoid; (x_{ti}, y_{ti}, z_{ti}) be the location of the center of the i-th ellipsoid; (x_i', y_i', z_i') be the coordinates of the specular point in the local coordinate system of the i-th ellipsoid; and x_i, y_i, and z_i be the coordinates of the specular point of the i-th ellipsoid in the target fixed coordinate system.

The starting point for each computation is the set of target aspect angles θ and φ. For each of the N ellipsoids, the following procedure is used:

(1) Transform from target aspect angles to local aspect angles using (2.28).

(2) Determine the location of the specular point in the local coordinate system using (2.23).

(3) Determine the RCS, S_i', of the specular point using (2.24).

(4) Transform the position of the specular point from local coordinates (x_i', y_i', z_i') to target coordinates (x_i, y_i, z_i) by

$$\begin{bmatrix} x_i \\ y_i \\ z_i \end{bmatrix} = \begin{bmatrix} T^{-1} \end{bmatrix} \begin{bmatrix} x_i' \\ y_i' \\ z_i' \end{bmatrix} + \begin{bmatrix} x_{ti} \\ y_{ti} \\ z_{ti} \end{bmatrix} \quad .$$

(5) Determine the magnitude of the modulating function G(i) and the value of the RCS to be used in (2.4) through (2.7) by

$$S_i = G(i) \; S_i' \quad .$$

The values of the scattering parameters for the aspect angles θ and φ are found by applying (2.4) through (2.7) where the location (x_i, y_i, z_i), and RCS, S_i, of the i-th scatterer are determined as described above.

2.5 Numerical Example

The results of the last three sections will now be applied to the special case of the BQM-34A Target Drone. Figures 2.2 and 2.3 depict the actual Target Drone and the ellipsoidal approximation. The ellipsoidal model in this case consists of eight ellipsoids. The configuration (as defined by the conjugate radii), location (x_t, y_t, z_t) and orientation (θ_t, φ_t) for each ellipsoid is given in Table 2.1. The modulating functions for these ellipsoids are given in Table 2.2.

Table 2.1

Conjugate Radii and Translations of Ellipsoids
in Model of BQM-34A Target Drone

Component Part	A (meters)	B (meters)	C (meters)	θ_t (deg)	ϕ_t (deg)	x_t (meters)	y_t (meters)	z_t (meters)
Fuselage	3.25	0.352	0.556	0	0	0.0	0.0	0.0
Left Wing	0.293	2.82	0.044	0	45	0.614	0.0	-0.3
Right Wing	0.293	2.82	0.044	0	-45	0.614	0.0	-0.3
Left Horizontal Stabilizer	0.235	1.41	0.033	0	45	-1.757	0.0	-0.1
Right Horizontal Stabilizer	0.235	1.41	0.033	0	-45	-1.757	0.0	-0.1
Vertical Stabilizer	0.322	0.066	1.5	-45	0	-1.728	0.0	0.0
Left Wing Pod	0.6	0.1	0.3	0	0	-0.41	1.46	-0.35
Right Wing Pod	0.6	0.1	0.3	0	0	-0.41	-1.46	-0.35

Table 2.2

Modulating Functions for RCS of Ellipsoids
in Model of BQM-34A Target Drone

Component Part	Element No.	Modulating Function, $G(i)$
Fuselage	1	$G(1) = 1 + \left|\cos\theta_1 \sin\varphi_1\right|$
Left Wing	2	$G(2) = \left(\max\left[0.0,\ \cos(0.9\ \varphi_2)\right]\right)^{\frac{1}{2}^2}$
Right Wing	3	$G(3) = \left(\max\left[0.0,\ \cos(0.9\ \varphi_3)\right]\right)^{\frac{1}{2}^2}$
Left Horizontal Stabilizer	4	$G(4) = G(2)$
Right Horizontal Stabilizer	5	$G(5) = G(3)$
Vertical Stabilizer	6	$G(6) = \max\left[0.0,\ \cos(0.9\ \theta_6)\right]$
Left Wing Pod	7	$G(7) = 1$
Right Wing Pod	8	$G(8) = 1$

NOTE: θ_i and φ_i are local aspect angles

The procedures derived in Sections 2.2 and 2.4 are used to compute the scattering parameters as functions of the aspect angles, θ and φ. Typical results are shown in Figures 2.4, 2.5, and 2.6.

Figure 2.4 is the calculated RCS for L-Band plotted in decibels referenced to 1-square meter (RCSdBM) versus yaw angle for zero roll and zero pitch. Zero yaw angle corresponds to nose-on, 90 degrees corresponds to broadside and 180 degrees corresponds to tail-on. As compared to measured data, the calculated RCS in the angular regions from 0 to about 35 degrees and from about 140 to 180 degrees is low. In the headon region the discrepancy is about 15 decibels and in the tail-on region about 10 decibels. These discrepancies are due largely to two factors. The first factor is the simplicity of the modeling approach used. The second factor is the transparency of certain parts of the target drone. The analytic model ignores the engine intake and exhaust ducts thereby ignoring significant scattering over certain aspect angles. The data on which the comparison is based were measured on a target drone with considerable transparent portions. In addition to the radome, the front cowl forward of the engine is transparent. Therefore, the RCS within about 35 degrees of nose-on is the RCS of the bulkheads, forward engine structure, autopilot and electronics packages, and other components. The end of the tail cone which houses the recovery parachute is also transparent. These factors make a comparison extremely difficult. However, the lobing structure is approximately correct as is the broadside RCS.

Figures 2.5 and 2.6 are the azimuth and elevation errors, AZER and ELER respectively, expressed as the linear error at the target. The conditions are identical to those for Figure 2.4.
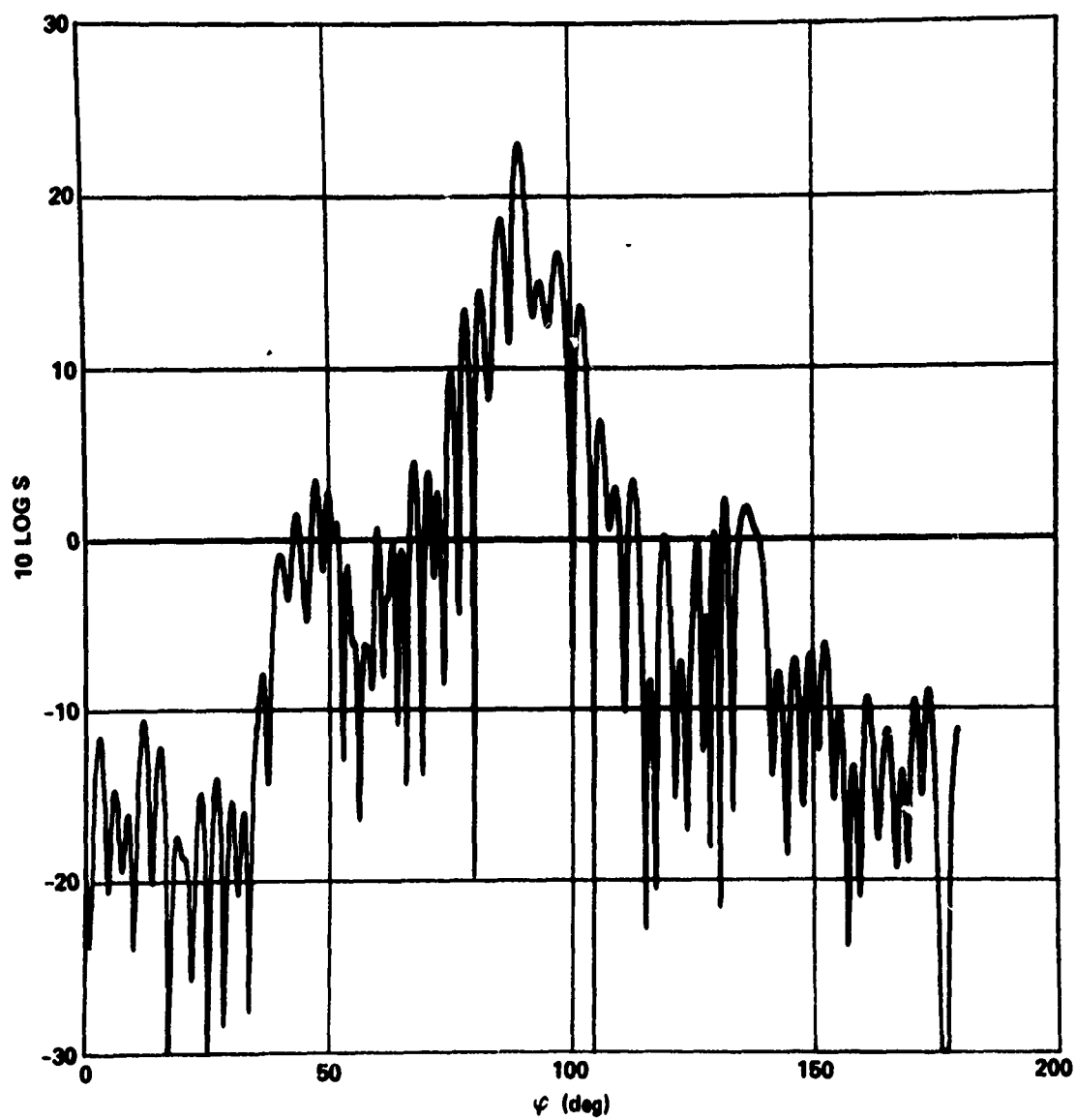
Figure 2.4 Radar Cross Section in dBM, 10 log S, Versus
Yaw Angle φ

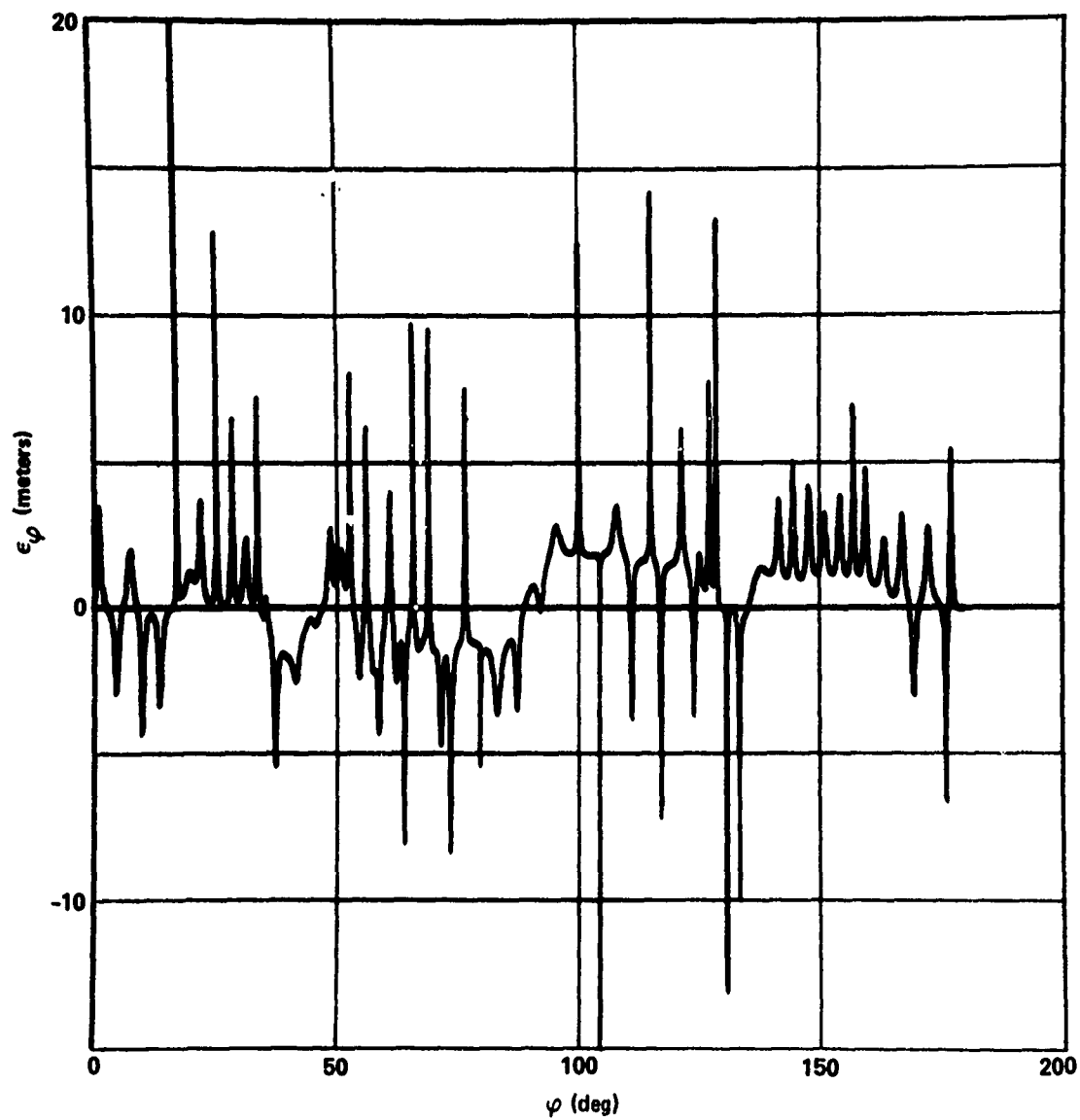Figure 2.5. Azimuth Error ϵ_φ Versus Yaw Angle φ
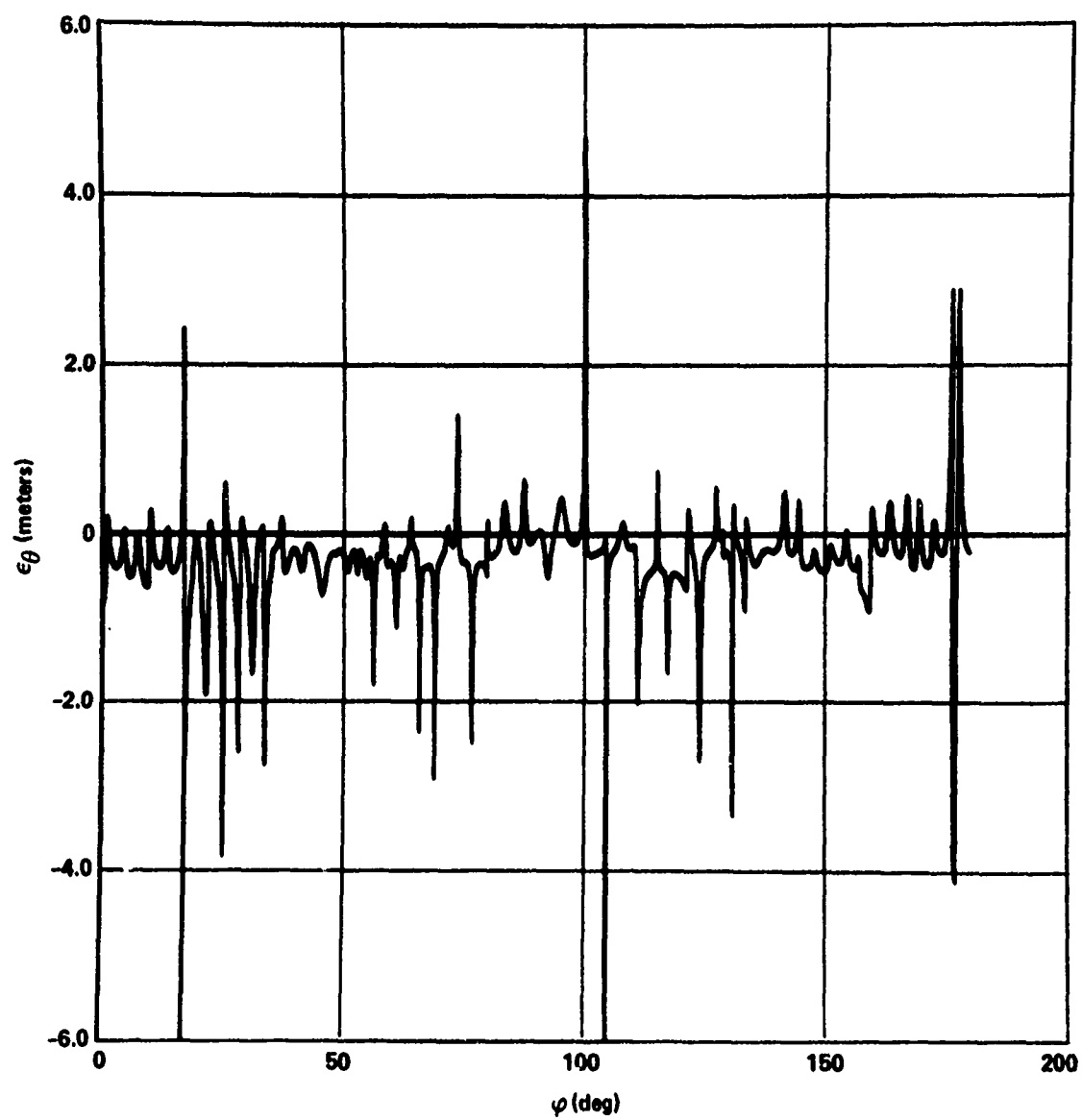
Figure 2.6. Elevation Error ϵ_θ Versus Yaw Angle φ

3. THE STATISTICAL PROPERTIES OF THE SCATTERING PARAMETERS

3.1 General

The primary objective of this research has been to develop techniques for computing the statistical parameters of a radar target, in particular an aircraft type target. These data can be used to generate a vector stochastic process representing the radar scattering parameters of the target which can be used in system simulations and evaluations. The data may also be used in the design of optimum filters for tracking systems.

Section 3.2 derives the statistics of the aspect angles using approximation techniques. Section 3.3 applies the aspect angle statistics to the analytic scattering model developed in Chapter 2 to derive the statistical properties of the scattering parameters.

3.1.1 The Statistical Properties Under Investigation

The available techniques for obtaining a dynamical representation of a stochastic process require that the probability density function and autocorrelation function be known, and that these functions satisfy certain criteria. These techniques can be generalized to N dimensions, when the matrix of covariance functions is known. One general approach requires only that the probability density function have finite variance and that the covariance functions be written as sums of exponentials.

The RCS, AZER, and ELER are complicated nonlinear functions of
the aspect angles as indicated in Chapter 2 so that the conventional
transformation of variables approach to obtain the probability density
function is impractical if not impossible. Therefore, other properties
of the probability density functions must be investigated. The most
descriptive properties which can be determined are the moments. A
complete description of a probability density function, in terms of its
moments, requires that all of the moments be known. For a Gaussian
density, all of the moments can be expressed in terms of the mean and
variance. These two moments are not sufficient, in general, to
characterize an unknown density function. However, computation of all
moments is not a practical undertaking so some compromise must be made.
A reasonable compromise appears to be the first four moments. The
third moment measures the skewness or asymmetry and the fourth moment
measures the shape of the distribution as compared to the Gaussian
distribution.

These moments can be used to approximate the fit of an unknown
probability density function by use of known techniques including the
use of Gram-Charlier series [57] where the unknown density functions
do not differ markedly from Gaussian density functions or those
derivable from Gaussian density functions. Another technique is
described by Wragg and Dowson [58] for density functions on [0, ∞).

The statistical properties of the scattering parameters under
investigation, then are the first four moments and the matrix of
covariance functions. Since it is not possible to assign probabilis-
tic properties to a target trajectory, the statistics to be derived are
all for a given trajectory. Therefore, the moments and the correlation

functions are defined as conditional expectations given the flight path in the ground fixed coordinate system.

3.1.2 The General Approach

The time history of the scattering parameters of an aircraft cannot be represented by a stationary process. The means and variances of the scattering parameters are time-varying functions of the aspect angles θ and φ, which are in general functions of the trajectory and hence of time. The relationship among the aspect angles and the target position and attitude in the ground fixed coordinate system are given by

$$
\begin{bmatrix}
\sin \theta(t) \cos \varphi(t) \\
\sin \theta(t) \sin \varphi(t) \\
\cos \theta(t)
\end{bmatrix}
= [T(t)]
\begin{bmatrix}
-\sin \theta_0(t) \cos \varphi_0(t) \\
-\sin \theta_0(t) \sin \varphi_0(t) \\
-\cos \theta_0(t)
\end{bmatrix}
\quad (3.1)
$$

where [T] is given in (2.3).

The target coordinate angles $\theta_0(t)$ and $\varphi_0(t)$ describe the target position in space as measured in the ground fixed coordinate system. The Euler angles, α, β, and γ, appearing in [T] are functions of the target motion, making the [T] a function of time for a known trajectory. Let $\bar{\alpha}(t)$, $\bar{\beta}(t)$, and $\bar{\gamma}(t)$ be the Euler angles corresponding to a given target trajectory (position, velocity, and acceleration). If these are substituted in [T] in (3.1) the resulting $\tilde{\theta}(t)$ and $\tilde{\varphi}(t)$ are then purely deterministic functions of time. However, in general, the Euler angles α, β, and γ contain a stochastic component due to perturbations in the motion, wind, vibrations, etc. For simplicity it may be assumed that the stochastic components of α, β, and γ are additive with zero mean and exponential autocorrelation function.

Therefore, $\alpha(t)$, $\beta(t)$, and $\gamma(t)$ are assumed to have time varying means $\bar{\alpha}(t)$, $\bar{\beta}(t)$, $\bar{\gamma}(t)$ and autocorrelation functions.

$$R_\nu\left(t_1, t_2\right) = \bar{\nu}\left(t_1\right) \bar{\nu}\left(t_2\right) + \sigma_\nu^2 \, e^{-k_\nu |t_2 - t_1|} \quad , \quad (3.2)$$

$$\nu = \alpha, \beta, \gamma \quad .$$

The perturbations have generally small time constants as compared to the time constants of aircraft trajectory. Consequently, $\alpha(t)$, $\beta(t)$, and $\gamma(t)$ may be considered to be wide-sense stationary for $|t_2 - t_1|$ small enough. Now $\theta(t)$ and $\varphi(t)$ in (3.1) are given by time varying nonlinear transformations of α, β, and γ. Since the time constants of the stochastic components are small compared to the time constants of the trajectory, and hence of the transformation, it can be shown that $\theta(t)$ and $\varphi(t)$ are therefore time varying random processes whose means and autocorrelation functions have the form

$$E\{\theta(t)\} = \bar{\theta}(t) \approx \tilde{\theta}(t)$$

$$E\{\varphi(t)\} = \bar{\varphi}(t) \approx \tilde{\varphi}(t) \quad (3.3)$$

$$R_\theta\left(t_1, t_2\right) = \bar{\theta}\left(t_1\right)\bar{\theta}\left(t_2\right) + \sigma_\theta\left(t_1\right)\sigma_\theta\left(t_2\right)\rho_\theta\left(t_2 - t_1\right)$$

$$R_\varphi\left(t_1, t_2\right) = \bar{\varphi}\left(t_1\right)\bar{\varphi}\left(t_2\right) + \sigma_\varphi\left(t_1\right)\sigma_\varphi\left(t_2\right)\rho_\varphi\left(t_2 - t_1\right) \quad . \quad (3.4)$$

Here, it has also been assumed that the stochastic perturbation of the Euler angles are relatively small. Consequently for a given flight path, $\theta(t)$ and $\varphi(t)$ have time varying means and variances. Furthermore, if $|t_2 - t_1|$ is small, then their covariance is approximately

$$c_\theta\left(t_1, t_2\right) \approx \sigma_\theta^2\left(t_1\right)\rho\left(t_2 - t_1\right)$$

$$c_\varphi\left(t_1, t_2\right) \approx \sigma_\varphi^2\left(t_1\right)\rho\left(t_2 - t_1\right) \tag{3.5}$$

while for large $|t_2 - t_1|$ they are uncorrelated. Similarly, for $|t_2 - t_1|$ small enough that $\rho(t_2 - t_1)$ is not negligible, $\bar{\theta}(t_1) \approx \bar{\theta}(t_2)$ and $\bar{\varphi}(t_1) \approx \bar{\varphi}(t_2)$. Hence, they are wide-sense stationary for sufficiently small time intervals.

The approach to estimating the aspect angle statistics is to expand the implicit expressions for θ and φ contained in (3.1) about the deterministic values $\tilde{\theta}$ and $\tilde{\varphi}$ which are obtained by substituting $\bar{\alpha}$, $\bar{\beta}$, and γ into (3.1) for α, β, and γ. The order of the approximation will be reduced to the minimum acceptable level.

3.2 Aspect Angle Statistics

The derivation of the statistical characteristics of the aspect angles, θ and φ, requires a knowledge of the target position in the ground fixed coordinate system and the target motion in each of its 6 degrees of freedom. The translational motion is specified in the ground fixed coordinate system. The angular motion is more difficult to define but relates the angular position of the target fixed coordinate system to the ground fixed coordinate system. Neglecting any random angular motions it is assumed that the target flies with its longitudinal axis, x axis, coincident with the velocity vector and its vertical axis, z axis, opposing the combined acceleration due to gravity and any maneuvers other than longitudinal acceleration. (This approach clearly ignores aerodynamic theories related to flight [59] but permits a reasonable analysis without requiring a detailed aerodynamic model of the target.) The yaw, pitch, and roll angles,

α, β, and γ respectively, required to go from axes parallel to the ground fixed Cartesian coordinate axes to the target fixed Cartesian coordinate axes are shown in Figure 3.1.

Let x', y', and z' be the Cartesian coordinate axes of the ground fixed coordinate system and x, y, and z be the Cartesian coordinates of the target fixed coordinate system. As defined previously, (1) the x axis is the longitudinal or roll axis of the target with the velocity vector pointing in the positive direction; (2) the y axis is the pitch axis; and (3) the z axis is the yaw axis. The yaw, pitch, and roll angles (Euler angles), α, β, and γ respectively, are defined such that α and γ are conventional right-handed angles, but β is left-handed. Let x*, y*, and z* be the intermediate axes during the sequence of angular transformations from one coordinate system to the other. The transformation between coordinate systems is unique only when the order of the angular transformations is defined. In this work, the order is defined to be β, γ, and α, in that order. Figure 3.1 depicts the angular coordinate transformation from the ground fixed coordinates to the target fixed coordinates. The first rotation is β about the y' axis, the second rotation is γ about x*, the intermediate x axis, and the third is α about the final z axis.

The aspect angles are related to the target position and motion by (3.1) where [T] is defined in (2.3). If the α rotation is factored out of φ, it is noted that α is additive to φ resulting in a simplification of the algebra.

$$[T] = \begin{bmatrix} \cos\alpha & \sin\alpha & 0 \\ -\sin\alpha & \cos\alpha & 0 \\ 0 & 0 & 1 \end{bmatrix} \begin{bmatrix} \cos\beta & 0 & \sin\beta \\ -\sin\beta\sin\gamma & \cos\gamma & \cos\beta\sin\gamma \\ -\sin\beta\cos\gamma & -\sin\gamma & \cos\beta\cos\gamma \end{bmatrix} \quad (3.6)$$
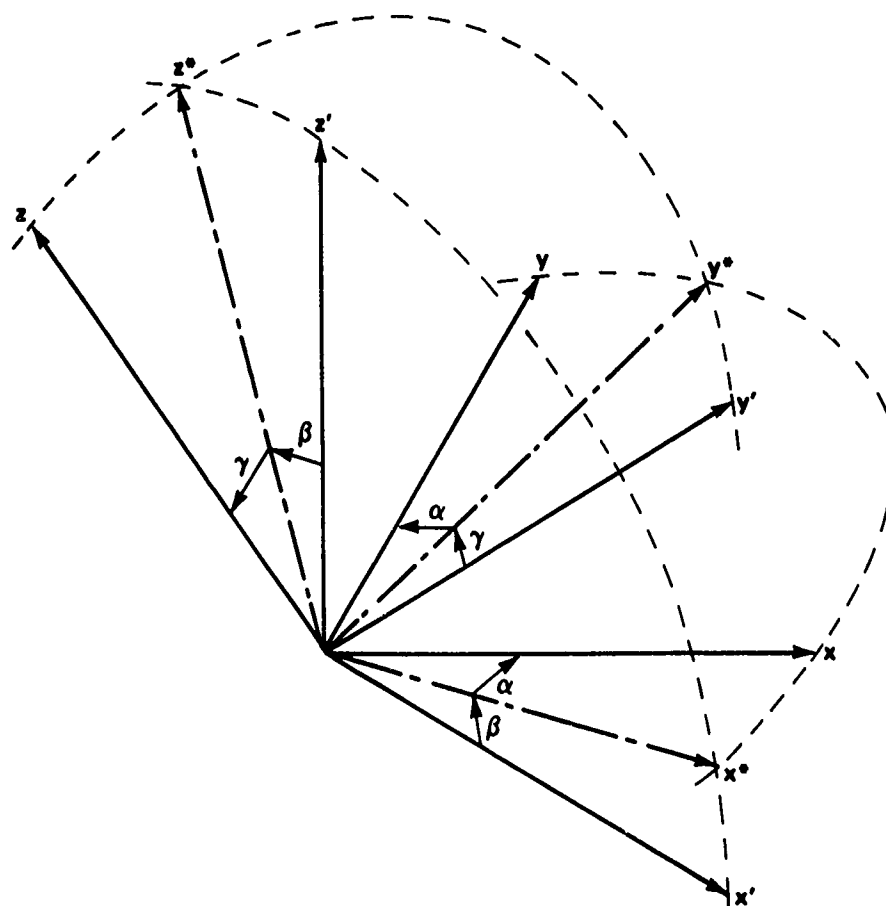
40

Figure 3.1. Angular Transformations from Ground Fixed
to Target Fixed Coordinates

It is possible now to find an exact analytic solution for the joint probability density function for θ and φ, as given in Appendix B. Clearly the equations in the right hand matrix are nonlinear and do not permit a visualization of the results even when the density functions for α, β, and γ are given. Numerical results can be obtained by implementing standard transformation of variables techniques on a digital computer. An even more formidable limitation exists. Although it is possible to obtain the moments by numerical integration, it is not possible to obtain the covariance functions for θ and φ which are necessary in computing the covariance functions of the scattering parameters.

The aspect angles θ and φ can be expanded in Taylor series about their quasi-means $\tilde{\theta}(t)$ and $\tilde{\varphi}(t)$. For notational convenience, the time dependence of the means and variances is being dropped from the notation for the rest of the analysis. If variances of the random components of the Euler angles are sufficiently small, θ and φ can be approximated by the first two terms of the Taylor series expansions.

$$\varphi \approx \tilde{\varphi} + \alpha_s + \beta_s \left.\frac{\partial \varphi}{\partial \beta}\right|_{\bar{\beta},\bar{\gamma}} + \gamma_s \left.\frac{\partial \varphi}{\partial \gamma}\right|_{\bar{\beta},\bar{\gamma}} + \beta_s \gamma_s \left.\frac{\partial^2 \varphi}{\partial \beta \partial \gamma}\right|_{\bar{\beta},\bar{\gamma}}$$

$$+ \frac{1}{2} \beta_s^2 \left.\frac{\partial^2 \varphi}{\partial \beta^2}\right|_{\bar{\beta},\bar{\gamma}} + \frac{1}{2} \gamma_s^2 \left.\frac{\partial^2 \varphi}{\partial \gamma^2}\right|_{\bar{\beta},\bar{\gamma}} \qquad (3.7)$$

42

$$\theta \approx \tilde{\theta} + \beta_s \left. \frac{\partial \theta}{\partial \beta} \right|_{\overline{\beta}, \overline{\gamma}} + \gamma_s \left. \frac{\partial \theta}{\partial \gamma} \right|_{\overline{\beta}, \overline{\gamma}} + \beta_s \gamma_s \left. \frac{\partial^2 \theta}{\partial \beta \partial \gamma} \right|_{\overline{\beta}, \overline{\gamma}}$$

$$+ \frac{1}{2} \beta_s^2 \left. \frac{\partial^2 \theta}{\partial \beta^2} \right|_{\overline{\beta}, \overline{\gamma}} + \frac{1}{2} \gamma_s^2 \left. \frac{\partial^2 \theta}{\partial \gamma^2} \right|_{\overline{\beta}, \overline{\gamma}} \qquad (3.8)$$

where

$$\alpha_s = \alpha - \overline{\alpha}$$

$$\beta_s = \beta - \overline{\beta}$$

$$\gamma_s = \gamma - \overline{\gamma} \qquad .$$

By use of implicit differentiation and algebraic manipulations the partial derivatives can be shown to be:

$$\left. \frac{\partial \theta}{\partial \beta} \right|_{\overline{\beta}, \overline{\gamma}} = \cos \overline{\gamma} \cos \tilde{\varphi} \qquad (3.9)$$

$$\left. \frac{\partial^2 \theta}{\partial \beta^2} \right|_{\overline{\beta}, \overline{\gamma}} = \frac{1}{2} \sin 2\overline{\gamma} \sin \tilde{\varphi} + \frac{1}{2} (1 + \cos 2\overline{\gamma}) \cot \tilde{\theta} \sin^2 \tilde{\varphi} \qquad (3.10)$$

$$\left. \frac{\partial \theta}{\partial \gamma} \right|_{\overline{\beta}, \overline{\gamma}} = \sin \tilde{\varphi} \qquad (3.11)$$

$$\left. \frac{\partial^2 \theta}{\partial \gamma^2} \right|_{\overline{\beta}, \overline{\gamma}} = \cot \tilde{\theta} \cos^2 \tilde{\varphi} \qquad (3.12)$$

$$\left. \frac{\partial^2 \theta}{\partial \beta \partial \gamma} \right|_{\overline{\beta}, \overline{\gamma}} = - \cos \tilde{\varphi} (\sin \overline{\gamma} - \cos \overline{\gamma} \cot \tilde{\theta} \sin \tilde{\varphi}) \qquad (3.13)$$

$$\frac{\partial \varphi}{\partial \beta}\bigg|_{\overline{\beta},\overline{\gamma}} = -\sin \overline{\gamma} - \cos \overline{\gamma} \cot \widetilde{\theta} \sin \widetilde{\varphi} \qquad (3.14)$$

$$\frac{\partial^2 \varphi}{\partial \beta^2}\bigg|_{\overline{\beta},\overline{\gamma}} = \frac{1}{2} \sin 2\overline{\gamma} \cot \widetilde{\theta} \cos \widetilde{\varphi} + \frac{1}{4} \sin 2\widetilde{\varphi}(1 + \cos 2\overline{\gamma})(1 + 2 \cot \widetilde{\theta})$$
$$(3.15)$$

$$\frac{\partial \varphi}{\partial \gamma}\bigg|_{\overline{\beta},\overline{\gamma}} = \cos \widetilde{\varphi} \cot \widetilde{\theta} \qquad (3.16)$$

$$\frac{\partial^2 \varphi}{\partial \gamma^2}\bigg|_{\overline{\beta},\overline{\gamma}} = -\frac{1}{2} \sin 2\widetilde{\varphi} (1 + 2 \cot^2 \widetilde{\theta}) \qquad (3.17)$$

$$\frac{\partial^2 \varphi}{\partial \beta \partial \gamma}\bigg|_{\overline{\beta},\overline{\gamma}} = \sin \overline{\gamma} \sin \widetilde{\varphi} \cot \widetilde{\theta} - \cos \gamma (\cos^2 \widetilde{\varphi} + \cot^2 \widetilde{\theta} \cos 2 \widetilde{\varphi}).$$
$$(3.18)$$

The accuracy of these expansions may be examined by obtaining the statistics of the resulting series:

$$\overline{\theta} = E\{\theta\} \approx \widetilde{\theta} + \frac{1}{2} \sigma_\beta^2 \left[\sin 2 \overline{\gamma} \sin \widetilde{\varphi} + \left(1 + \cos 2 \overline{\gamma}\right) \cot \widetilde{\theta} \sin^2 \widetilde{\varphi} \right]$$
$$+ \sigma_\gamma^2 \cot \widetilde{\theta} \cos^2 \widetilde{\varphi} \qquad (3.19)$$

$$\overline{\varphi} = E\{\varphi\} \approx \widetilde{\varphi} + \frac{1}{2} \sigma_\beta^2 \left[\sin 2 \overline{\gamma} \cot \widetilde{\theta} \cos \widetilde{\varphi} \right.$$

$$+ \frac{1}{2} \sin 2 \widetilde{\varphi} \left(1 + \cos 2 \overline{\gamma}\right) \left(1 + 2 \cot \widetilde{\theta}\right) \Big]$$

$$- \frac{1}{2} \sigma_\gamma^2 \sin 2 \widetilde{\varphi} \left(1 + 2 \cot^2 \widetilde{\theta}\right) \qquad (3.20)$$

44

$$\sigma_\theta^2 = E\left\{(\theta - \tilde{\theta})^2\right\} = \sigma_\beta^2 \cos^2 \bar{\gamma} \cos^2 \tilde{\phi} + \sigma_\gamma^2 \sin^2 \tilde{\phi}$$

$$+ \sigma_\beta^2 \sigma_\gamma^2 \cos^2 \tilde{\phi} \left(\sin \bar{\gamma} - \cos \bar{\gamma} \cot \tilde{\theta} \sin \tilde{\phi}\right)^2$$

$$+ \frac{1}{4} \sigma_\beta^4 \left[\sin 2 \bar{\gamma} \sin \tilde{\phi} + (1 + \cos 2 \bar{\gamma}) \cot \tilde{\theta} \sin^2 \tilde{\phi}\right]^2$$

$$\div \sigma_\gamma^4 \cot^2 \tilde{\theta} \cos^2 \tilde{\phi} \qquad (3.21)$$

$$\sigma_\phi^2 = E\left\{(\phi - \bar{\phi})^2\right\} = \sigma_\alpha^2 + \sigma_\beta^2 (\sin \bar{\gamma} + \cos \bar{\gamma} \cot \tilde{\theta} \sin \tilde{\phi})^2$$

$$+ \sigma_\gamma^2 \cot^2 \tilde{\theta} \cos^2 \tilde{\phi} + \sigma_\beta^2 \sigma_\gamma^2 \left[\sin \bar{\gamma} \sin \tilde{\phi} \cot \tilde{\theta}\right.$$

$$\left. - \cos \bar{\gamma} \left(\cos^2 \tilde{\phi} + \cot^2 \tilde{\theta} \cos 2 \tilde{\phi}\right)\right]^2$$

$$+ \frac{1}{4} \sigma_\beta^4 \left[\sin 2 \bar{\gamma} \cot \tilde{\theta} \cos \tilde{\phi} + \frac{1}{2} \sin 2 \tilde{\phi} (1 + \cos 2 \bar{\gamma})\left(1 + 2 \cot^2 \tilde{\theta}\right)\right]^2$$

$$+ \frac{1}{4} \sigma_\gamma^4 \sin^2 2 \tilde{\phi} \left(1 + 2 \cot^2 \tilde{\theta}\right)^2 \qquad (3.22)$$

$$\sigma_\theta \sigma_\phi \, \rho_{\theta,\tau} = E\{(\theta - \bar{\theta})(\phi - \bar{\phi})\} = \sigma_\beta^2 \cos \bar{\gamma} \cos \tilde{\phi}$$

$$\times (- \sin \bar{\gamma} - \cos \bar{\gamma} \cot \tilde{\theta} \sin \tilde{\omega}) + \frac{1}{2} \sigma_\gamma^2 \sin 2 \tilde{\phi} \cot \tilde{\theta}$$

$$+ \frac{1}{4} \sigma_\beta^4 \left[\sin 2 \bar{\gamma} \sin \tilde{\phi} + (1 + \cos 2 \bar{\gamma}) \cot \tilde{\theta} \sin^2 \tilde{\phi}\right]$$

$$\times \left[\sin 2 \bar{\gamma} \cot \tilde{\theta} \cos \tilde{\phi} + \frac{1}{2} \sin 2 \tilde{\phi} (1 + \cos 2 \bar{\gamma})(1 + 2 \cot^2 \tilde{\theta})\right]$$

$$- \sigma_\beta^2 \sigma_\gamma^2 \cos \tilde{\phi} (\sin \bar{\gamma} - \cos \bar{\gamma} \cot \tilde{\theta} \sin \tilde{\phi})$$

$$\times \left[\sin \bar{\gamma} \sin \tilde{\phi} \cot \tilde{\theta} - \cos \bar{\gamma} \left(\cos^2 \tilde{\phi} + \cot^2 \tilde{\theta} \cos 2 \tilde{\phi}\right)\right]$$

$$- \frac{1}{2} \sigma_\gamma^4 \cot \tilde{\theta} \cos^2 \tilde{\phi} \sin 2 \tilde{\phi} \left(1 + 2 \cot^2 \tilde{\theta}\right) \qquad . \qquad (3.23)$$

Some knowledge of the statistics of the Euler angles is necessary in order to establish bounds on the errors, and hence evaluate the accuracy of the expansions.

There is, unfortunately, a lack of published or available data on the angular motions of an aircraft in flight. An aircraft is designed to fly and perform a mission safely. Only those flight characteristics which affect safety or the ability to perform the specified mission are investigated and reported. The small scale random motions of interest here are generally ignored. The pilot, or autopilot, can handle these as a minor part of the normal flight activities. The coupling among yaw, pitch and roll, especially when flying with the autopilot operating, is familiar to many. It would seem reasonable, based upon this and other factors, to expect that the quasi-random angular motions would be similarly coupled. However, the lack of data make it impossible to determine what the coupling or covariance function should be.

It is necessary to assume some probability and covariance functions for the Euler angles. The most useful family of probability density functions for angles is that used by Viterbi [60]. It is given by

$$f_\theta(\theta) = \frac{\exp\ (s\ \cos\ \theta)}{2\pi\ I_0(s)} \quad , \qquad 0 \leq \theta \leq 2\pi \qquad (3.24)$$

where θ is the angle and s is a parameter related to the variance of the distribution. For s = 0, the density is uniform over the range of $-\pi$ to τ, and for s = ∞, the density is a delta function at θ = 0. This density is closely approximated by a normal density for s >> 1, as shown by Viterbi. Due to the lack of published data, it is assumed

46

that the random angular motions of the target are independent normal (Gaussian) processes with exponential autocorrelation functions. This is an arbitrary and perhaps simplistic approach, but represents a practical and mathematically tractable approach. The choice of a normal process is based upon the fact that the random motions are small. The only justification for the exponential autocorrelation function is mathematical convenience.

For a basically stable aircraft under cruising flight conditions, standard deviations of the Euler angles of less than 100 milliradians or about 5.7 degrees seem reasonable. Autocorrelation time constants on the order of 1.0 to 5.0 seconds also seem reasonable.

Without loss of generality, but in the interest of simplifying the algebra, it is assumed that the aircraft is flying a rectilinear flight path. This implies that $\bar{\beta} = \bar{\gamma} = 0$, and that $\tilde{\theta} = \theta_0$ and $\tilde{\varphi} = \varphi_0 + \bar{\alpha}$. From practical considerations, the area of prime interest in the elevational aspect angle θ is for $\pi/2 \leq \theta \leq 3\pi/4$. In this region $-1 \leq \cot \theta \leq 0$. With this information it is possible to evaluate the general accuracy of the Taylor series expansions of θ and φ, (3.7) and (3.8). Equations (3.19) through (3.23) can be written as:

$$\bar{\theta} = \tilde{\theta} + \frac{1}{2} \cot \tilde{\theta} \left(\sigma_\beta^2 \sin^2 \tilde{\varphi} + \sigma_\gamma^2 \cos^2 \tilde{\varphi} \right) \qquad (3.19A)$$

$$\bar{\varphi} = \tilde{\varphi} + \frac{1}{2} \sin 2 \tilde{\varphi} \left(1 + 2 \cot^2 \tilde{\theta} \right)\left(\sigma_\beta^2 - \sigma_\gamma^2 \right) \qquad (3.20A)$$

$$\sigma_\theta^2 = \sigma_\beta^2 \cos^2 \tilde{\varphi} + \sigma_\gamma^2 \sin^2 \tilde{\varphi} + \frac{1}{4} \sigma_\beta^2 \sigma_\gamma^2 \cot^2 \tilde{\theta} \sin^2 2 \tilde{\varphi}$$

$$+ \cot^2 \tilde{\theta} \left(\sigma_\beta^4 \sin^4 \tilde{\varphi} + \sigma_\gamma^4 \cos^4 \tilde{\varphi} \right) \qquad (3.21A)$$

$$\sigma_\varphi^2 = \sigma_\alpha^2 + \cot^2 \tilde{\theta} \left(\sigma_\beta^2 \sin^2 \tilde{\varphi} + \sigma_\gamma^2 \cos^2 \tilde{\varphi} \right)$$

$$+ \sigma_\beta^2 \sigma_\gamma^2 \left(\cos^2 \tilde{\varphi} + \cot^2 \tilde{\theta} \cos 2 \tilde{\varphi} \right)^2$$

$$+ \frac{1}{4} \sin^2 2 \tilde{\varphi} \left(1 + 2 \cot^2 \tilde{\theta} \right)^2 \left(\sigma_\beta^4 + \sigma_\gamma^4 \right) \qquad (3.22A)$$

$$\sigma_\theta \sigma_\varphi \rho_{\theta, \varpi} = \frac{1}{2} \sin 2 \tilde{\varphi} \cot \tilde{\theta} \left(\sigma_\gamma^2 - \sigma_\beta^2 \right)$$

$$+ \frac{1}{2} \cot \tilde{\theta} \sin 2 \tilde{\varphi} \left(1 + 2 \cot^2 \theta \right) \left(\sigma_\beta^4 \sin^2 \tilde{\varphi} - \sigma_\gamma^4 \cos^2 \tilde{\varphi} \right)$$

$$- \frac{1}{2} \sigma_\beta^2 \sigma_\gamma^2 \sin 2 \tilde{\varpi} \cot \tilde{\theta} \left(\cos^2 \tilde{\varphi} + \cot^2 \tilde{\theta} \cos 2 \tilde{\varphi} \right) . \qquad (3.23A)$$

By inspection, it is clear that the second order terms generally add less than 0.1 sup $(\sigma_\beta, \sigma_\gamma)$ to the means and standard deviations of the aspect angles. First order (linear) approximations will be sufficient for this analysis. The following equations will be used in the computations later in this chapter.

$$\theta = \theta_0 + \beta_s \cos \tilde{\varphi} + \gamma_s \sin \tilde{\varpi} \qquad (3.25)$$

$$\varpi = \varpi_0 + \alpha - \beta_s \cot \theta_0 \sin \tilde{\varpi} + \gamma_s \cot \theta_0 \cos \tilde{\varphi} \qquad (3.26)$$

where $\tilde{\varpi} = \varpi_0 + \bar{\alpha}$. The means and covariance functions of the aspect angles are given by:

$$\bar{\theta} = \theta_0 \qquad (3.27)$$

$$\bar{\varpi} = \varpi_0 + \bar{\alpha} \qquad (3.28)$$

$$C_\theta \left(t_1, t_2 \right) = \sigma_\beta^2 \cos^2 \bar{\varphi} \, e^{-k_\beta \tau} + \sigma_\gamma^2 \sin^2 \bar{\varphi} \, e^{-k_\gamma \tau} \qquad (3.29)$$

$$C_\varphi \left(t_1, t_2 \right) = \sigma_\alpha^2 \, e^{-k_\alpha \tau} + \sigma_\beta^2 \cot^2 \theta_0 \sin^2 \bar{\varphi} \, e^{-k_\beta \tau}$$

$$+ \sigma_\gamma^2 \cot^2 \theta_0 \cos^2 \bar{\varphi} \, e^{-k_\gamma \tau} \qquad (3.30)$$

$$C_{\theta,\varphi}\left(t_1, t_2\right) = \frac{1}{2}\sin 2\,\overline{\varphi}\,\cot\theta_0\left(\sigma_\gamma^2\,e^{-k_\gamma\tau} - \sigma_\beta^2\,e^{-k_\beta\tau}\right) \quad (3.31)$$

where $\tau = |t_2 - t_1|$ and k_α, k_β, and k_γ are the inverses of the time constants of the autocorrelation functions of α, β, and γ, respectively. The linearization also implies that the joint density function of θ and φ is approximately Gaussian.

3.3 Statistics of the Scattering Parameters

3.3.1 Derivation of General Approach

The previous chapter and previous sections of this chapter have developed the necessary background and inputs to the derivation of the statistics of the scattering parameters. The following development holds true for all of the scattering parameters, so only the RCS will be mentioned. The application to the other scattering parameters will be made when appropriate.

As mentioned in Section 3.1, it is not possible to obtain the probability density function for the RCS using conventional transformation of variables techniques. Therefore, the first four moments of the probability density function and the covariance functions will be derived.

The characteristic function approach is to be used in the derivation of the expectation as follows:

$$E\{S\} \triangleq E\{S(\theta,\varphi)\} = E\left\{\frac{1}{(2\pi)^2}\iint A(u,v)e^{j(u\theta + v\varphi)}\,du\,dv\right\}$$

$$= \frac{1}{(2\pi)^2}\iint A(u,v)\,E\left\{e^{j(u\theta + v\varphi)}\right\}\,du\,dv$$

$$= \frac{1}{(2\pi)^2}\iint A(u,v)\,\Phi_{\theta,\varphi}(u,v)\,du\,dv \quad (3.32)$$

where

$$A(u, v) = \iint S(\theta,\varphi)\, e^{-j(u\theta + v\varphi)}\, d\theta\, d\varphi \qquad (3.33)$$

is the Fourier transform of $S(\theta,\varphi)$, and $\Phi_{\theta,\varphi}$ is the characteristic function of θ and φ. Similarly, for higher order moments, the expressions become

$$E\left\{S^r\right\} = E\left\{\frac{1}{(2\pi)^{2r}} \left(\iint A(u, v)\, e^{j(u\theta + v\varphi)}\, dudv\right)^r\right\}$$

$$= \frac{1}{(2\pi)^{2r}} \iint \cdots \iint A(u_1, v_1)\, \cdots\, A\left(u_2, v_2\right)\, \Phi\left(u_1 + \cdots\right.$$

$$\left. + u_r, v_1 + \cdots + v_r\right) \times du_1 dv_1 \cdots du_r dv_r \qquad (3.34)$$

and

$$E\left\{S_1 S_2\right\} \triangleq E\left\{S_1\left[\theta\left(t_1\right),\, \varphi\left(t_1\right)\right]\, S_2\left[\theta\left(t_2\right),\, \varphi\left(t_2\right)\right]\right\}$$

$$= \frac{1}{(2\pi)^4} \iiiint A_1\left(u_1, v_1\right)\, A_2\left(u_2, v_2\right)\, \Phi_{\theta_1, \theta_2, \varphi_1, \varphi_2}\left(u_1, v_1, u_2, v_2\right)$$

$$\times du_1\, dv_1\, du_2\, dv_2 \qquad . \qquad (3.35)$$

Thus, the moments and the correlation functions of the scattering parameters can be computed, at least in theory. From a practical point of view, however, this approach appears to have the same difficulty as determining the densities using the transformation of variables. The digital computer makes the computations of the moments and the covariance functions possible.

The procedure used in the computational process is basically to reduce the integrals to summations using approximation techniques. The general steps are:

(1) Compute the Fourier integral A(u, v) in (3.33).

(2) Compute the characteristic function $\Phi_{\theta,\varphi}(u,v)$ which for the assumption of a jointly Gaussian density for the aspect angles is given by

$$\Phi_{\theta,\varphi}(u,v) = e^{j\left(\bar{\theta}u + \bar{\varphi}v\right)}e^{-\frac{1}{2}\left(\sigma_\theta^2 u^2 + 2\rho_{\theta,\varphi}\sigma_\theta\sigma_\varphi uv + \sigma_\varphi^2 v^2\right)}$$

(3) Compute the integral (3.32).

There are practical considerations which influence the detailed procedures, which will be discussed as they are encountered.

It was shown in Section 3.2 that the conditional variances for θ and φ are small. It is reasonable, therefore, to consider only the portion of the $\theta - \varphi$ plane having a reasonable probability of occurring. Let $\bar{\theta}$ and $\bar{\varphi}$ be the conditional means and σ_θ^2 and σ_φ^2 be the conditional variances of θ and φ. Let M be a positive integer. Then the area of the plane having coordinates such that $\bar{\theta} - M\sigma_\theta \leq \theta \leq \bar{\theta} + M\sigma_\theta$ and $\bar{\varphi} - M\sigma_\varphi \leq \varphi \leq \bar{\varphi} + M\sigma_\varphi$ will be used for the actual computations.

Now, let $S_T(\theta,\varphi)$ be a periodic function which is identical to $S(\theta, \varphi)$ in the area defined above, i.e.,

$$- M\sigma_\theta \leq \theta - \bar{\theta} \leq M\sigma_\theta , \quad - M\sigma_\varphi \leq \varphi - \bar{\varphi} \leq M\sigma_\varphi \quad ,$$

and

$$S_T\left(\theta + 2kM\sigma_\theta, \varphi + 2\ell M\sigma_\varphi\right) = S_T(\theta,\varphi)$$

for k, ℓ integers.

The periodic function $S_T(\theta,\varphi)$ instead of $S(\theta,\varphi)$ will be used in computing the expectations. A bound on the resulting error in using a finite M is found in Appendix C. A reasonable compromise seems to

be M = 4 if θ and φ are assumed to be Gaussian. Since $S_T(\theta,\varphi)$ is periodic, it can be represented by its Fourier series.

$$S_T(\theta,\varphi) = \sum_{m=-\infty}^{\infty} \sum_{n=-\infty}^{\infty} A(m,n) \, e^{j\left(mu_0\theta + nv_0\varphi\right)} \tag{3.36}$$

where

$$u_0 = \frac{\pi}{M\sigma_\theta}$$

and

$$v_0 = \frac{\pi}{M\sigma_\varphi} \quad .$$

Substitution of (3.36) in the expectation results in a discrete version of (3.32).

$$E\{S\} \approx E\left\{ \sum_{m=-\infty}^{\infty} \sum_{n=-\infty}^{\infty} A(m,n) \, e^{j\left(mu_0\theta + nv_0\varphi\right)} \right\}$$

$$= \sum_{m=-\infty}^{\infty} \sum_{n=-\infty}^{\infty} A(m,n) \, \Phi_{\theta,\varphi}\left(mu_0, \, nv_0\right) \tag{3.37}$$

so the double integral in (3.32) becomes a double summation. The only approximation made at this point is the substitution of $S_T(\theta,\varphi)$ for $S(\theta,\varphi)$ as mentioned above. In practice only finite number of terms will be used in the summation (3.37). A bound on the resulting error is also discussed in Appendix C.

Similarly (3.33) and (3.34) become, respectively,

$$E\left\{S^r\right\} = \sum_{m_1=-\infty}^{\infty} \sum_{n_1=-\infty}^{\infty} \cdots \sum_{m_r=-\infty}^{\infty} \sum_{n_r=-\infty}^{\infty} A\left(m_1,n_1\right) \cdots A\left(m_r, \, n_r\right)$$

$$\times \, \Phi_{\theta,\varphi}\left(u_0 \sum_{i=1}^{r} m_i, \, v_0 \sum_{i=1}^{r} n_i\right) \tag{3.38}$$

52

$$E\left\{S_1 S_2\right\} = \sum_{m_1=-\infty}^{\infty} \sum_{n_1=-\infty}^{\infty} \sum_{m_2=-\infty}^{\infty} \sum_{n_2=-\infty}^{\infty} A_1\left(m_1,n_1\right) A_2\left(m_2,n_2\right)$$

$$\times \; \Phi_{\theta_1,\varphi_1,\theta_2,\varphi_2}\left(m_1 u_0, \; m_2 u_0, \; n_1 v_0, \; n_2 v_0\right) \; .$$

$$(3.39)$$

Now, it is necessary to obtain the Fourier coefficients, $A(m,n)$. These will be estimated using the Fast Fourier Transform.

3.3.2 The Fast Fourier Transform

The Fast Fourier Transform (FFT) is a digital computer algorithm for fast and efficient computation of the Discrete Fourier Transform (DFT)[61, 62]. The DFT is defined by

$$A_r = \frac{1}{N} \sum_{n=0}^{N-1} x_n \exp\left(\frac{-2\pi j r n}{N}\right) \qquad (3.40)$$

where A_r is the r-th coefficient of the DFT and x_n is the n-th sample of the time series x_n which consists of N samples. The inverse transform is given by

$$x_n = \sum_{n=0}^{N-1} A_r \exp\left(\frac{2\pi j r n}{N}\right) \qquad . \qquad (3.41)$$

One of the consequences of using the DFT is that both the time series and the coefficients of the harmonic frequencies can be defined for all integers (positive and negative). This results in the familiar periodic form

$$A_r = A_{r+N} = A_{r+2N} = \quad \cdot \; \cdot \; \cdot$$

$$x_n = X_{n+N} = x_{n+2N} = \quad \cdot \; \cdot \; \cdot \qquad \cdot$$

The approximation of the Fourier Transform or Fourier Series by by the DFT is not without its pitfalls and hazards. A distortion due

to aliasing occurs in the frequency domain for real functions which
are not sampled at sufficiently high rates [62, 63].

In addition to the aliasing error, there is an error due to the
fact that the FFT acts like a bank of filters, each with a sin Nx/sin x
response, where N is the number of samples used (Appendix C). Let B_r
be the r-th Fourier series coefficient of a periodic time function,
$x_T(t) = x(t)$, $0 \leq t \leq T$, then the FFT estimate, A_r, of B_r is given by

$$A_r = \frac{1}{N} \sum_{m=-\infty}^{\infty} B_m e^{j(m - r)\left(\frac{N - 1}{N}\right)\pi} \frac{\sin(m - r)\pi}{\sin(m - r)\frac{\pi}{N}}$$

$$= \sum_{i=-\infty}^{\infty} B_{r+iN} \quad . \quad (3.42)$$

The error in estimating the Fourier transform of a non-periodic
function due to the "sidelobes" of the filter is called leakage [64].
The replacement of x(t) by its periodic version $x_T(t)$, as mentioned in
the previous section, reduces this error to the error introduced by the
harmonic components B_m outside the unambiguous range of A_r. This error
is due to failure to satisfy the Nyquist sampling rate for the function
being analyzed. In the work here, the sampling rate is sufficient to
make this error insignificant.

The DFT and FFT, can be generalized to two dimensions. The two-
dimensional DFT is defined by

$$A_{r,s} = \frac{1}{N^2} \sum_{m=0}^{N-1} \sum_{n=0}^{N-1} X_{m,n} \exp\left(\frac{-2\pi j(rm + sn)}{N}\right) \quad (3.43)$$

where A_{rs} is the coefficient corresponding the r-th harmonic in one
dimension and the s-th harmonic in the other dimension, and x_{mn} is the
m-th by n-th sample of x. In this case there are N samples in each

dimension of x and A. Just as in the one dimensional case, A_{rs} and x_{mn} can be defined so that they are periodic functions, but in each dimension, i.e.,

$$A_{r,s} = A_{r,s+N} = A_{r+N,s} = A_{r+N,s+N} \cdots$$

$$x_{m,n} = x_{m,n+N} = x_{m+N,n} = x_{m+N,n+N} \cdots \quad .$$

The inverse transform is defined by

$$x_{m,n} = \sum_{r=0}^{N-1} \sum_{s=0}^{N-1} A_{r,s} \exp\left(\frac{2\pi j(rm + sn)}{N}\right) \quad . \quad (3.44)$$

The two-dimensional FFT is used to obtain the coefficients necessary to compute the moments and covariances in (3.37), (3.38), and (3.39). The characteristic function is computed directly by assuming that θ and φ are jointly Gaussian random processes.

3.3.3 Practical Limitations

A slight regression is in order at this point to aid in visualization of the problems encountered in actually implementing these equations. Equations (3.37), (3.38), and (3.39) represent a rather significant problem in terms of the capacity of a computer, i.e., in terms of memory capacity and number of operations required. By proper choice of the origin, the characteristic function can be made a real function. The coefficients of the two dimensional transform, however, are generally complex functions. If $N = 128$, then there are 16,384 real numbers required for the characteristic function and equally as many complex numbers required for the A in (3.37). In terms of memory requirements, the characterisitic function requires $16,384_{10} = 40,000_8$ words in memory and the A requires $32,768_{10} =$

$100,000_8$. This represents a significant portion of the resources of even a large scientific computer. Even more significant, however, is the number of operations, or iterations implied by the multiple sums.

Assume that (3.37), (3.38), and (3.39) are to be implemented as written, which is to say by brute force. Equation (3.37) would require 16,384 iterations, (3.39) would require 268,435,456, and (3.38) would require $(16,384)^r$ where r is the moment desired. If each iteration required 1 microsecond (an optimistic estimate), a second moment would require about 268 seconds, clearly an unreasonable length of time for one number. It is possible, however, to significantly reduce this time, but higher order moments are clearly beyond consideration using this approach.

It is shown in Appendix C, that for the data used here, the size of the arrays required for the Fourier coefficients can be reduced by a factor of approximately 4. This means that the number of iterations required for (3.37) is also reduced by a factor of about 4. The reductions are more significant for (3.39). The four-dimensional characteristic function requires only about 1/16 of the original memory requirements and only about 1/16 as many iterations are required. Further reductions in computation time are possible due to the rate at which the characteristic function converges toward zero.

The third and fourth central moments are also desired to characterize the probability density functions. These are more appropriately calculated using numerical integration techniques. Use of numerical integration provides the moments by using only N^2 iterations. For rectangular (Euler) integration, the moments are computed by

$$E\left\{S^r\right\} = \sum_{m=0}^{N-1} \sum_{n=0}^{N-1} S^r(m\Delta\theta, n\Delta\phi) \ f_{\theta,\phi}(m\Delta\theta, n\Delta\phi) \ \Delta\theta \ \Delta\phi \quad (3.45)$$

where

$$\Delta\theta = \frac{2M\sigma_\theta}{N}$$

and

$$\Delta\phi = \frac{2M\sigma_\phi}{N} \qquad ,$$

and where the coordinates have been shifted appropriately. The first two moments computed using rectangular integration have been compared with those computed using (3.36) and (3.38) with excellent results.

3.3.4 The Computation of the Statistics

The previous sections of this chapter have developed the techniques for the computation of the statistical characteristics when the aspect angles are jointly Gaussian random processes and the scattering parameters are known. These techniques will now be applied to the scattering model developed in Chapter 2.

The application to the moments and the covariance of the radar cross section, S, has already been discussed in Section 3.3.1. The azimuth and elevation errors given in (2.5), (2.6), and (2.13) will now be discussed. Consider (2.5), (2.6), and (2.13). The azimuth and elevation errors, AZER and ELER, are obtained by dividing the nonradial components of power by the radial component of power. This means that the correlation or covariance between RCS and AZER or RCS and ELER will, in general, be small since AZER and ELER are bipolar functions with small means. In fact

$$E\left\{S \times AZER\right\} = E\left\{\sum_{i=1}^{M} \sum_{j=1}^{M} \sqrt{S_i S_j} \ f_{2i} \cos\left(\alpha_i - \alpha_j\right)\right\} \quad (3.46)$$

$$E\left\{S \times ELER\right\} = E\left\{\sum_{i=1}^{M} \sum_{j=1}^{M} \sqrt{S_i S_j} \; f_{1i} \; \cos\left(\alpha_i - \alpha_j\right)\right\} \quad .(3.47)$$

Therefore, more meaningful variables are the nonradial components of normalized power instead of AZER and ELER, i.e., the numerators of (2.5) and (2.6), namely

$$\epsilon_1 \triangleq \sum_{i=1}^{M} \sum_{j=1}^{M} \sqrt{S_i S_j} \; f_{1i} \; \cos\left(\alpha_i - \alpha_j\right) = S \times ELER \qquad (3.48)$$

$$\epsilon_2 \triangleq \sum_{i=1}^{M} \sum_{j=1}^{M} \sqrt{S_i S_j} \; f_{2i} \; \cos\left(\alpha_i - \alpha_j\right) = S \times AZER \quad . \qquad (3.49)$$

The statistics of these two functions and S have been computed for a number of different conditions. Sample points on a straight and level flight were selected and combinations of the variances and time constants of the Euler angles were used to examine the moments and time constants of these scattering parameters.

Figures 3.2, 3.3, and 3.4 are computer plots of S, ϵ_1, and ϵ_2, respectively, for the region of the θ - φ plane for $1.5677 \leq \theta \leq 1.7317$ and $-0.28241 \leq \varphi \leq -0.12131$. These data represent a region of $\pm 4\sigma$ from the mean in each direction for $\bar{\theta} = 1.6497$, $\bar{\varphi} = -0.20186$, $\sigma_\theta = 0.02050$, and $\sigma_\varphi = 0.02014$. If the variances are reduced by 1/4 these data represent a region of $\pm 8\sigma$. Table 3.1 contains the moments of the scattering parameters, S, ϵ_1, and ϵ_2 for the two different conditions. It is clear that the moments of these scattering parameters are highly sensitive to the statistics of the aspect angles.

Chapter 4 presents data from a number of sample points on the flight path with different sets of conditions on the Euler angles. The results of the analytic solutions are compared with the results of simulation to verify the techniques derived in this chapter.

58
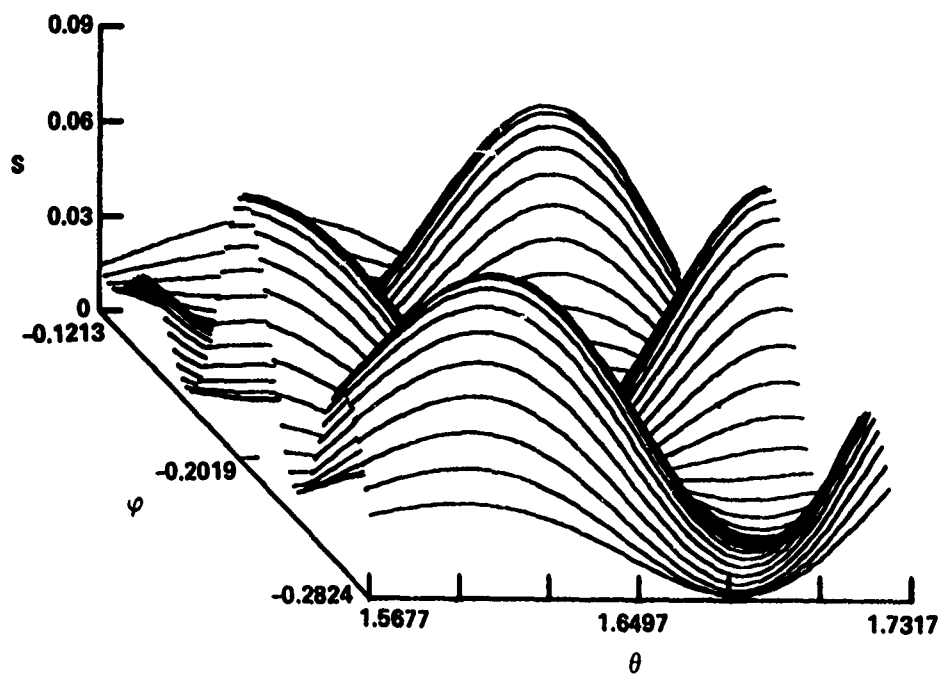
Figure 3.2. The Radar Cross Section, S, Versus the Aspect Angles
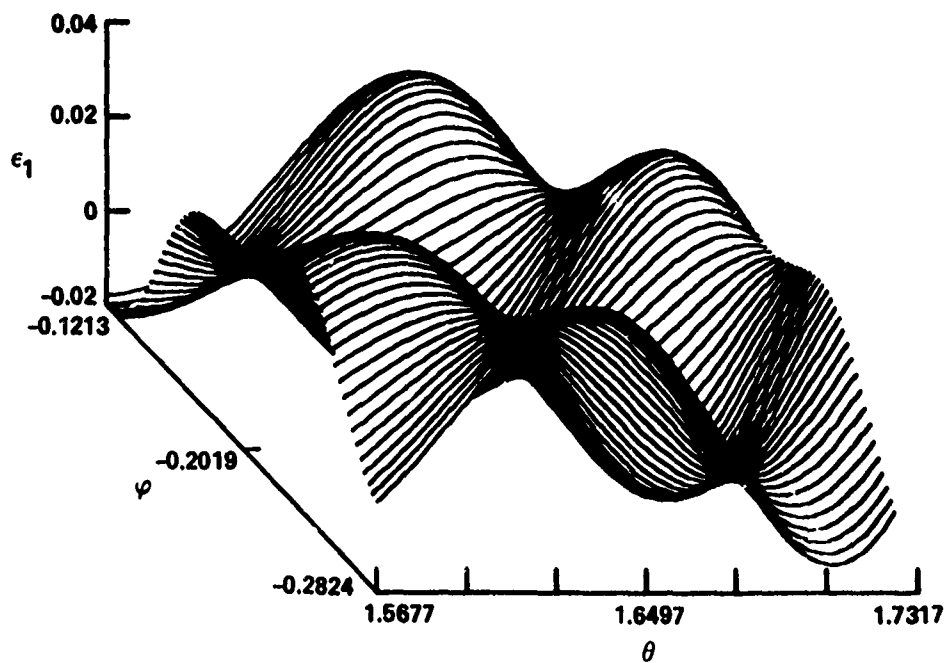
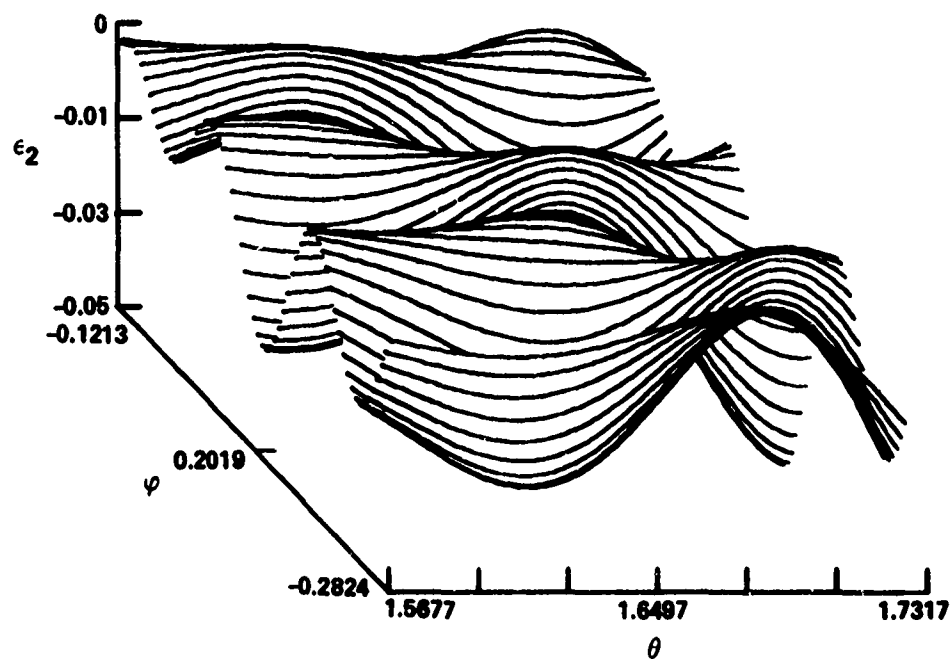Figure 3.3. Scattering Parameter ϵ_1 Versus the Aspect Angles

Figure 3.4.   Scattering Parameter ϵ_2 Versus the Aspect Angles

Table 3.1

Moments of the Scattering Parameters

Scattering Parameter	Run No.	σ_θ	σ_φ	Mean	Variance	Third Central Moment	Fourth Central Moment
S	1	0.0204963	0.020137	1.641×10^{-2}	2.334×10^{-4}	6.004×10^{-5}	3.273×10^{-7}
	2	0.0102482	0.0100685	9.537×10^{-3}	4.668×10^{-5}	4.598×10^{-7}	1.27×10^{-8}
ϵ_1	1	0.0204963	0.020137	-2.899×10^{-3}	1.460×10^{-4}	1.464×10^{-5}	7.38×10^{-8}
	2	0.0102482	0.0100685	-6.666×10^{-3}	4.077×10^{-5}	6.17×10^{-8}	6.5×10^{-9}
ϵ_2	1	0.0204963	0.020137	-8.746×10^{-3}	6.346×10^{-5}	-8.182×10^{-7}	2.48×10^{-8}
	2	0.0102482	0.0100685	-6.674×10^{-2}	1.548×10^{-5}	-4.14×10^{-8}	9.0×10^{-10}

4. COMPARISON OF ANALYTIC SOLUTIONS AND SIMULATIONS

4.1 General

A straight and level incoming flight path with a small crossing angle was selected as being typical of the conditions of interest. Three sample points on this flight path were selected at which computations of the statistics of the scattering parameters were to be calculated. Figure 4.1 depicts the flight path and the sample points. The coordinates of the three sample points are (30, 10, and 2.5 km), (20, 4.238, and 2.5 km), and (10, -1.524, and 2.5 km). In order to investigate the sensitivity of the scattering parameters to the aspect angle statistics, three different combinations of Euler angle statistics were applied at each sample point, and the resulting aspect angle statistics were computed analytically and by simulation.

Table 4.1 contains the data on the resulting aspect angle statistics used for each run. Figures 4.2 through 4.10 show the scattering parameters for each of the three sample points as functions of the aspect angles. The limits on θ and φ are $\pm 4\sigma$ for the largest values of σ_θ and σ_φ at each sample point. Figures 4.2 through 4.4 represent S, ϵ_1, and ϵ_2 at sample point 1; Figures 4.5 through 4.7 represent S, ϵ_1, and ϵ_2 at sample point 2; and Figures 4.8 through 4.10 represent S, ϵ_1, and ϵ_2 at sample point 3.

4.2 Simulation Results

A simulation program has been written which performs a Monte Carlo simulation of the time history of the EM scattering. The simulation

uses the same assumptions and models that are used in the analytic

solutions, except that the angular transformation is not linearized

about the mean aspect angles. The simulation is fairly general in

that the flight path, velocity, random motion statistics, and sampling

interval are input variables. The output data are 2048 time samples,

taken at 50-millisecond intervals, of each of the scattering parameters

and their statistics. The aspect angles statistics are also available

as output data. The simulation permits an investigation of many

characteristics not conducive to analytic solution. For example,

by changing the velocity it is possible to investigate the limits the

flight path and flight characteristics place on the assumptions used in

Chapter 3 regarding the wide-sense stationarity of the aspect angles.

Figures 4.11 through 4.19 are the outputs of the simulation for

run 6. Figures 4.11 through 4.13 represent S, ϵ_1, and ϵ_2; Figures 4.14

through 4.16 represent the autocovariances of S, ϵ_1, and ϵ_2; and

Figures 4.17 through 4.19 represent the cross-covariances of S and ϵ_1,

S and ϵ_2, and ϵ_1 and ϵ_2.

4.3 Data Comparison

The statistics of the scattering parameters have been computed

analytically and from simulations for each of the runs defined in

Table 4.1. The means and variances of the aspect angles are given for

the linearized solutions and the simulations to indicate the general

level of errors encountered. Tables 4.2, 4.3, and 4.4 compare the

statistics of the scattering parameters for the nine runs actually

made. Figures 4.20 through 4.37 compare the covariance functions for

runs 1, 6, and 9.

It is clear from the data that the statistics of the scattering parameters are very sensitive to the statistics of the aspect angles. Some of the differences between the analytic results and simulations can be explained by the apparently small differences in the means and variances of the aspect angles. More important than the differences are the similarities between the sets of data. It indicates that the general approach will permit the analytic determination of the statistics of the scattering parameters with some degree of accuracy.

The sensitivity of the scattering parameters to the statistics of the aspect angles emphasizes the need for actual data on the flight characteristics of aircraft. This may become even more important when higher frequencies are used since the lobing structure of the scattering parameters increases with increasing frequency.
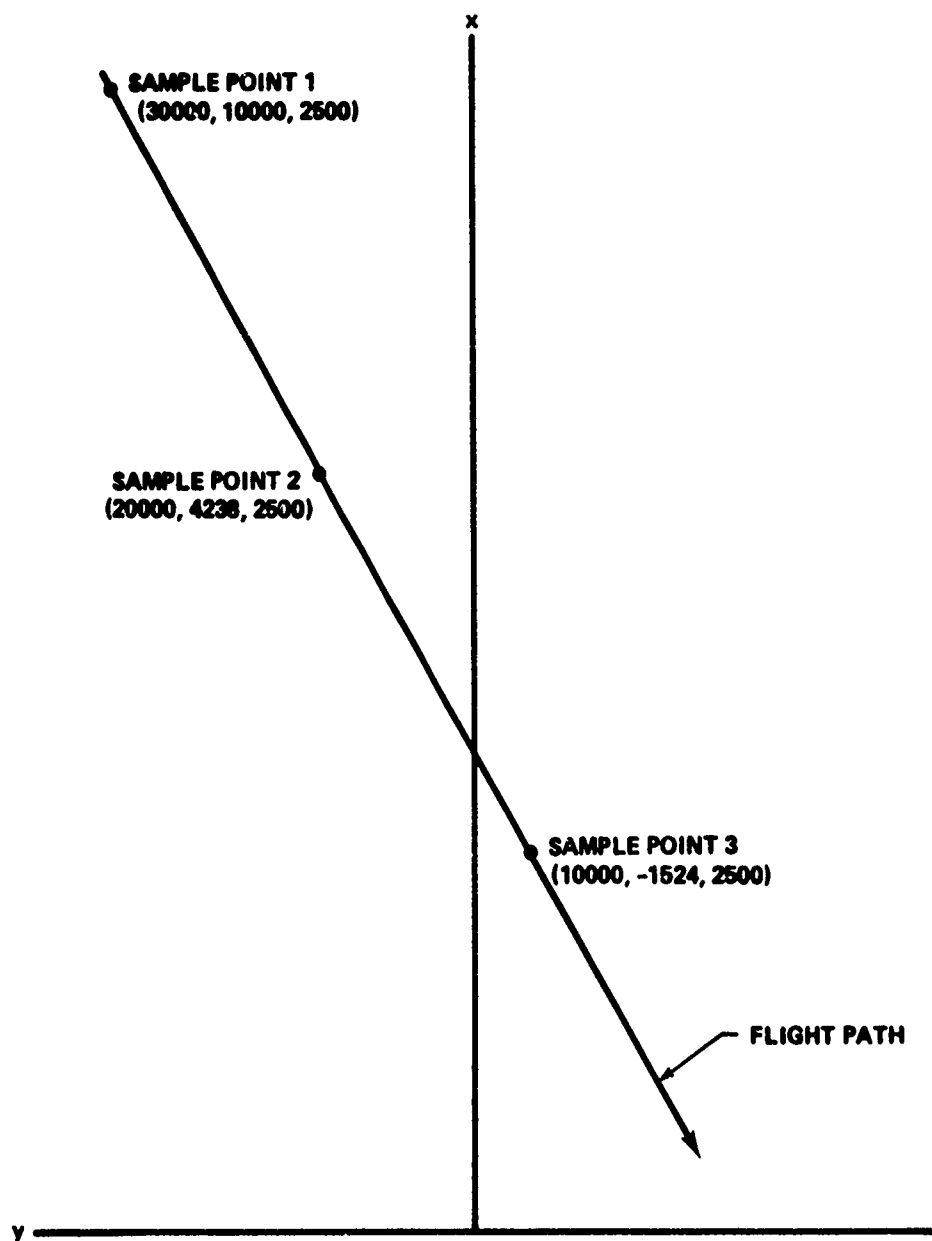
Figure 4.1. Target Flight Path in the Ground Fixed
Coordinate System

Table 4.1

Comparison of Aspect Angle Statistics

Sample Point No.	Run No.	$\sigma_\alpha = \sigma_\beta$ (radians)	σ_γ (radians)	$\tau_\alpha = \tau_\beta$ (sec)	τ_γ (sec)	Analytic Solutions				Simulations			
						θ_0	φ_0	σ_θ	σ_φ	$\bar{\theta}$	$\bar{\varphi}$	σ_θ	σ_φ
1	1	0.02	0.03	5.0	2.5	1.64967	-0.20186	0.020495	0.020137	1.64980	-0.20002	0.023652	0.021236
	2	0.01	0.015	5.0	2.5	1.64967	-0.20186	0.010248	0.010069	1.64967	-0.20115	0.011820	0.010630
	3	0.02	0.1	2.5	1.0	1.64967	-0.20186	0.028034	0.021450	1.64824	-0.2001	0.029953	0.022350
2	4	0.02	0.03	5.0	2.5	1.69248	-0.31480	0.021164	0.020316	1.69246	-0.31379	0.022863	0.020675
	5	0.02	0.1	2.5	1.0	1.69248	-0.31480	0.036336	0.023147	1.68985	-0.31299	0.036645	0.023873
	6	0.01	0.04	5.0	2.5	1.69248	-0.31480	0.015614	0.011035	1.69140	-0.31453	0.015103	0.035085
3	7	0.01	0.04	5.0	2.5	1.81309	-0.674848	0.026182	0.012727	1.81020	-0.67490	0.023216	0.012758
	8	0.02	0.03	5.0	2.5	1.81309	-0.674848	0.024396	0.021049	1.81153	-0.67429	0.02384	0.021966
	9	0.02	0.1	2.5	1.0	1.81309	-0.674848	0.064400	0.027963	1.80723	-0.67295	0.060154	0.028261
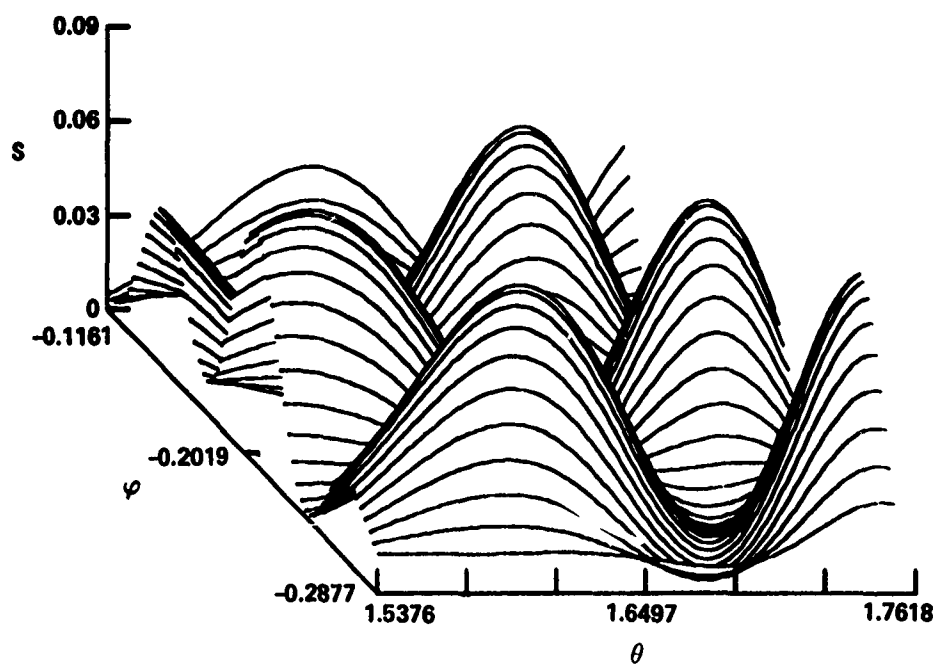
Figure 4.2. The Radar Cross Section, S, at Sample Point 1
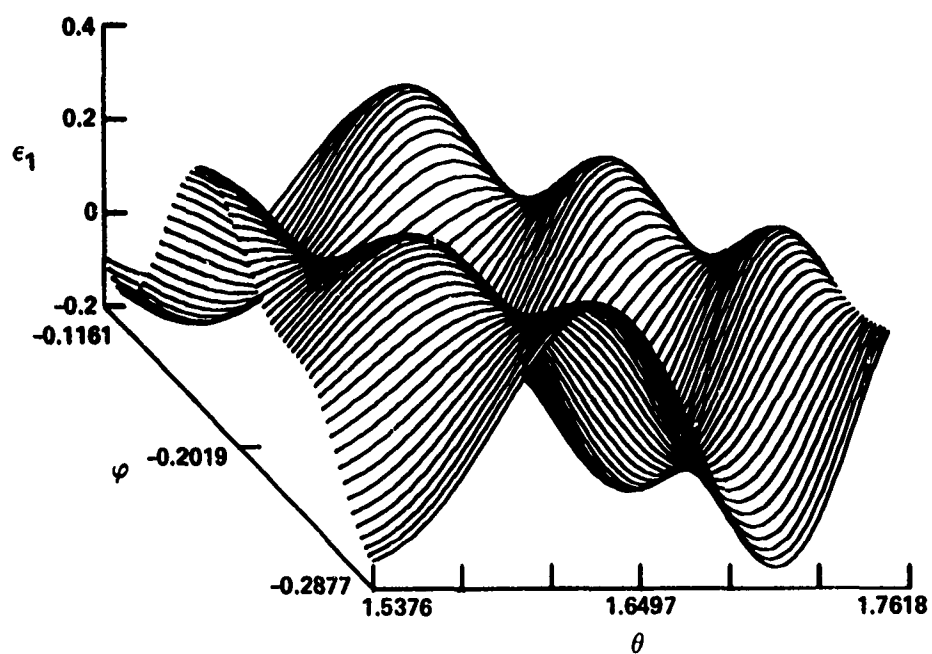
Figure 4.3. Elevation Component of Nonradial Power,
ϵ_1, at Sample Point 1
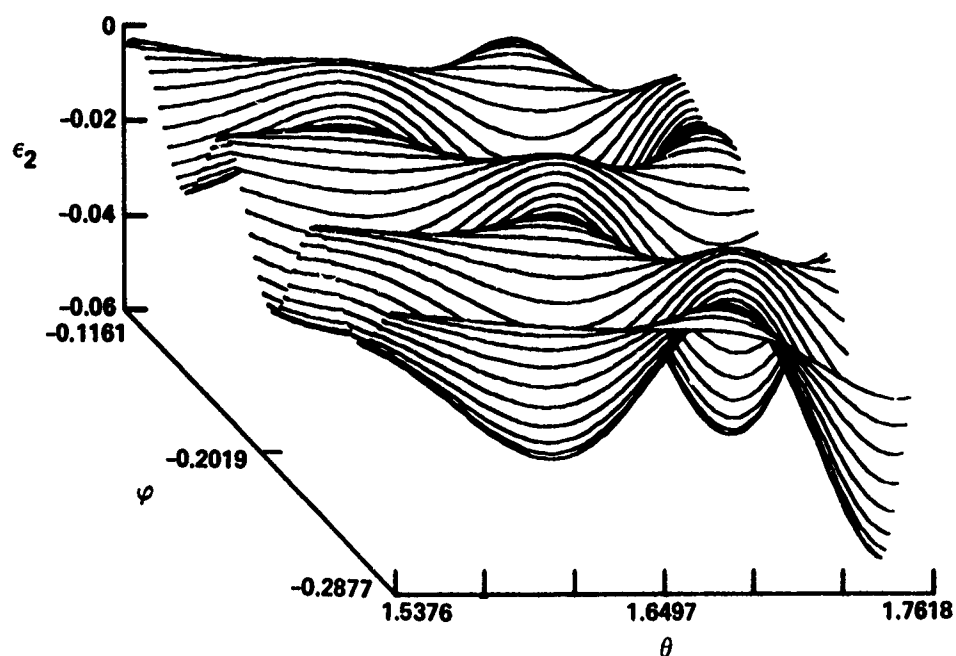
Figure 4.4. Azimuth Component of Nonradial Power, ϵ_2, at Sample Point 1
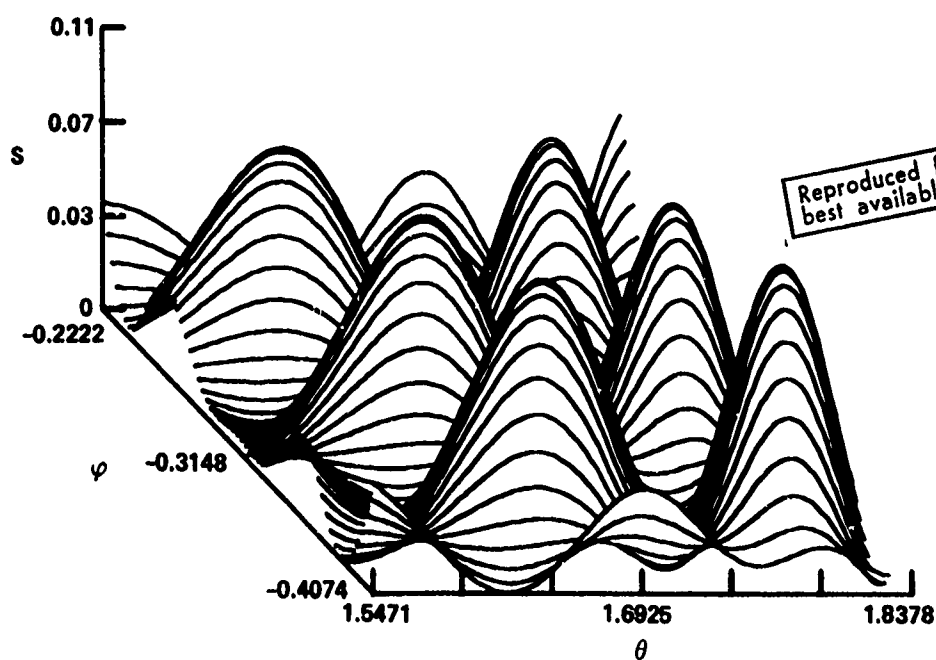
Figure 4.5. The Radar Cross Section, S, at Sample Point 2
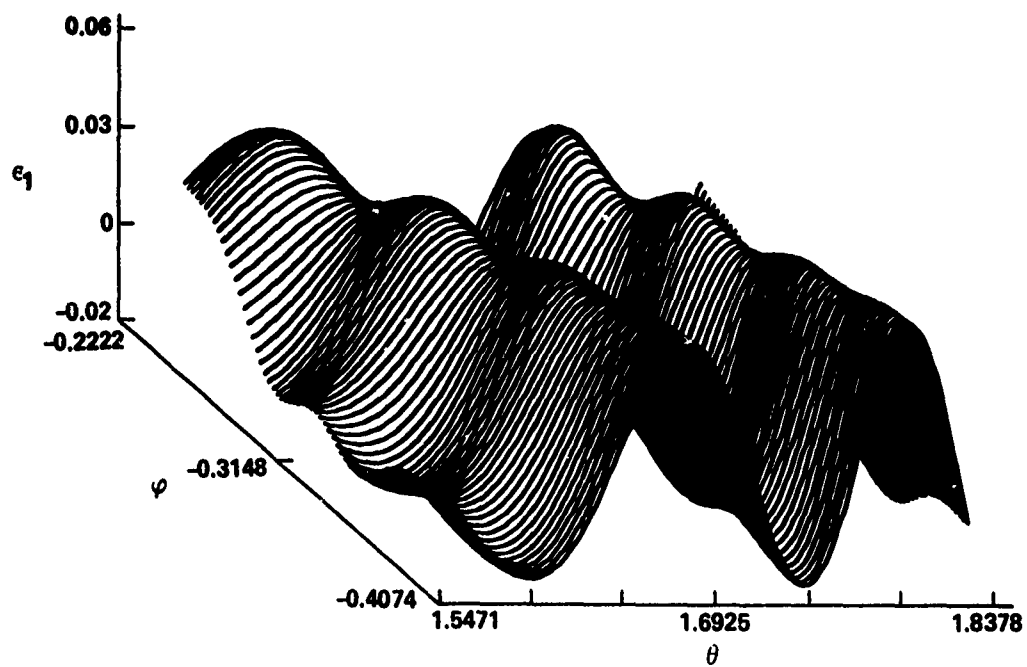
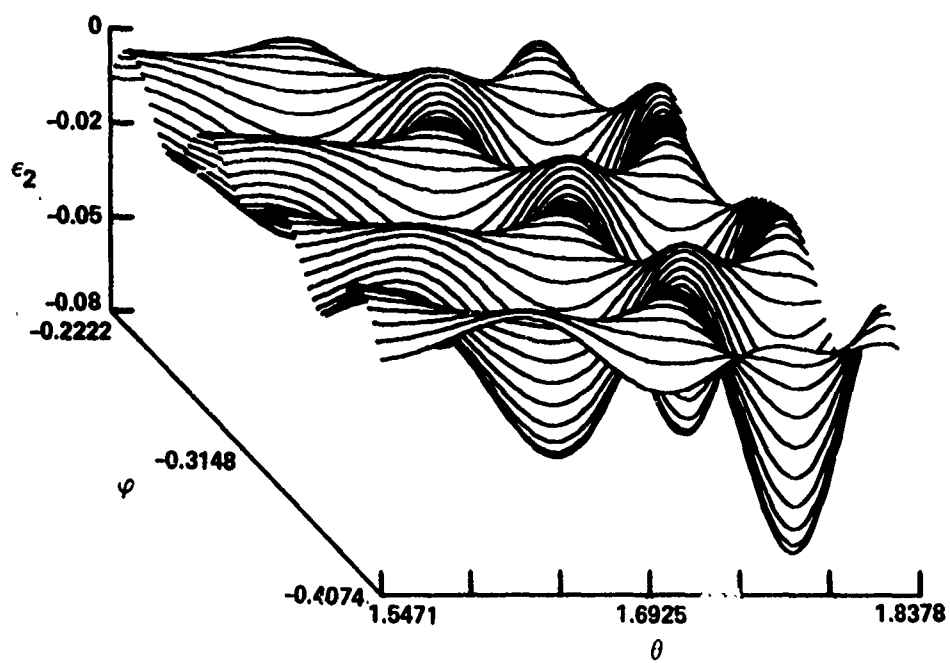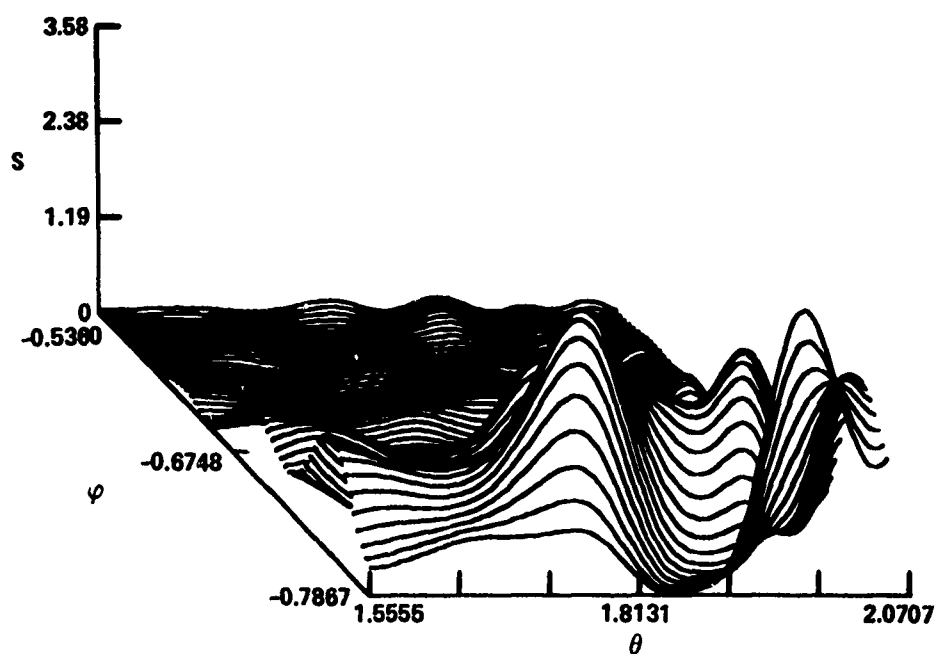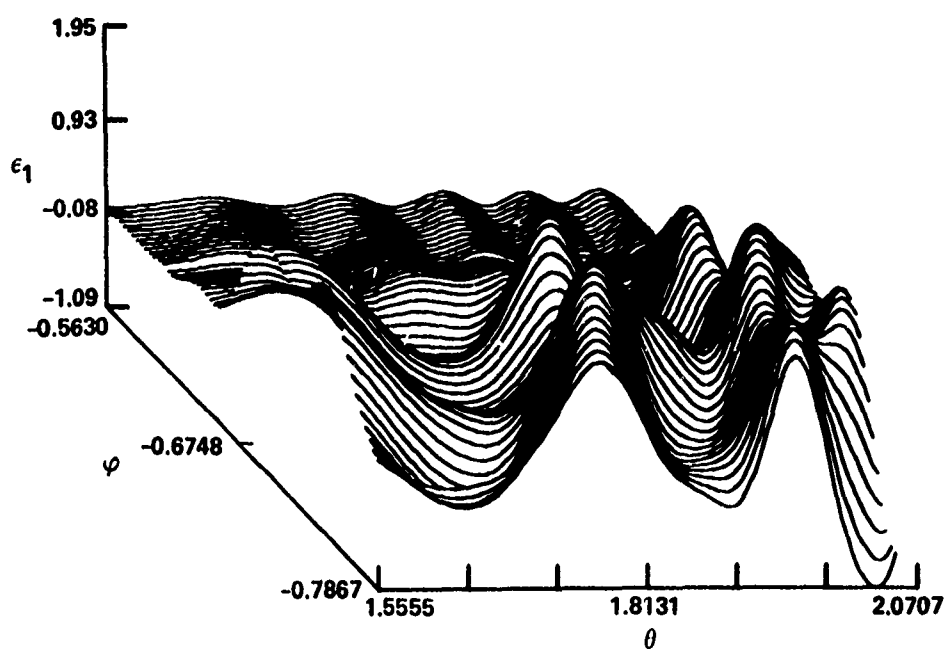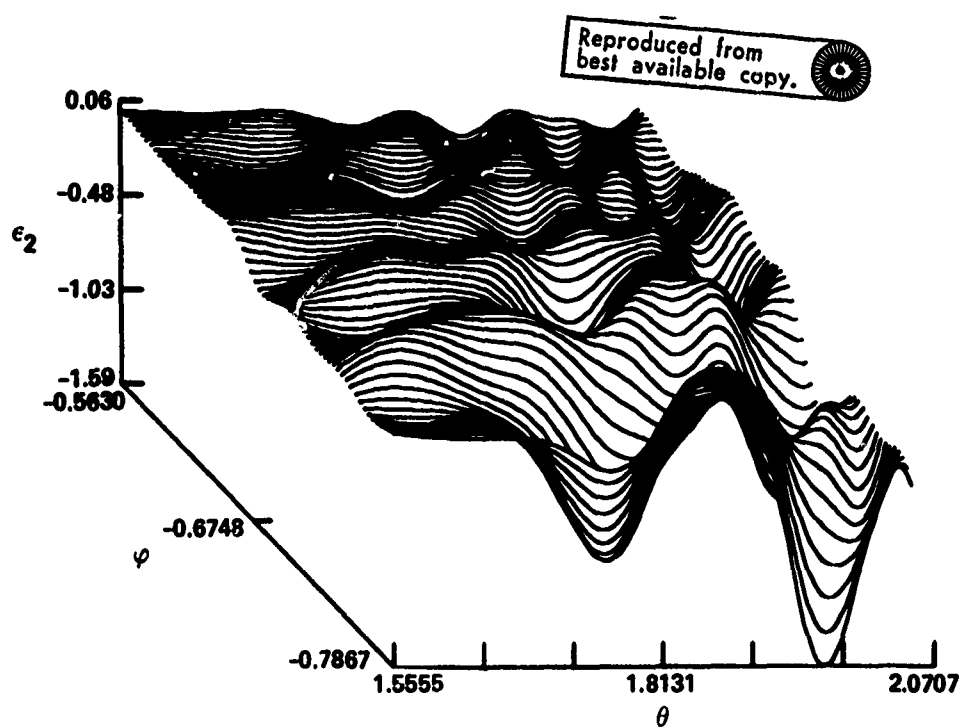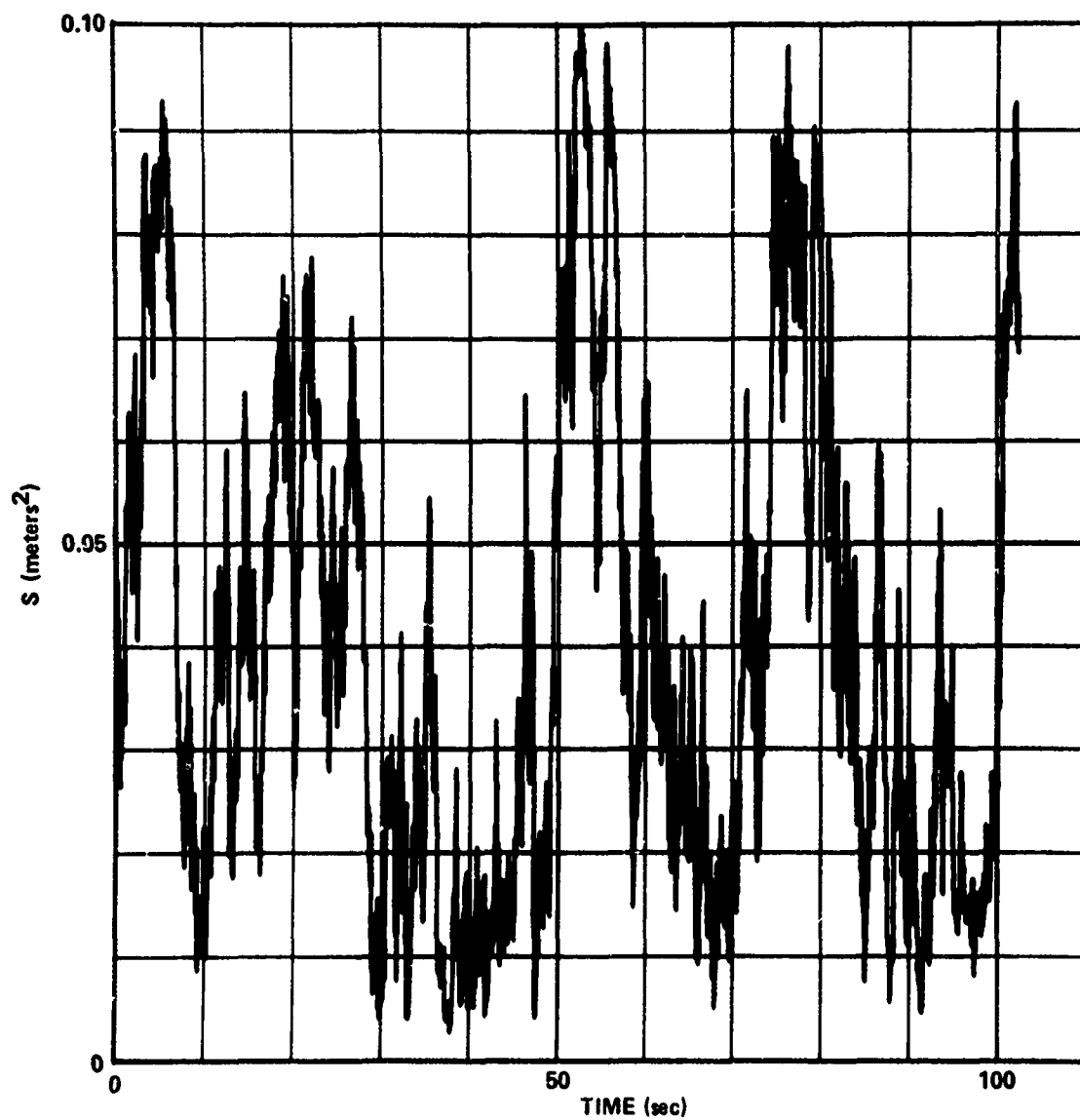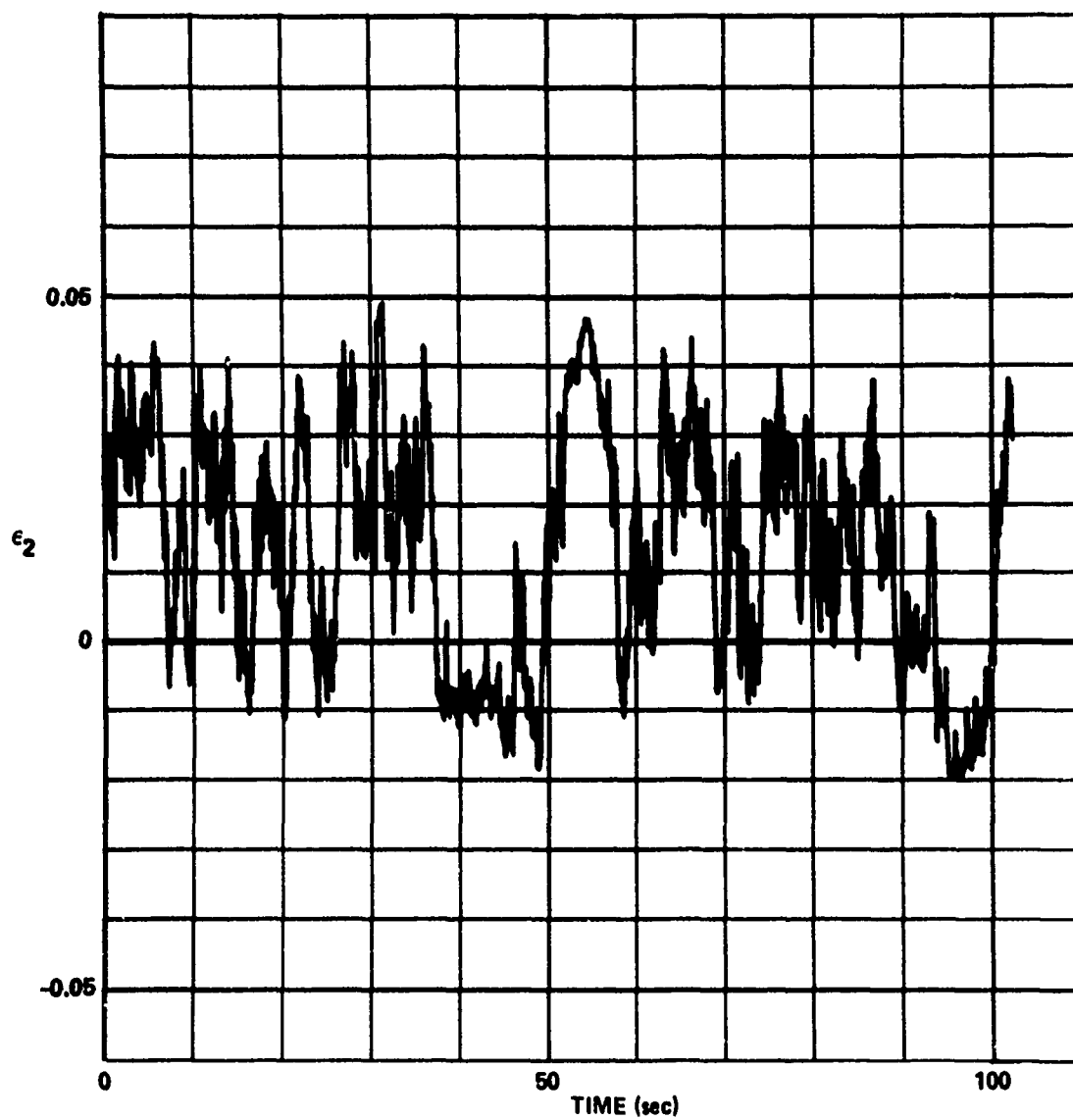Figure 4.6. Elevation Component of Nonradial Power, ϵ_1, at Sample Point 2

Figure 4.7. Azimuth Component of Nonradial Power, ϵ_2, at Sample Point 2

Figure 4.8. The Radar Cross Section, S, at Sample Point 3

Figure 4.9. Elevation Component of Nonradial Power, ϵ_1, at Sample Point 3

Figure 4.10. Azimuth Component of Nonradial Power, ϵ_2 ,
at Sample Point 3

Figure 4.11. Radar Cross Section, S, Versus Time

Figure 4.12. Elevation Component of Nonradial Power,
ϵ_1 Versus Time
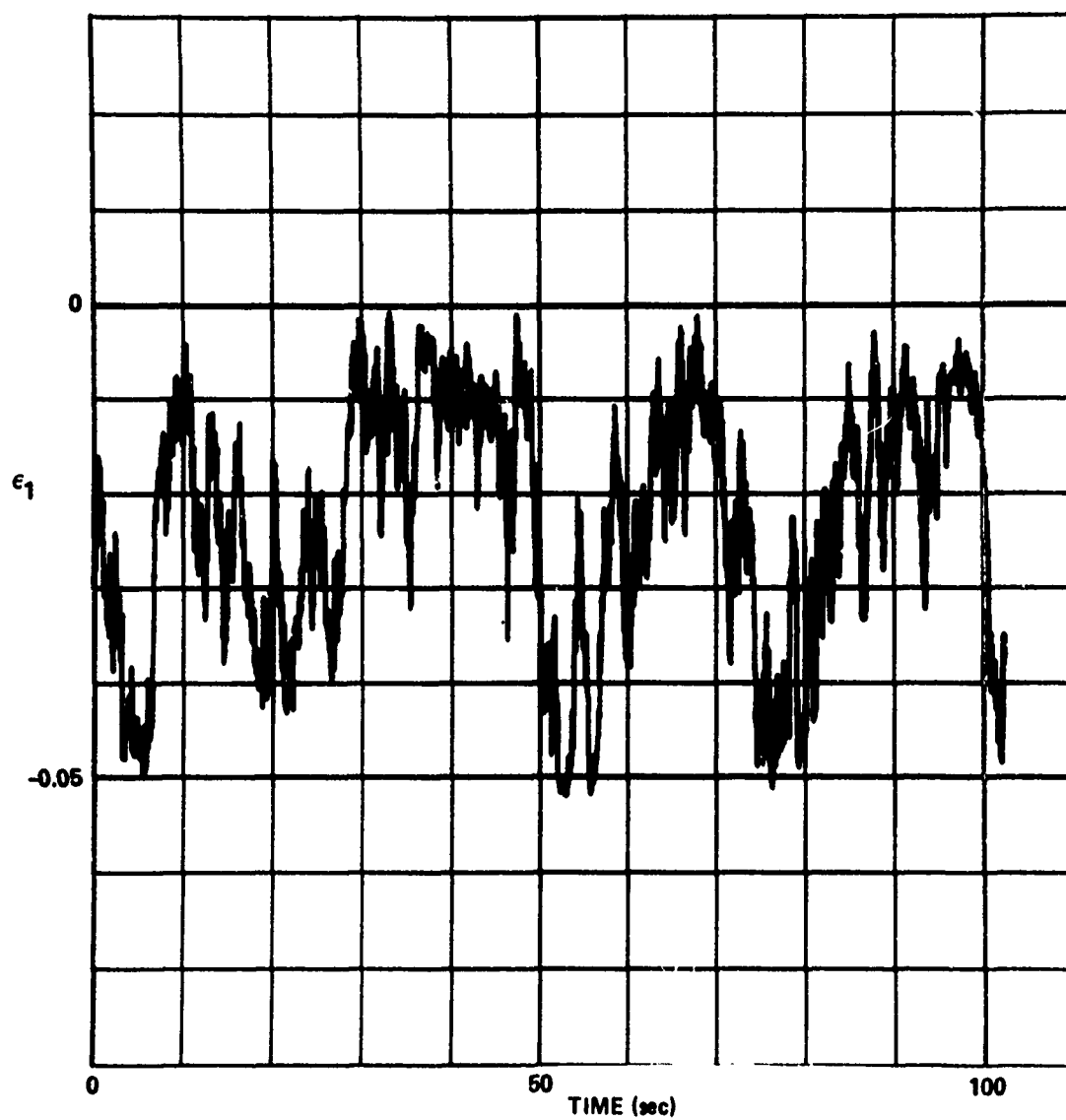
Figure 4.13. Azimuth Component of Nonradial Power, ϵ_2, Versus Time
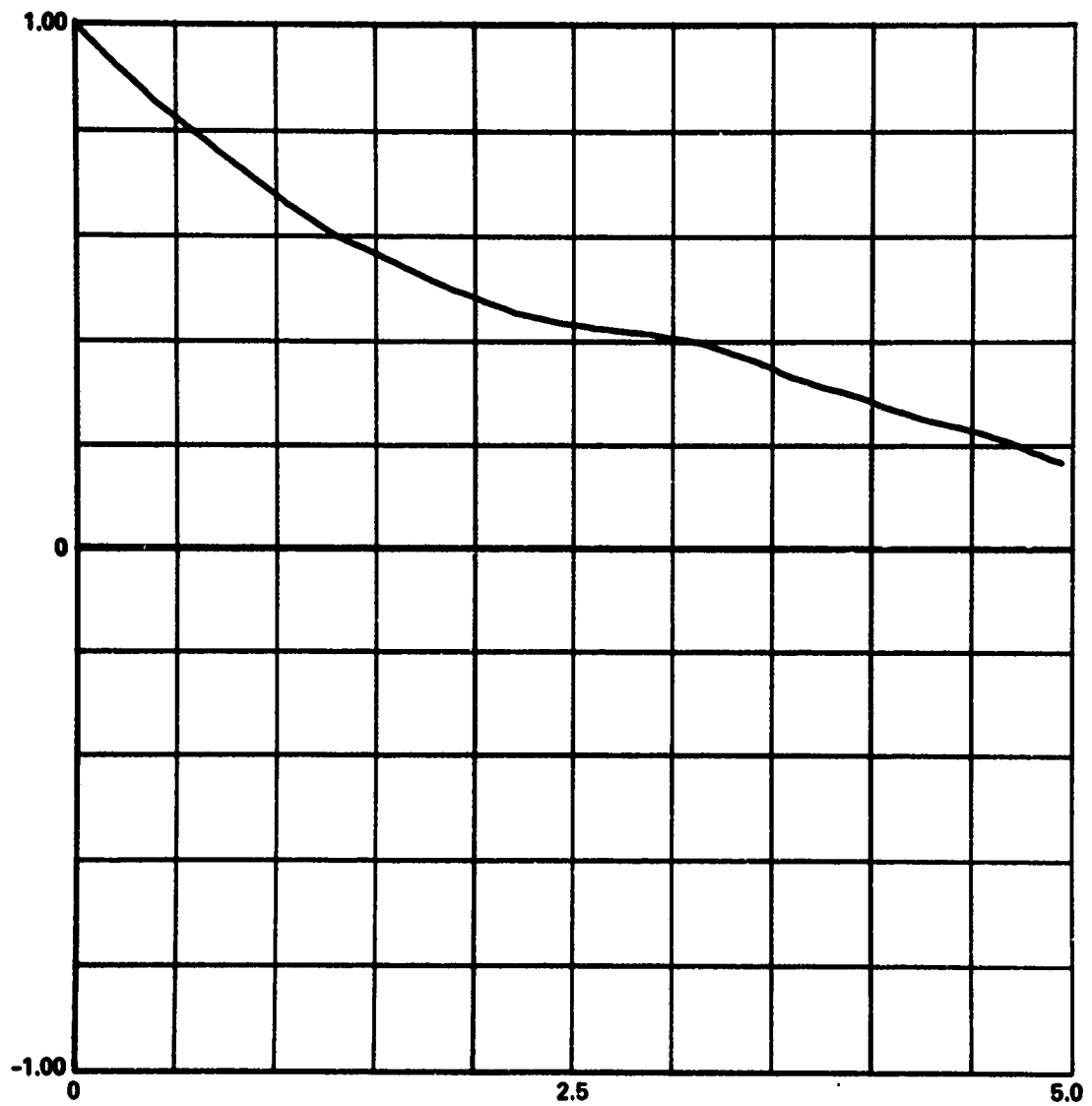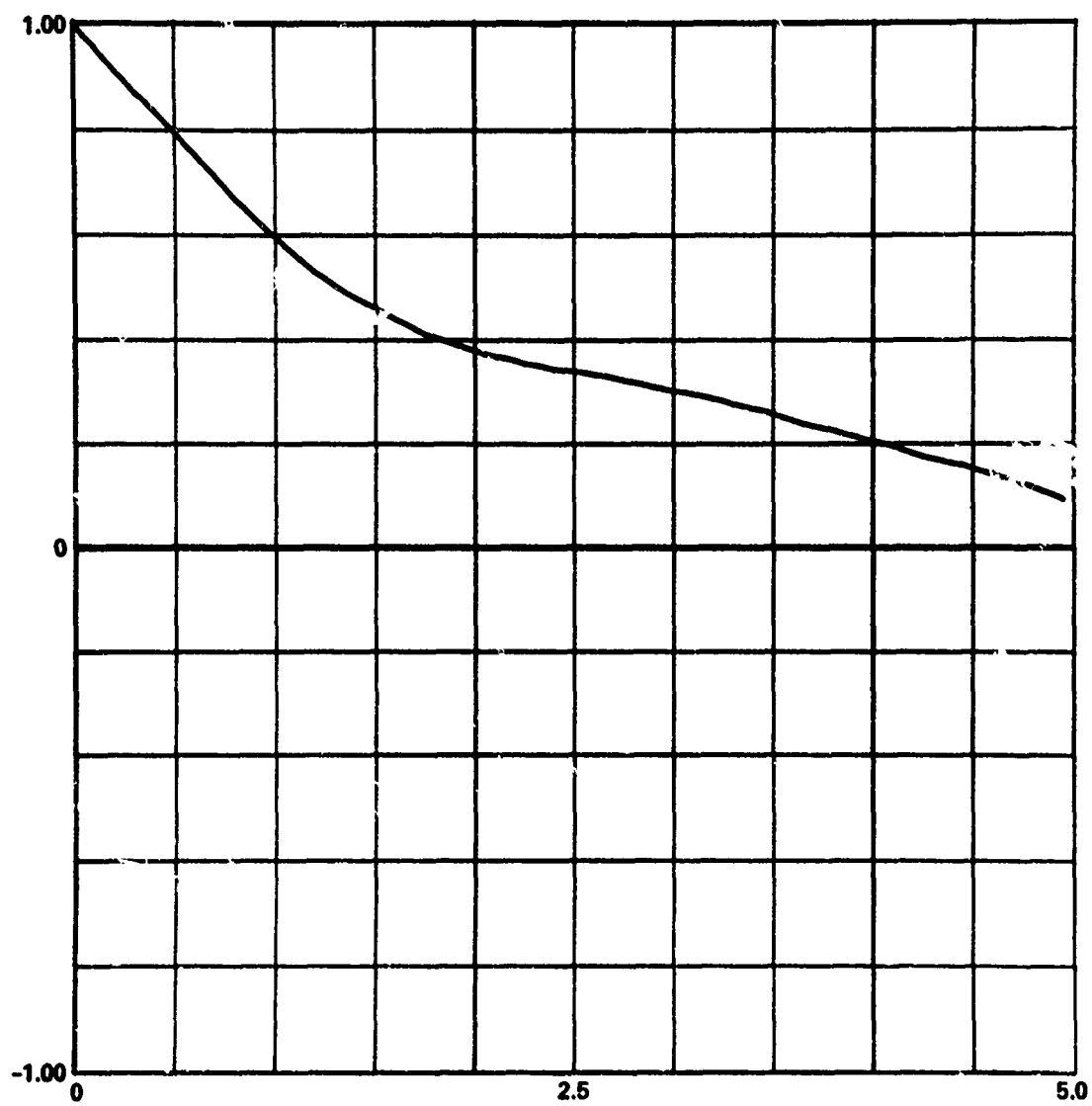
Figure 4.14. Autocovariance of S Versus Delay Time

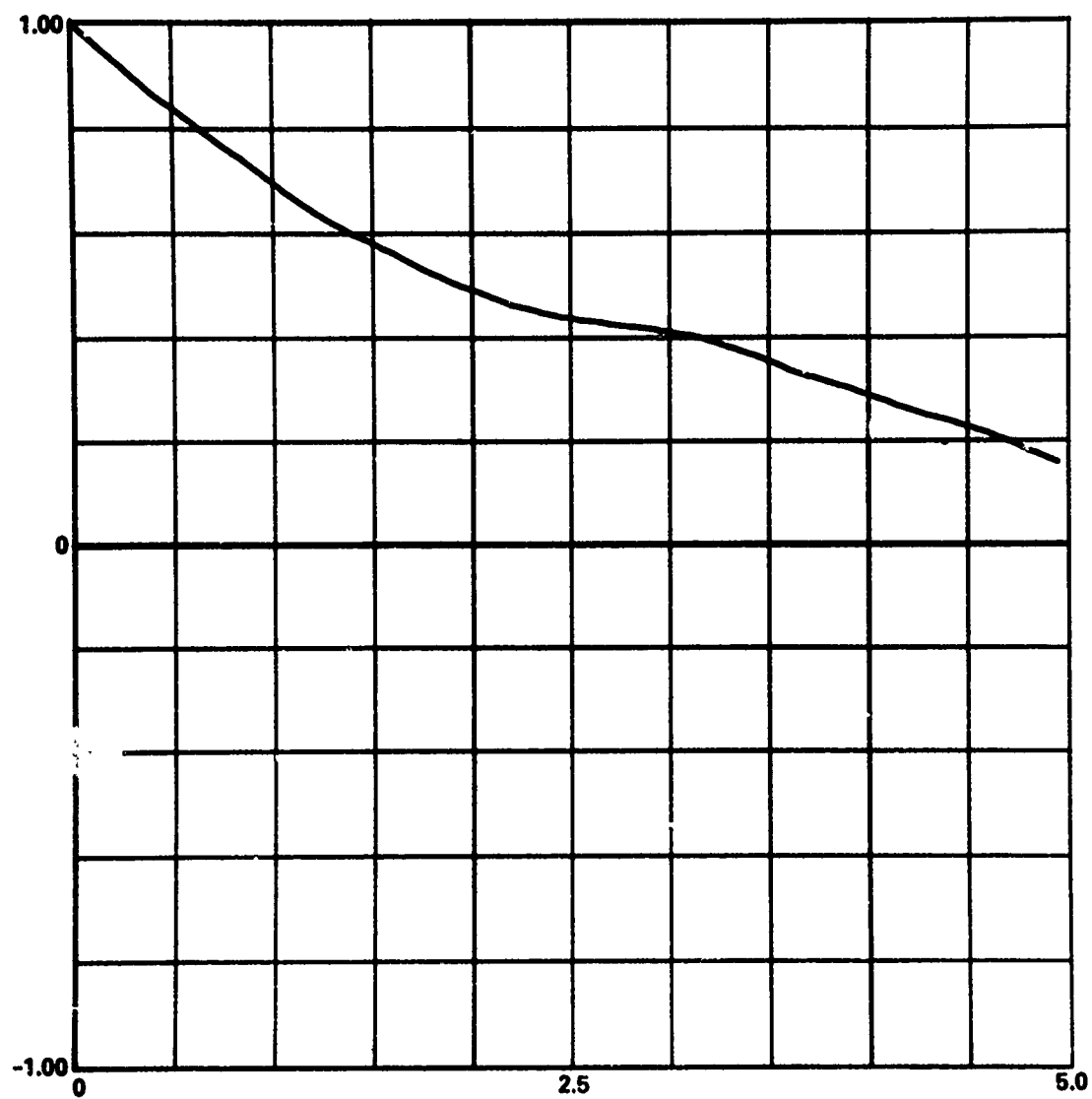Figure 4.15. Autocovariance of ϵ_1 Versus Delay Time

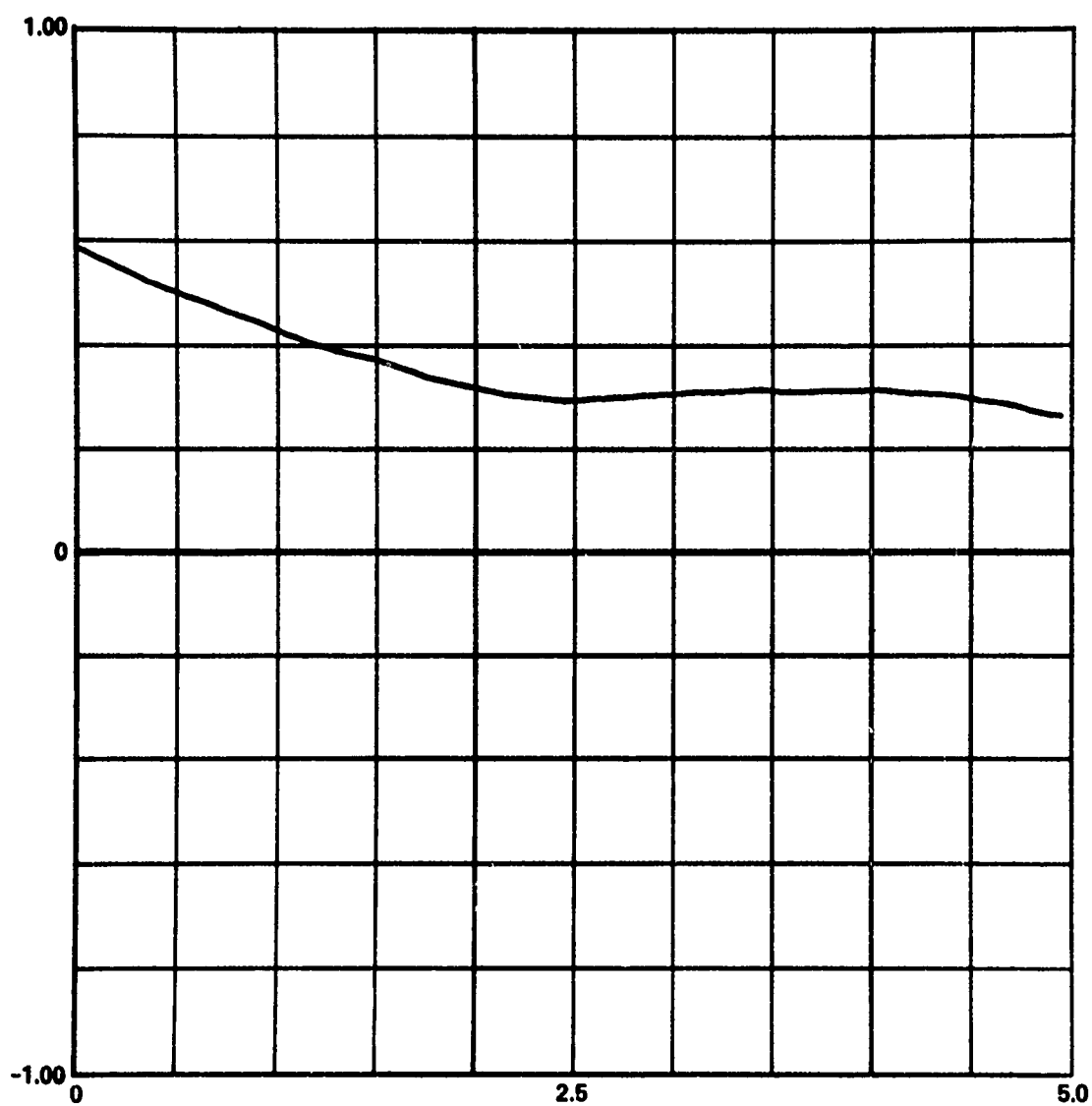Figure 4.16. Autocovariance of ϵ_2 Versus Delay Time

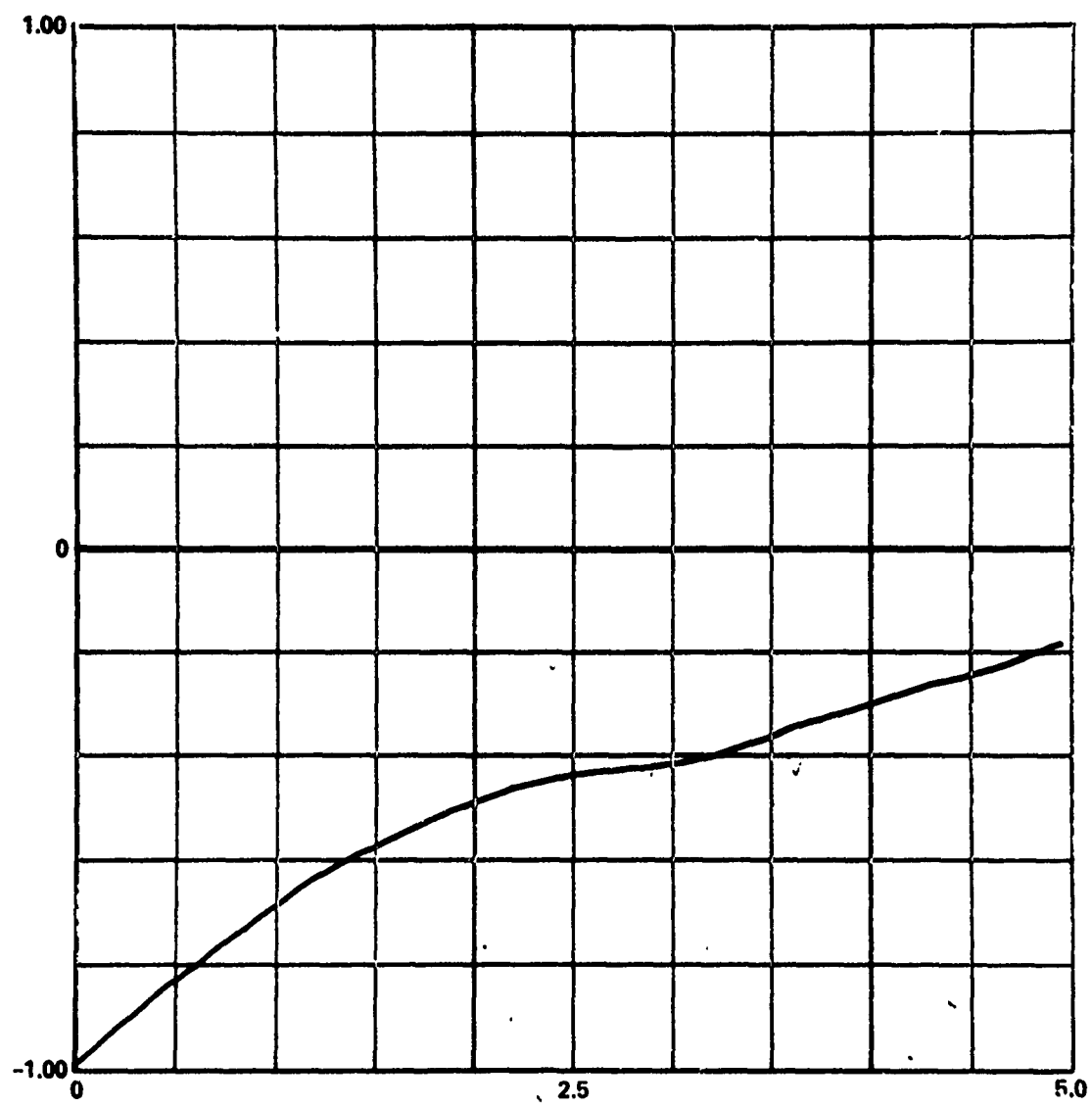Figure 4.17. Crosscovariance of S and ϵ_1 Versus Delay Time

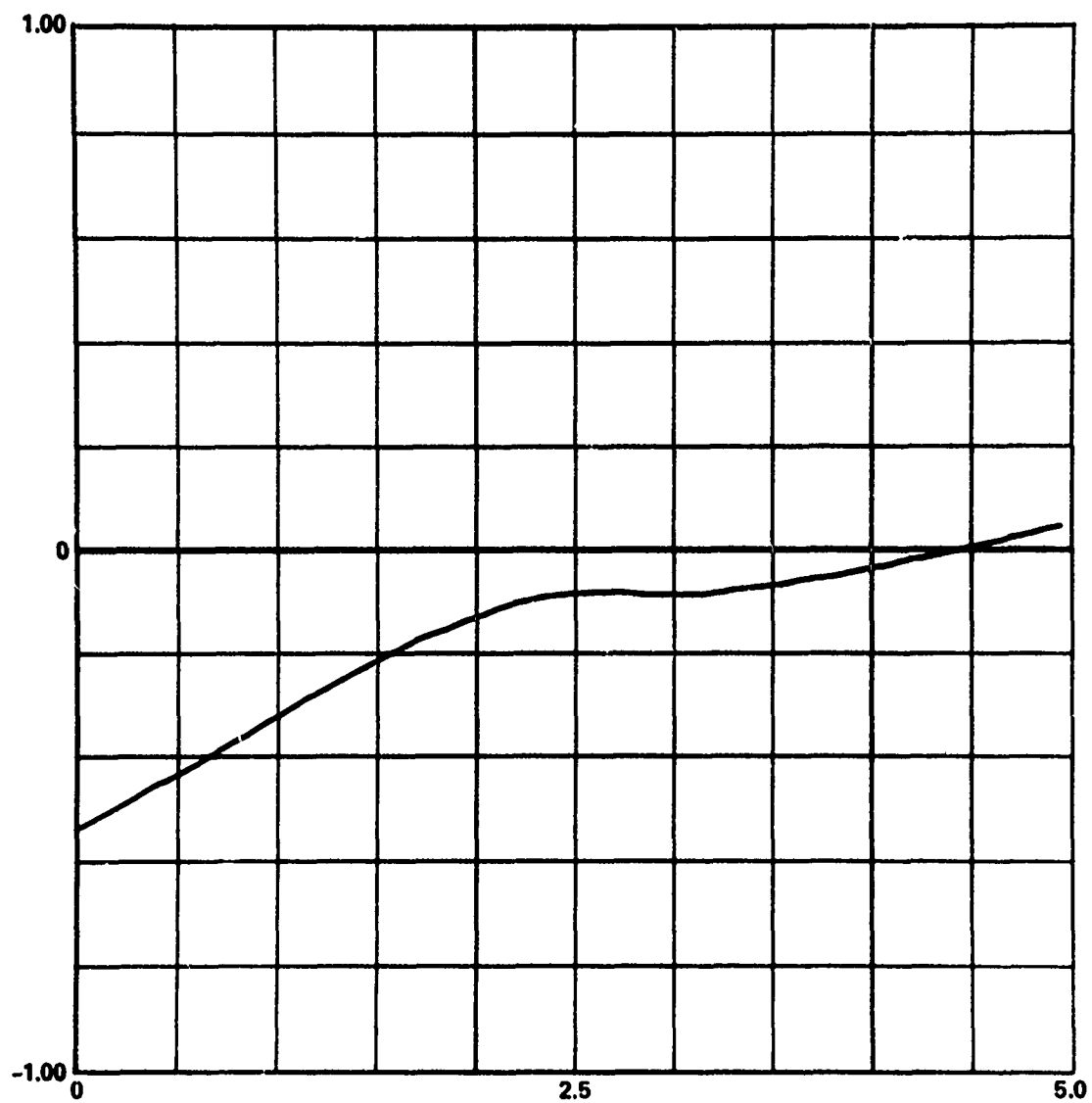Figure 4.18. Crosscovariance of S and ϵ_2 Versus Delay Time

Figure 4.19. Crosscovariance of ϵ_1 and ϵ_2 Versus Delay Time

Table 4.2

Comparison of Statistics of S

Run No.	Analytic Solutions				Simulations			
	$\bar{s}$	σ^2_S	$E\{(s-\bar{s})^3\}$	$E\{(s-\bar{s})^4\}$	$\bar{s}$	σ^2_S	$E\{(s-\bar{s})^3\}$	$E\{(s-\bar{s})^4\}$
1	0.016412	0.0002334	0.00006004	0.0000003273	0.017125	0.0002383	0.00000530	0.0000002755
2	0.009537	0.00004668	0.0000004598	0.0000000127	0.010529	0.00006490	0.0000008695	0.0000000257
3	C.020674	0.00036290	0.0000096023	0.0000005792	0.021348	0.00035559	0.0000082277	0.0000005045
4	0.032749	0.00066696	0.0000137447	0.0000011662	0.027306	0.00056145	0.0000145054	0.0000010688
5	0.034734	0.00076269	0.0000161271	0.0000014223	0.032199	0.00079452	0.000019532	0.0000016402
6	0.038411	0.000546743	0.0000053270	0.0000006828	0.039501	0.000602424	0.0000085751	0.0000008343
7	0.396596	0.133496	0.04995094	0.05565703	0.439472	0.137639	0.033670	0.042143
8	0.465423	0.1935265	0.0784095	0.1013614	0.0542582	0.214844	0.0561858	0.0868845
9	0.350875	0.1383598	0.08025367	0.09521217	0.379367	0.156015	0.0790915	0.0856024

Table 4.3

Comparison of Statistics of ϵ_1

Run No.	Analytic Solutions				Simulations			
	$\bar{\epsilon}_1$	$\sigma^2_{\epsilon_1}$	$E\{(\epsilon_1-\bar{\epsilon}_1)^3\}$	$E\{(\epsilon_1-\bar{\epsilon}_1)^4\}$	$\bar{\epsilon}_1$	$\sigma^2_{\epsilon_1}$	$E\{(\epsilon_1-\bar{\epsilon}_1)^3\}$	$E\{(\epsilon_1-\bar{\epsilon}_1)^4\}$
1	-0.002899	0.0001460	0.00001464	0.0000000738	-0.003002	0.0001429	0.00001740	0.0000000840
2	-0.006666	0.00004077	0.0000000617	0.0000000065	-0.007139	0.0000492156	0.0000001807	0.0000000136
3	0.001944	0.00022519	0.0000019789	0.0000001261	0.00183427	0.00021164	0.0000021430	0.0000001240
4	0.012623	0.00039518	0.0000017082	0.0000002819	0.011444	0.00033034	0.000001186	0.0000001973
5	0.016106	0.00045885	-0.0000000136	0.0000003365	0.016686	0.00044711	-0.0000003346	0.0000003096
6	0.012473	0.000312043	0.0000010321	0.0000001926	0.013345	0.00027981	-0.0000003492	0.0000001548
7	0.487953	0.1493125	0.430148	0.0658982	0.496217	0.158814	0.025233	0.057052
8	0.560294	0.207472	0.06202304	0.100759798	0.614113	0.235021	0.0472224	0.103608
9	0.379846	0.17110128	0.0838016	0.1072965	0.410458	0.2014778	0.0956061	0.1244495

Table 4.4

Comparison of Statistics of ϵ_2

| Run No.	Analytic Solutions				Simulations			
	$\bar{\epsilon}_2$	$\sigma^2_{\epsilon_2}$	$E\{(\epsilon_2-\bar{\epsilon}_2)^3\}$	$E\{(\epsilon_2-\bar{\epsilon}_2)^4\}$	$\bar{\epsilon}_2$	$\sigma^2_{\epsilon_2}$	$E\{(\epsilon_2-\bar{\epsilon}_2)^3\}$	$E\{(\epsilon_2-\bar{\epsilon}_2)^4\}$
1	-0.008746	0.00006346	-0.0000008182	0.0000000248	-0.009156	0.0000609	-0.0000005978	0.0000000166
2	-0.066739	0.000015478	-0.0000000414	0.0000000009	-0.007153	0.000017025	-0.0000000766	0.0000000014
3	-0.010615	0.000099126	-0.000014158	0.0000000482	-0.010961	0.00009915	-0.000001348	0.0000000500
4	-0.018025	0.0002006	-0.0000019877	0.0000000970	-0.015054	0.00016261	-0.0000019248	0.0000000789
5	-0.018655	0.0000023444	-0.0000027613	0.0000001409	-0.017290	0.00023587	-0.0000033349	0.0000001596
6	-0.022183	0.000163065	-0.0000005250	0.0000000560	-0.022745	0.0001710J	-0.0000009602	0.0000000623
7	-0.152579	0.020656	-0.0038344	0.00175901	-0.167468	0.020723	-0.00243582	0.00119589
8	-0.195725	0.0324476	-0.0060155442	0.00321499&44	-0.220511	0.0573493	-0.0049607	0.0029793
9	-0.144943	0.023260	-0.00581941	0.002876394	-0.155008	0.0277703	-0.0065453	0.0030783
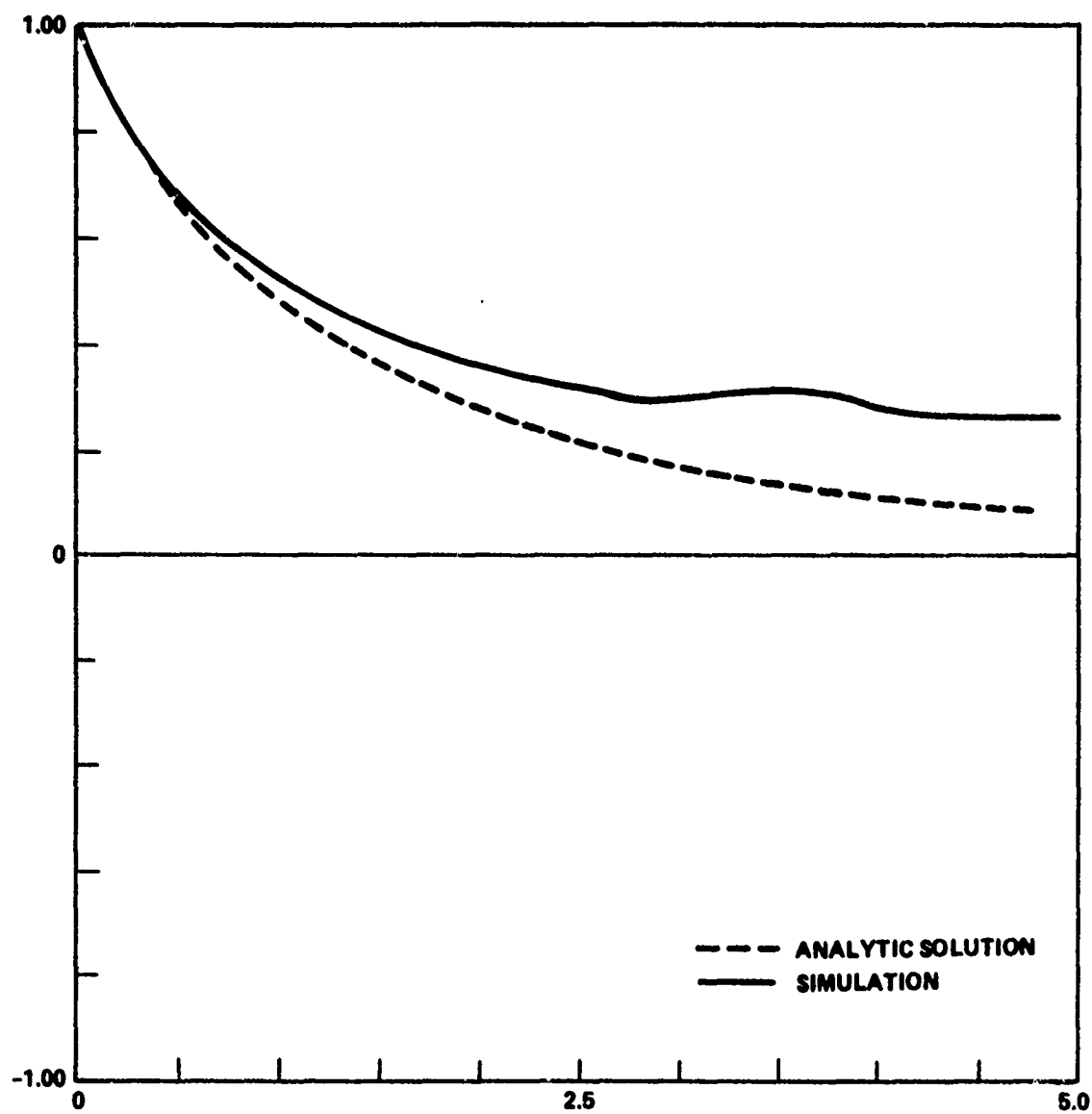
Figure 4.20. Autocovariance of S, Run 1
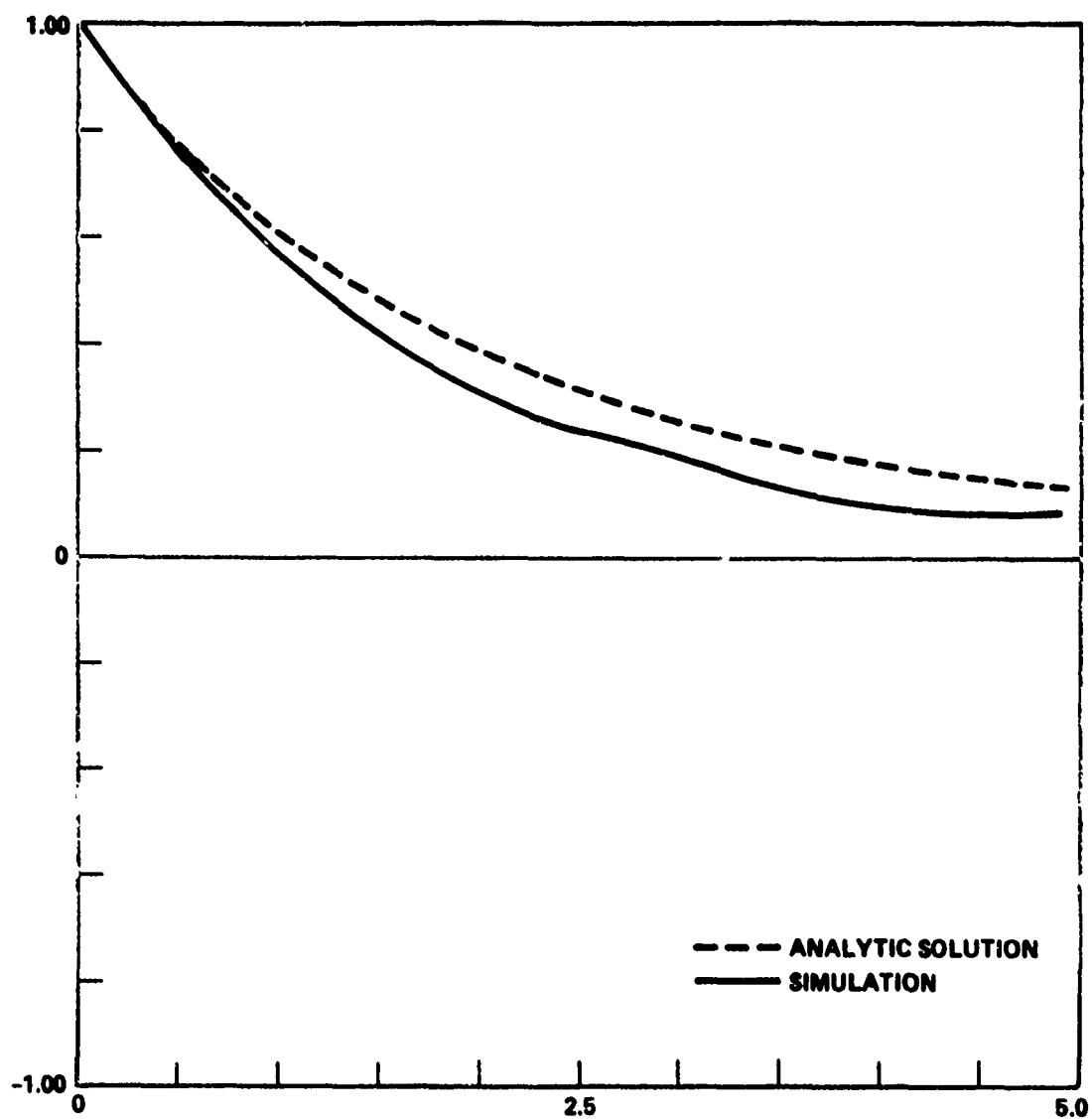
Figure 4.21. Autocovariance of ϵ_1, Run 1
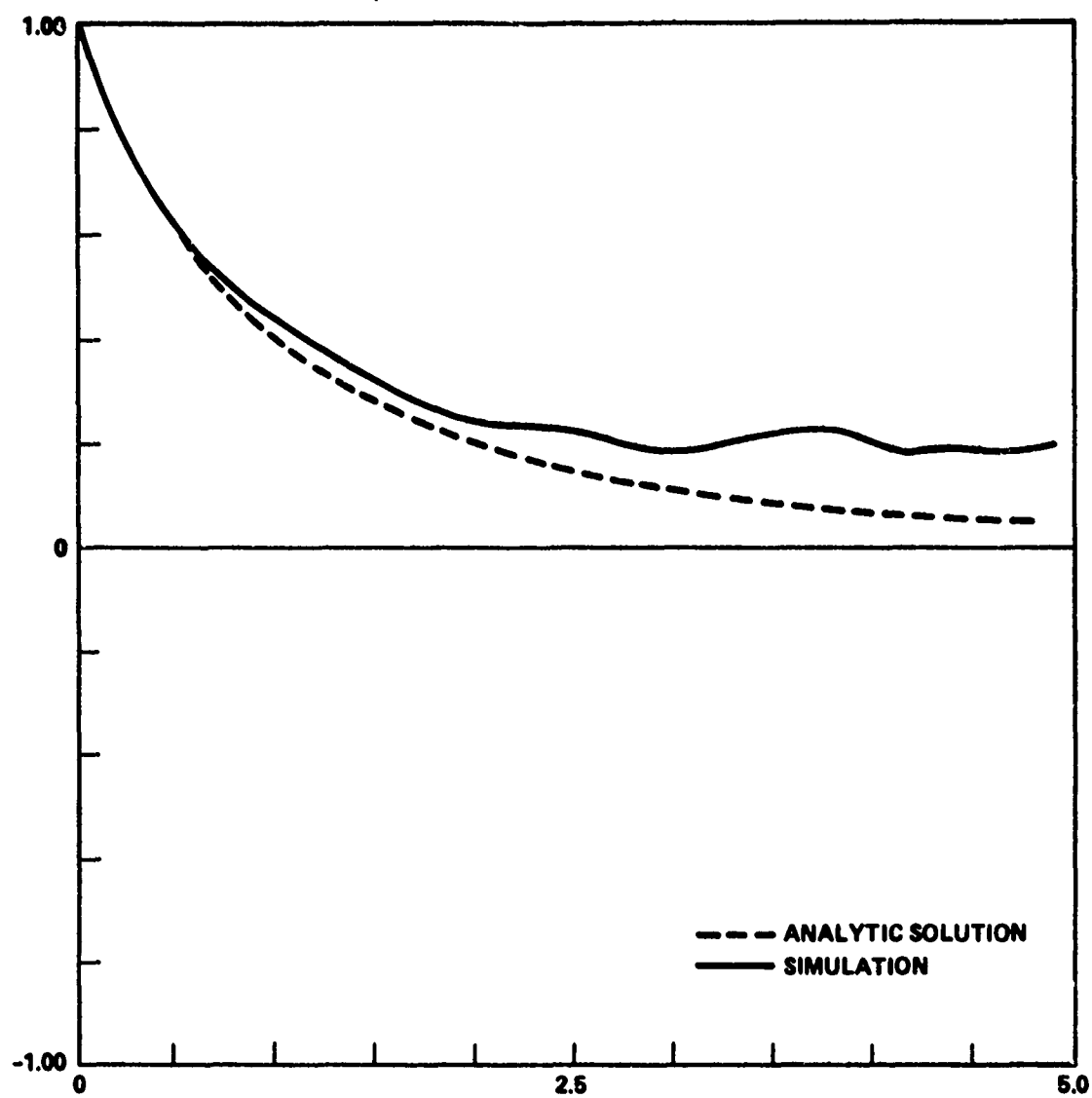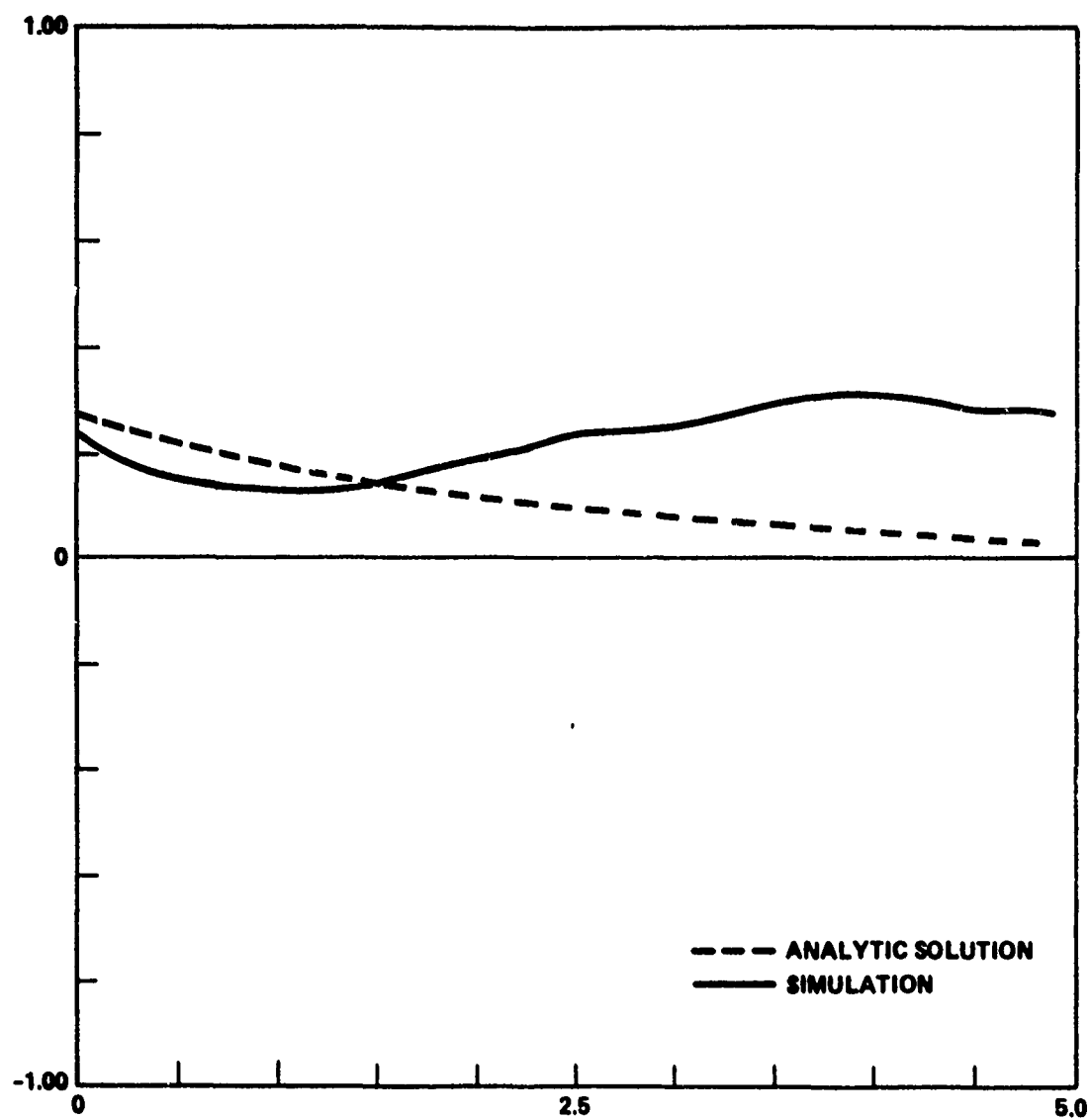
Figure 4.22. Autocovariance of ϵ_2, Run 1
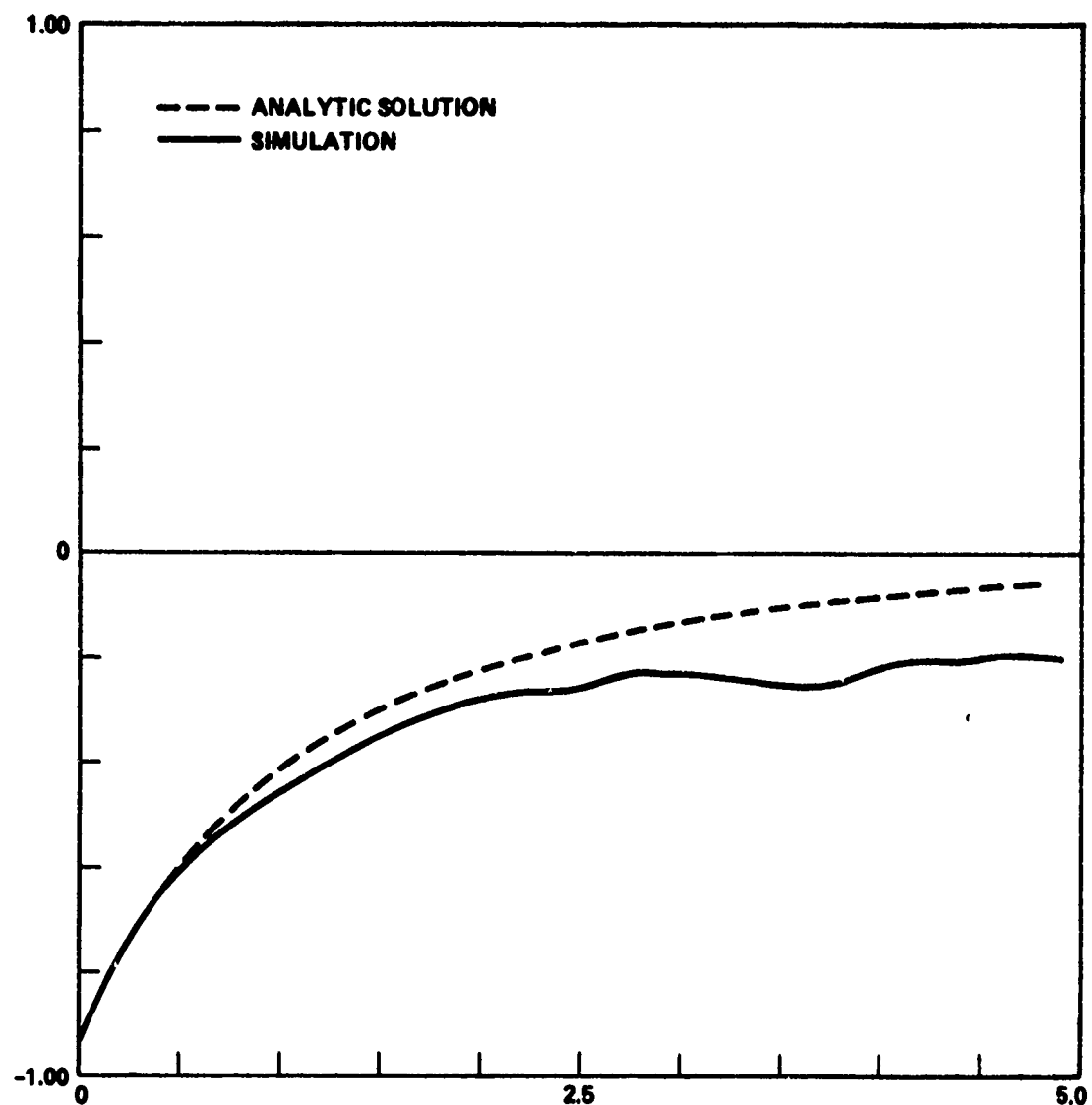
Figure 4.23. Crosscovariance of S and ϵ_1, Run 1

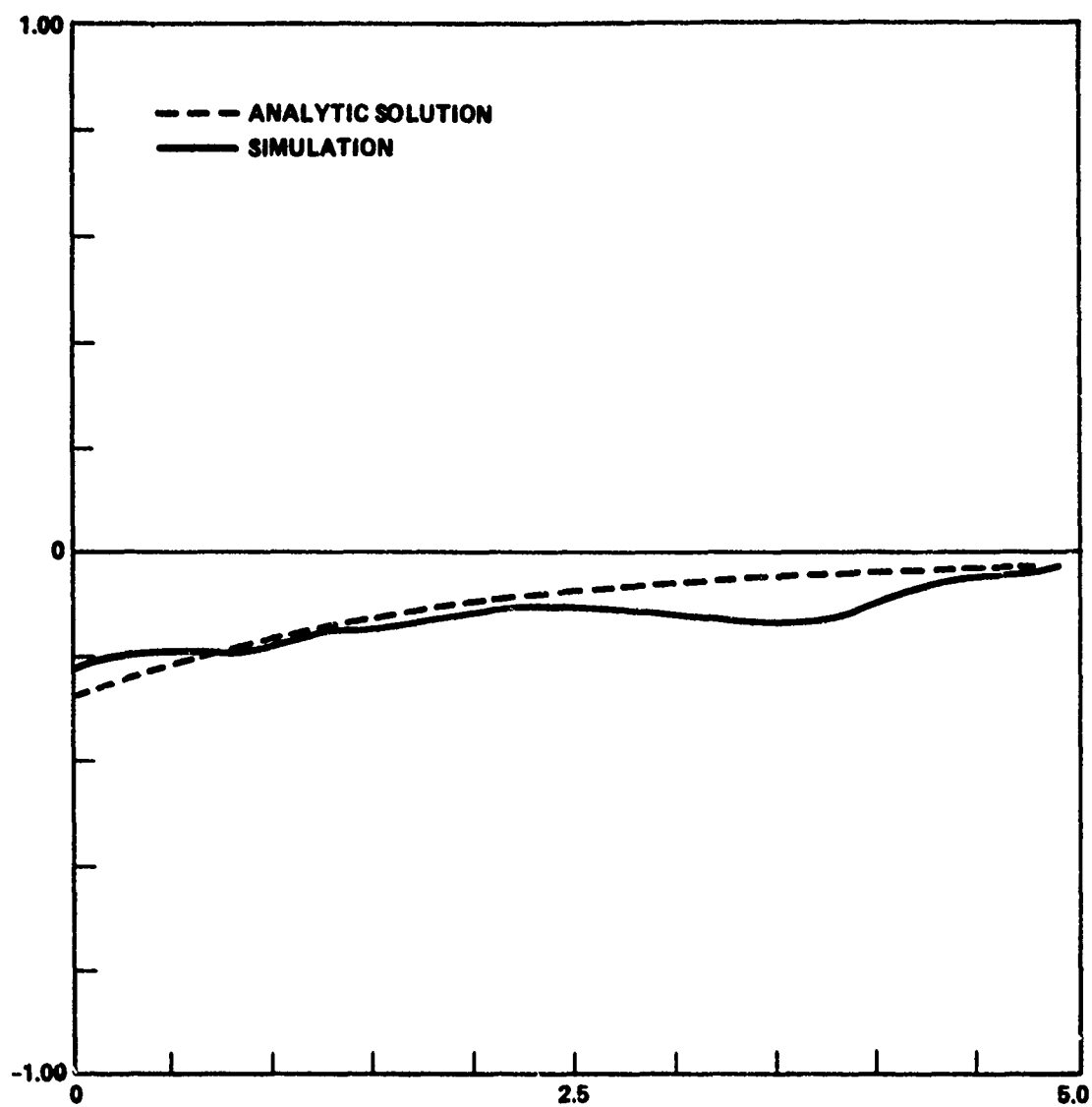Figure 4.24. Crosscovariance of S and ϵ_2, Run 1

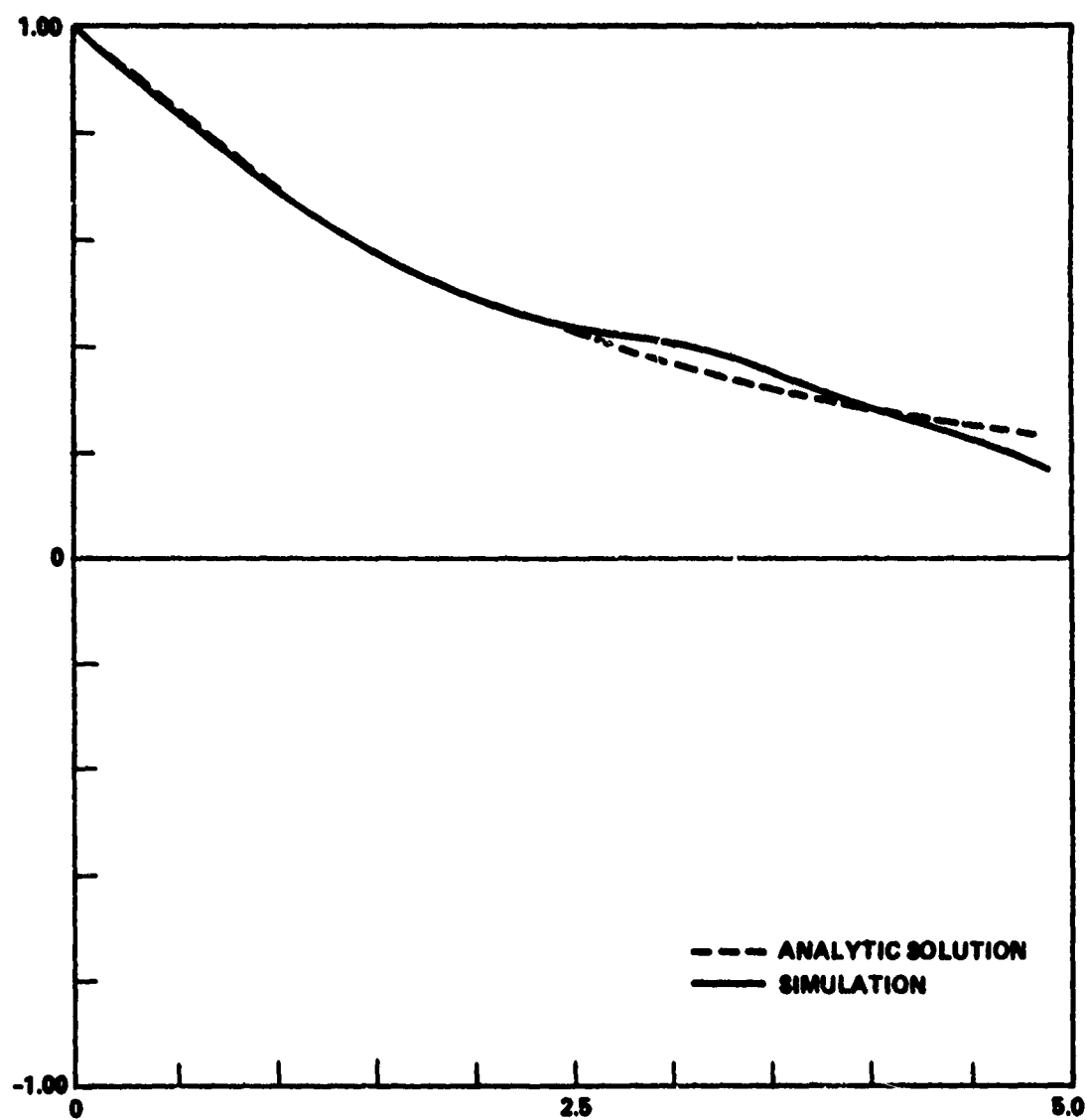Figure 4.25. Crosscovariance of ϵ_1 and ϵ_2, Run 1
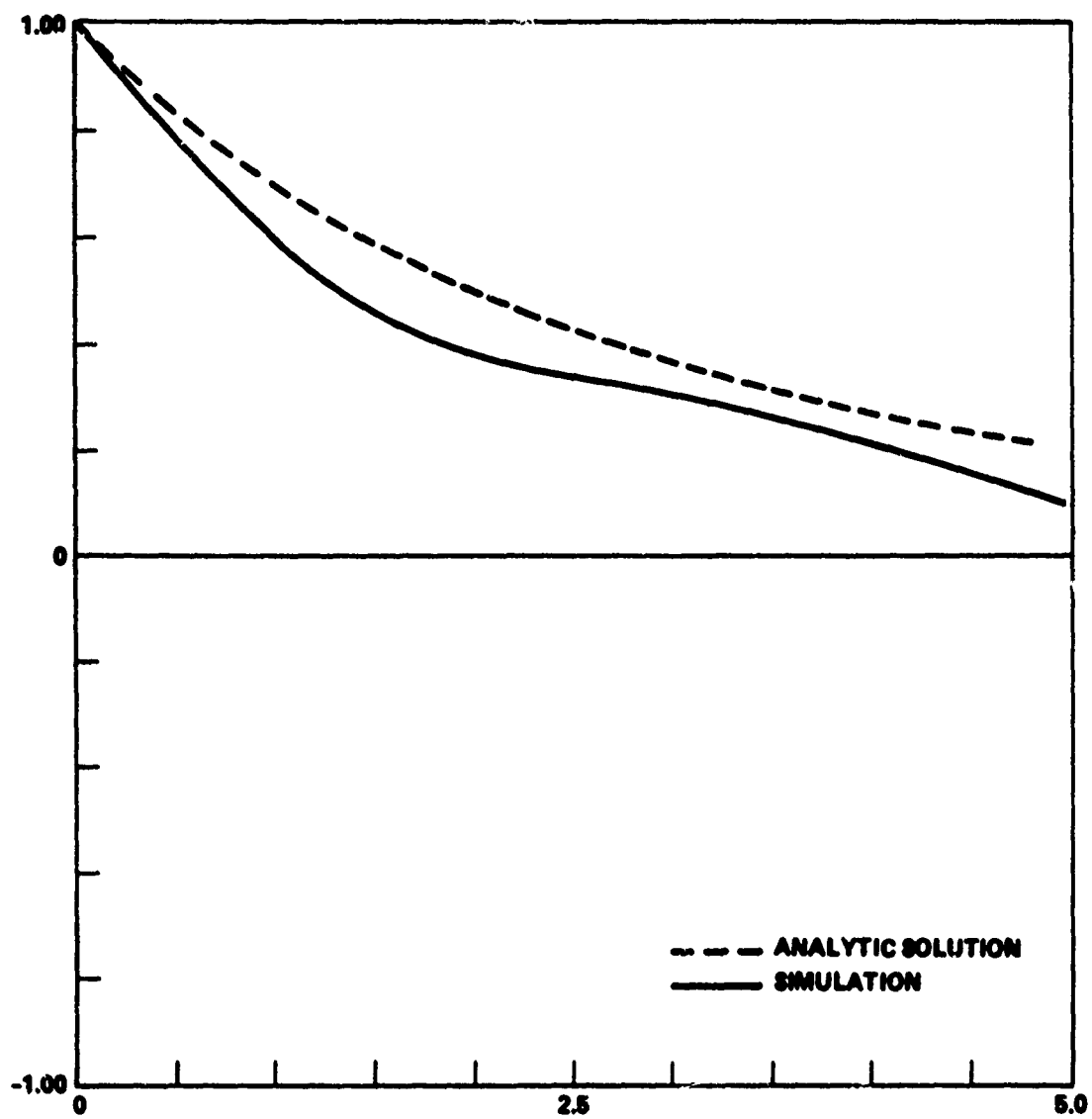
Figure 4.26. Autocovariance of S, Run 6

Figure 4.27. Autocovariance of ϵ_1, Run 6

Figure 4.28. Autocovariance of ϵ_2, Run 6

Figure 4.29. Crosscovariance of S and ϵ_1, Run 6

Figure 4.30. Crosscovariance of S and ϵ_2, Run 6

Figure 4.31. Crosscovariance of ϵ_1 and ϵ_2, Run 6

Figure 4.32. Autocovariance of S, Run 9
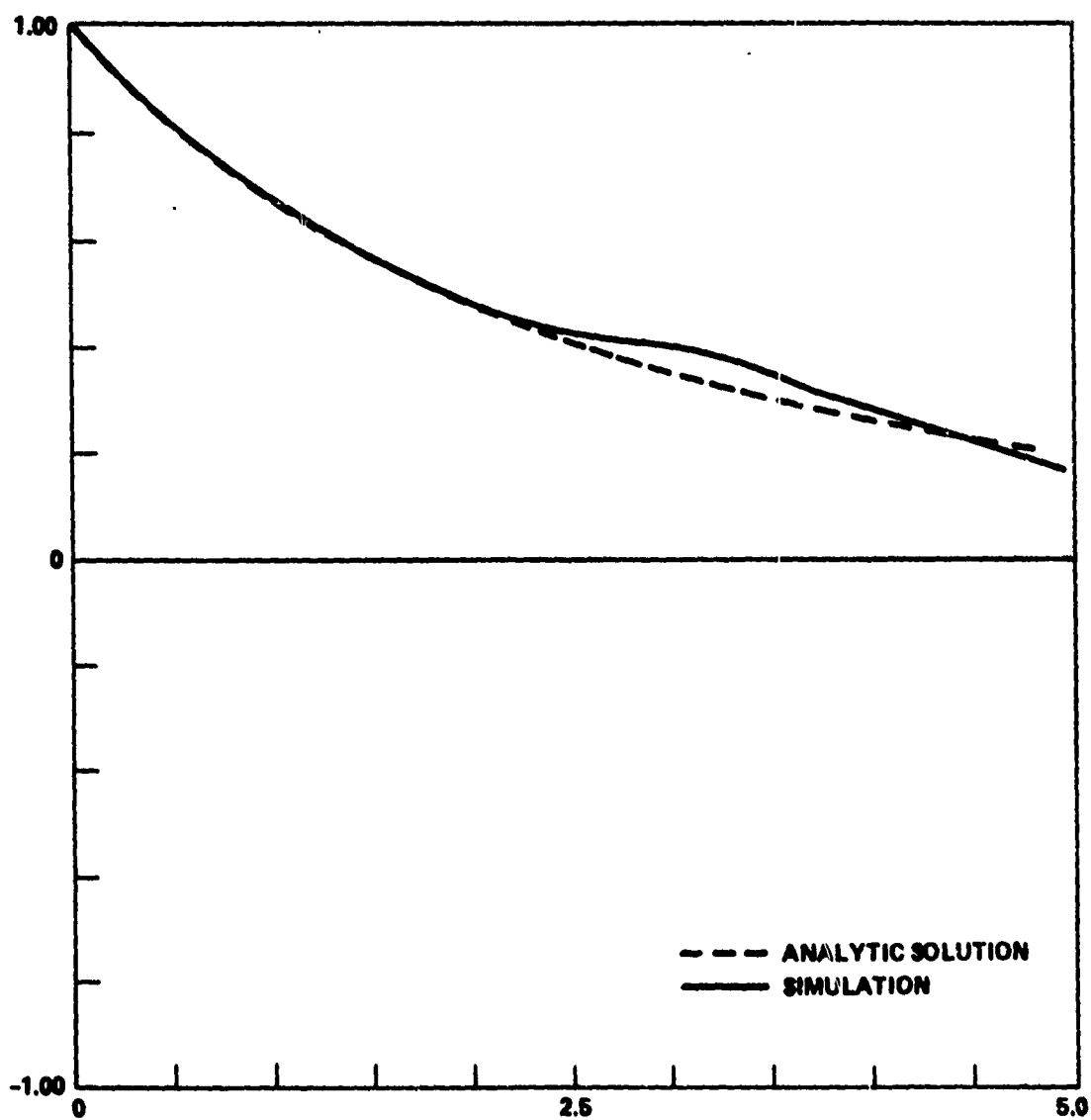
Figure 4.33. Autocovariance of ϵ_1, Run 9

Figure 4.34. Autocovariance of ϵ_2, Run 9

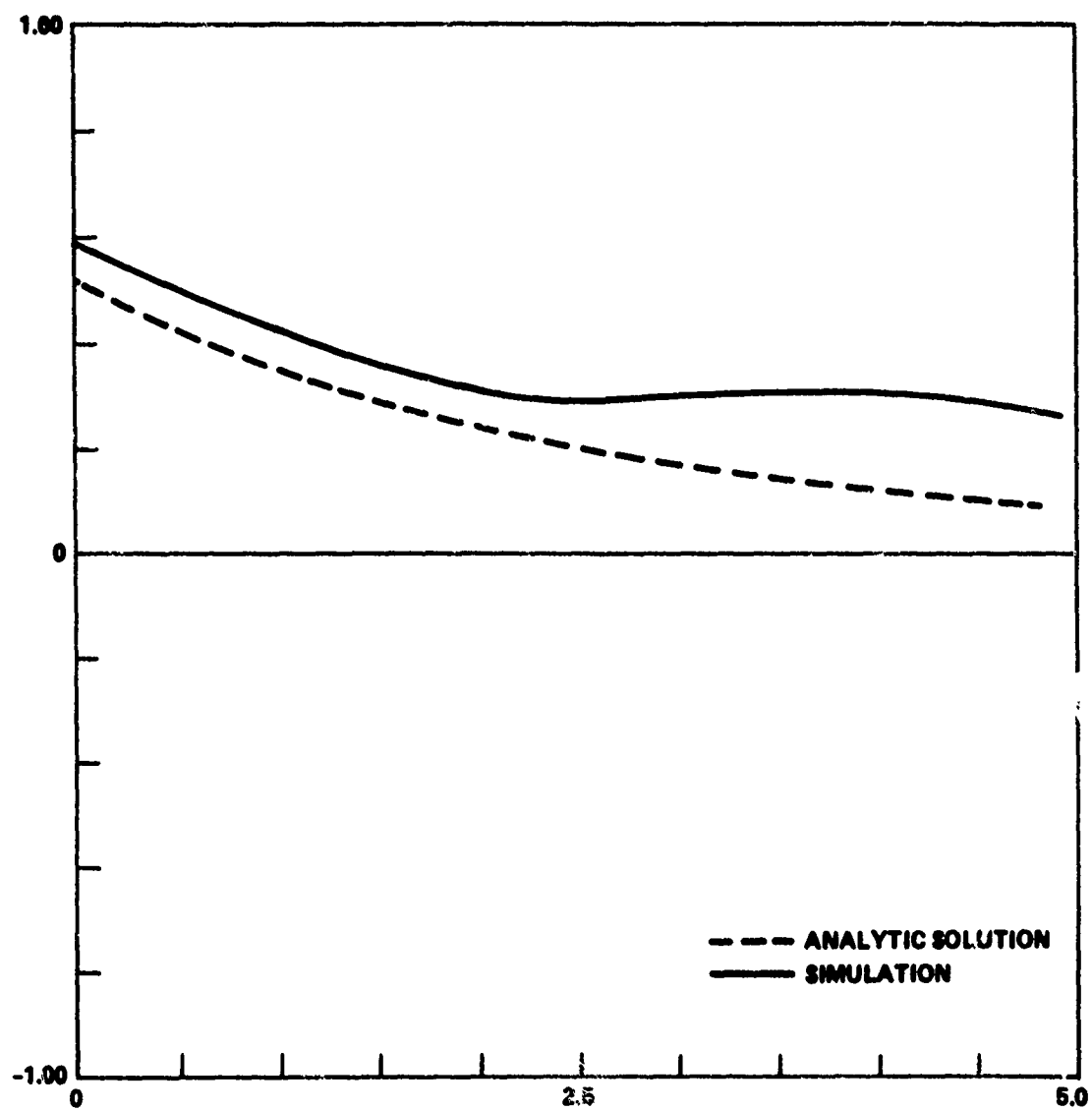Figure 4.35. Crosscovariance of S and ϵ_1, Run 9

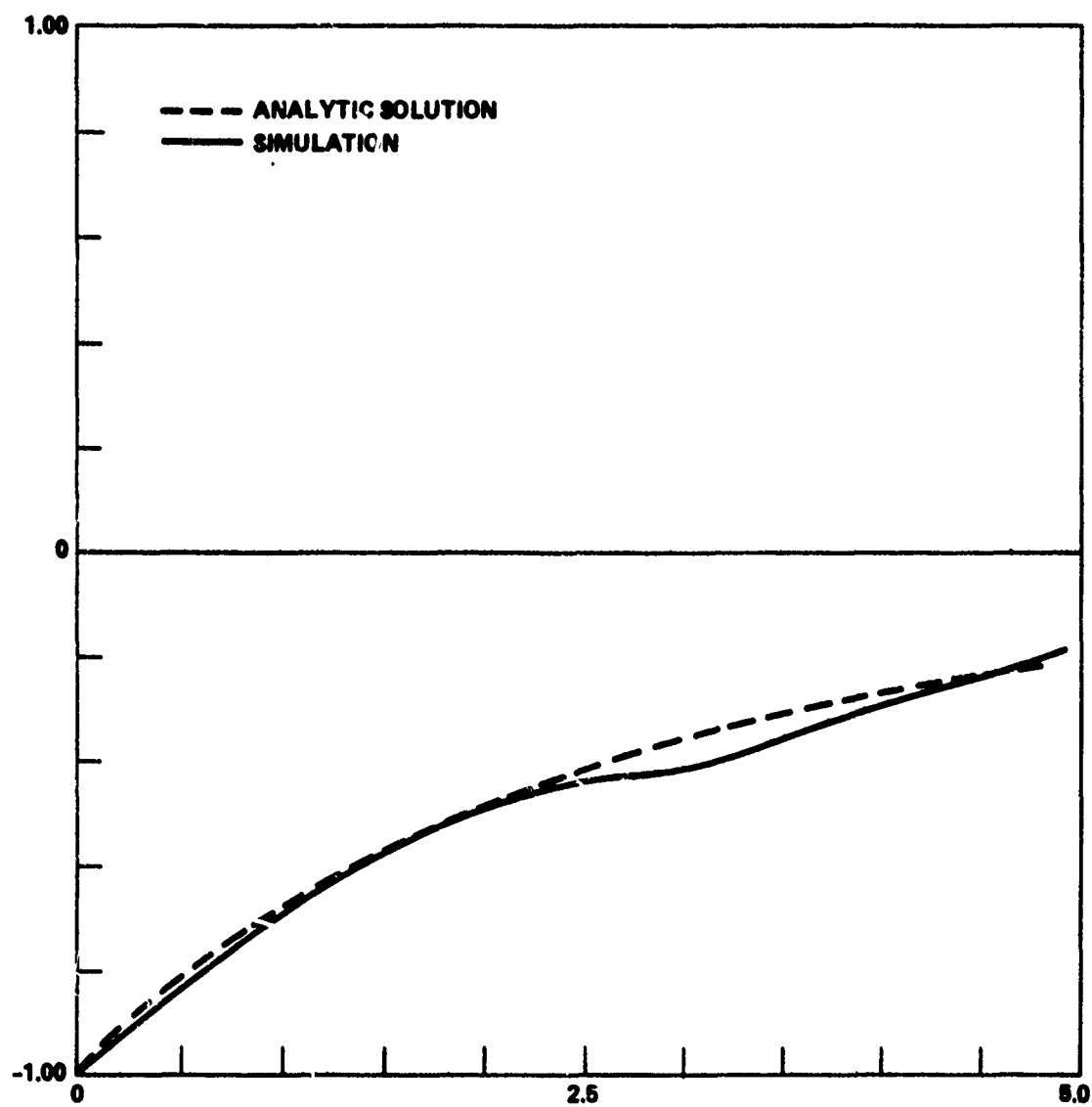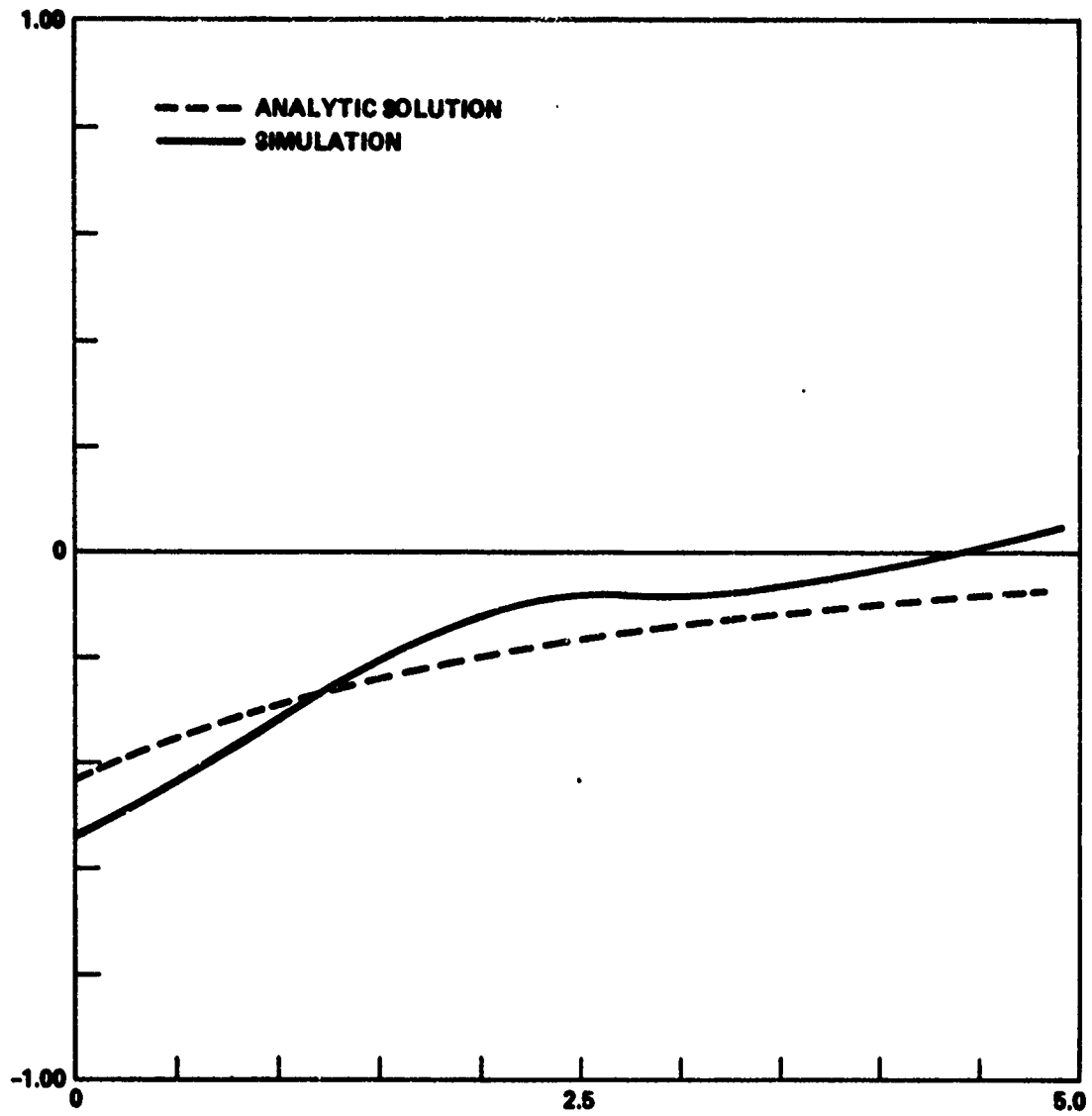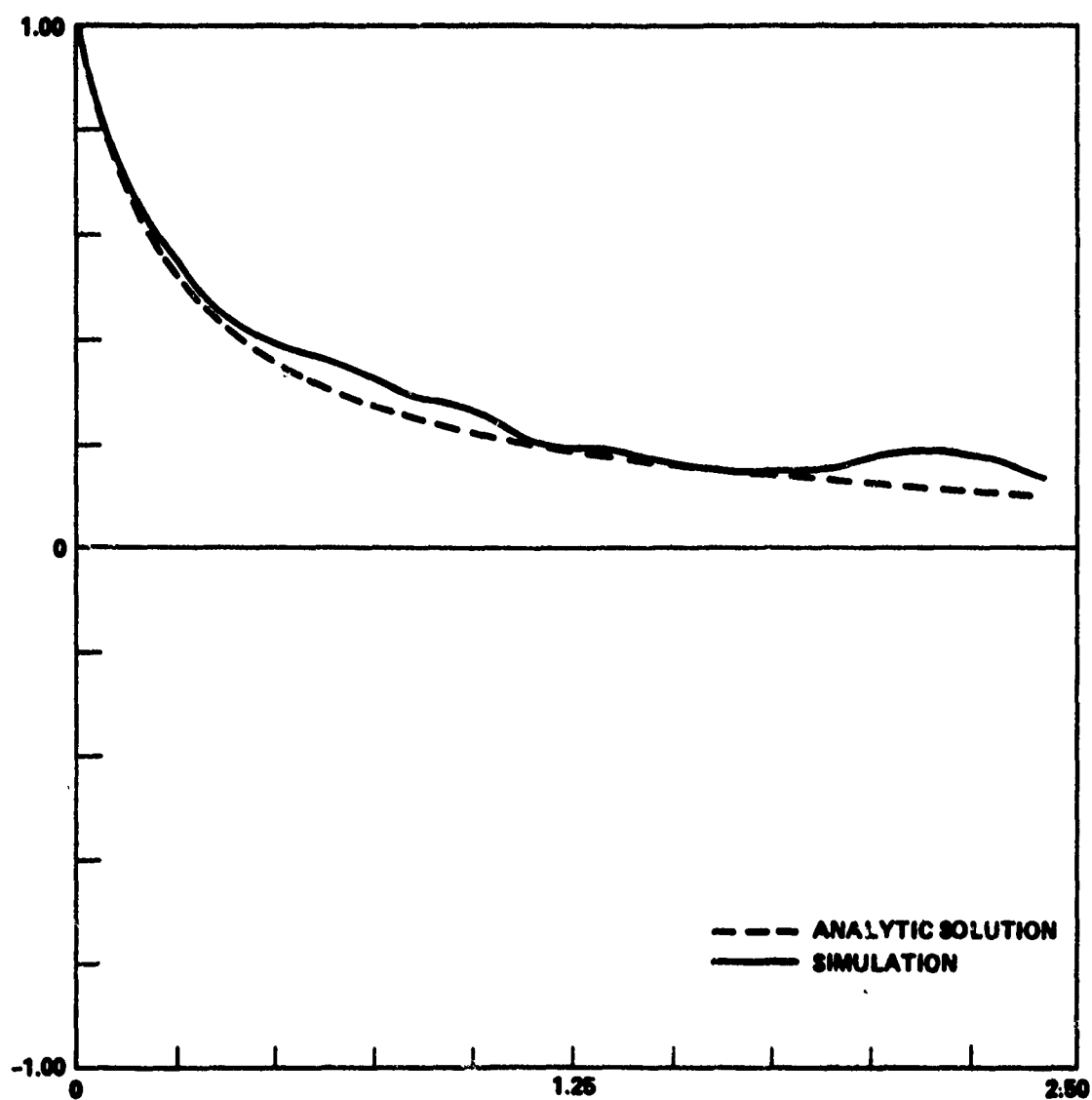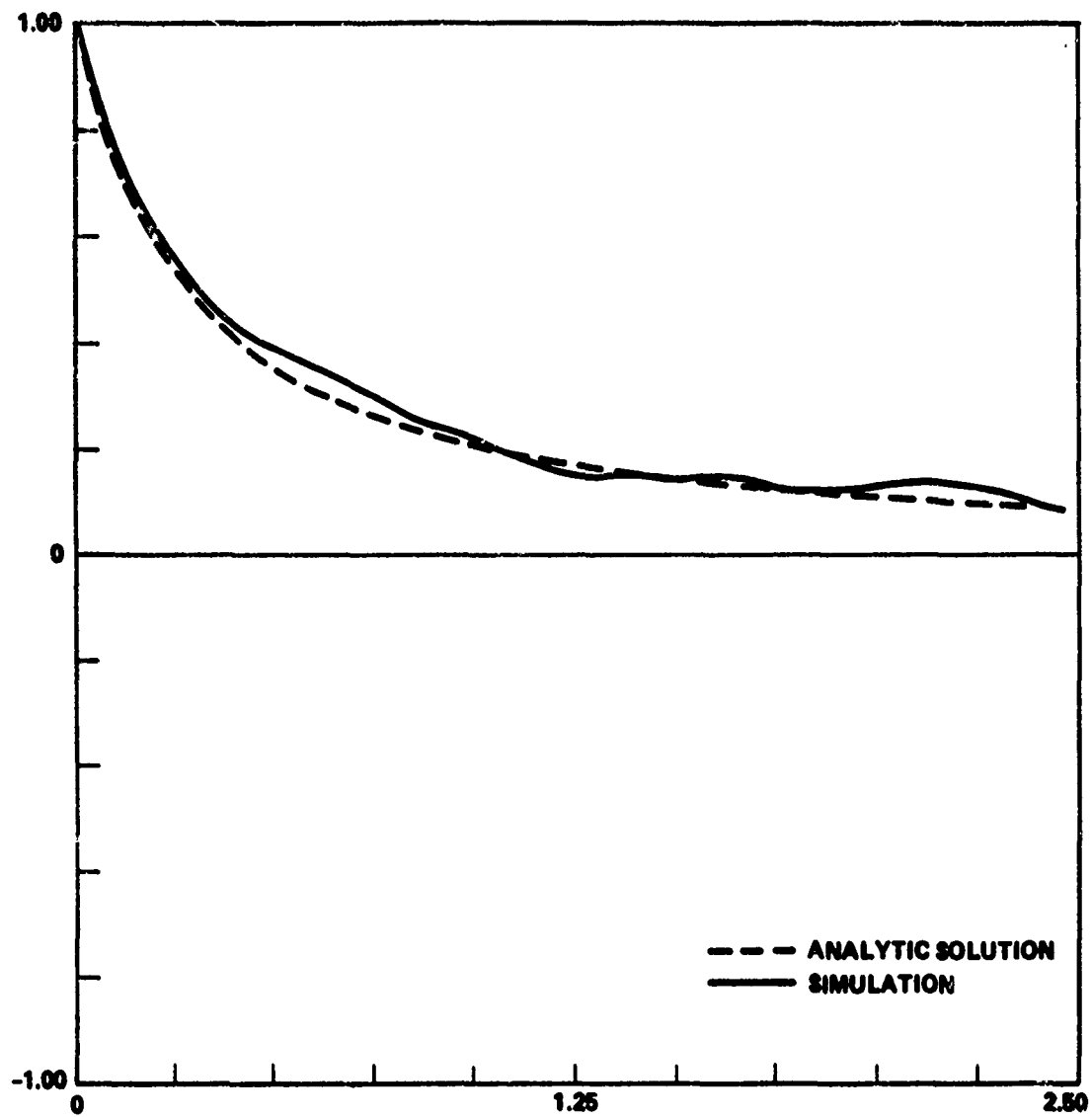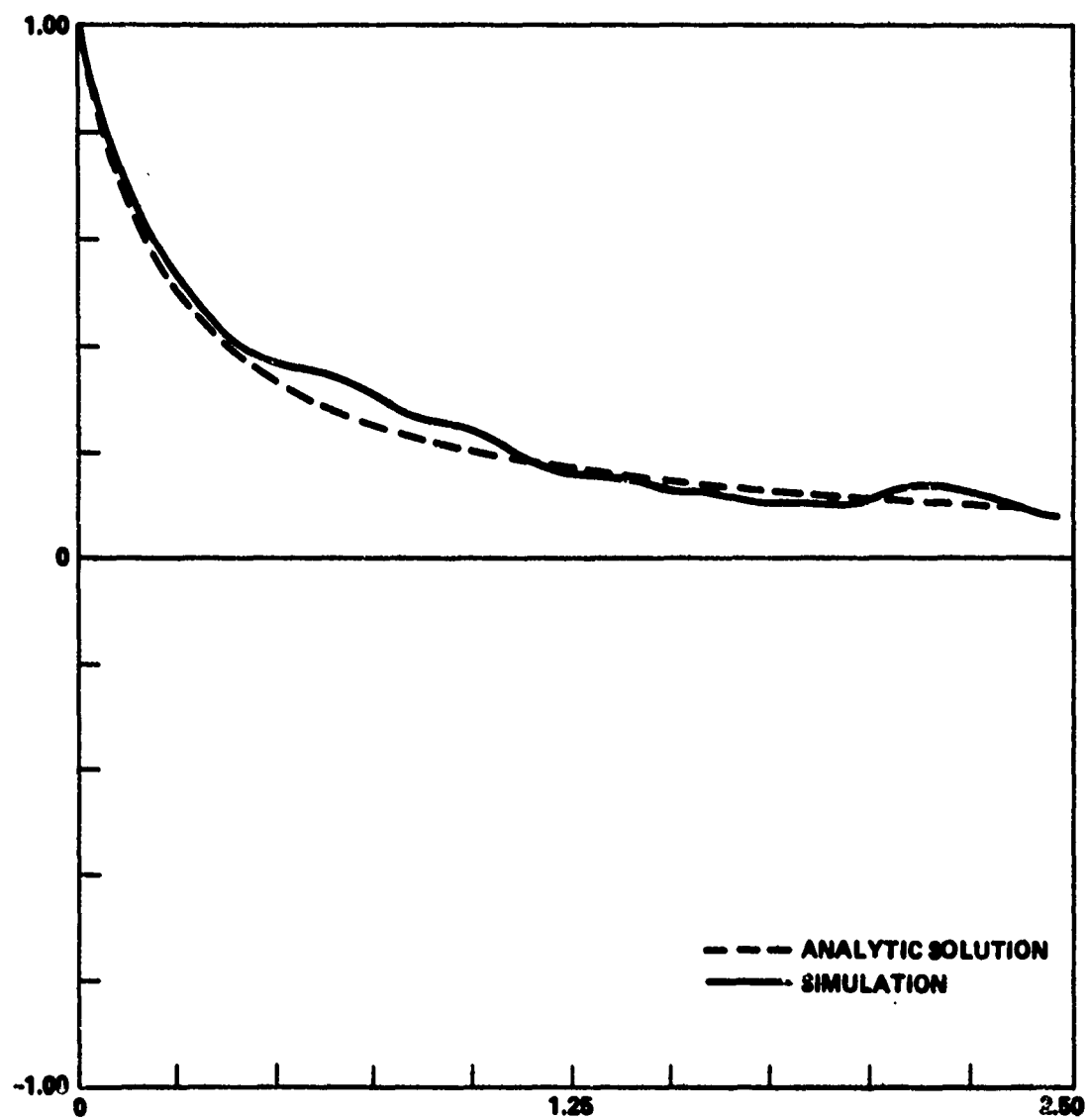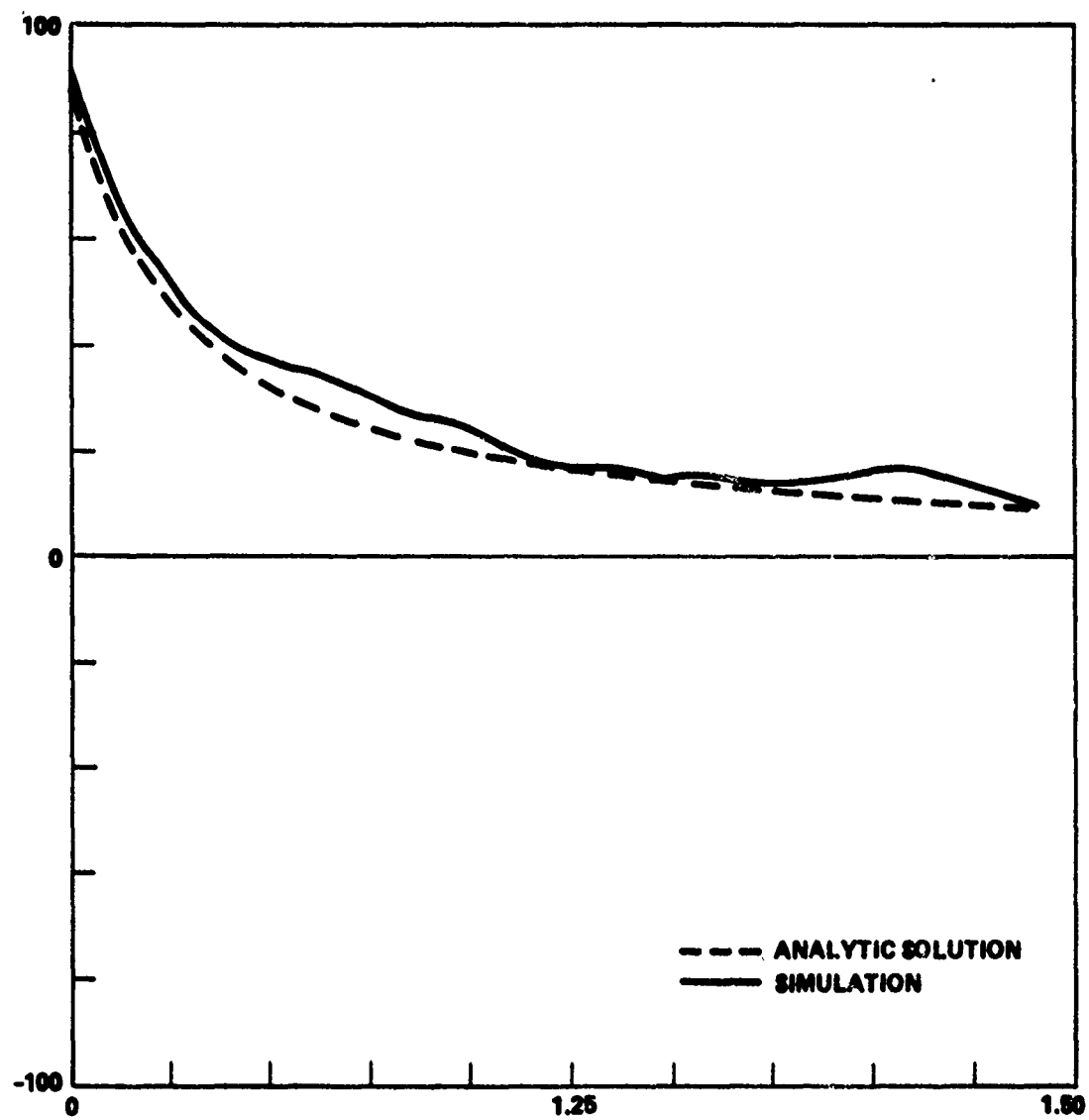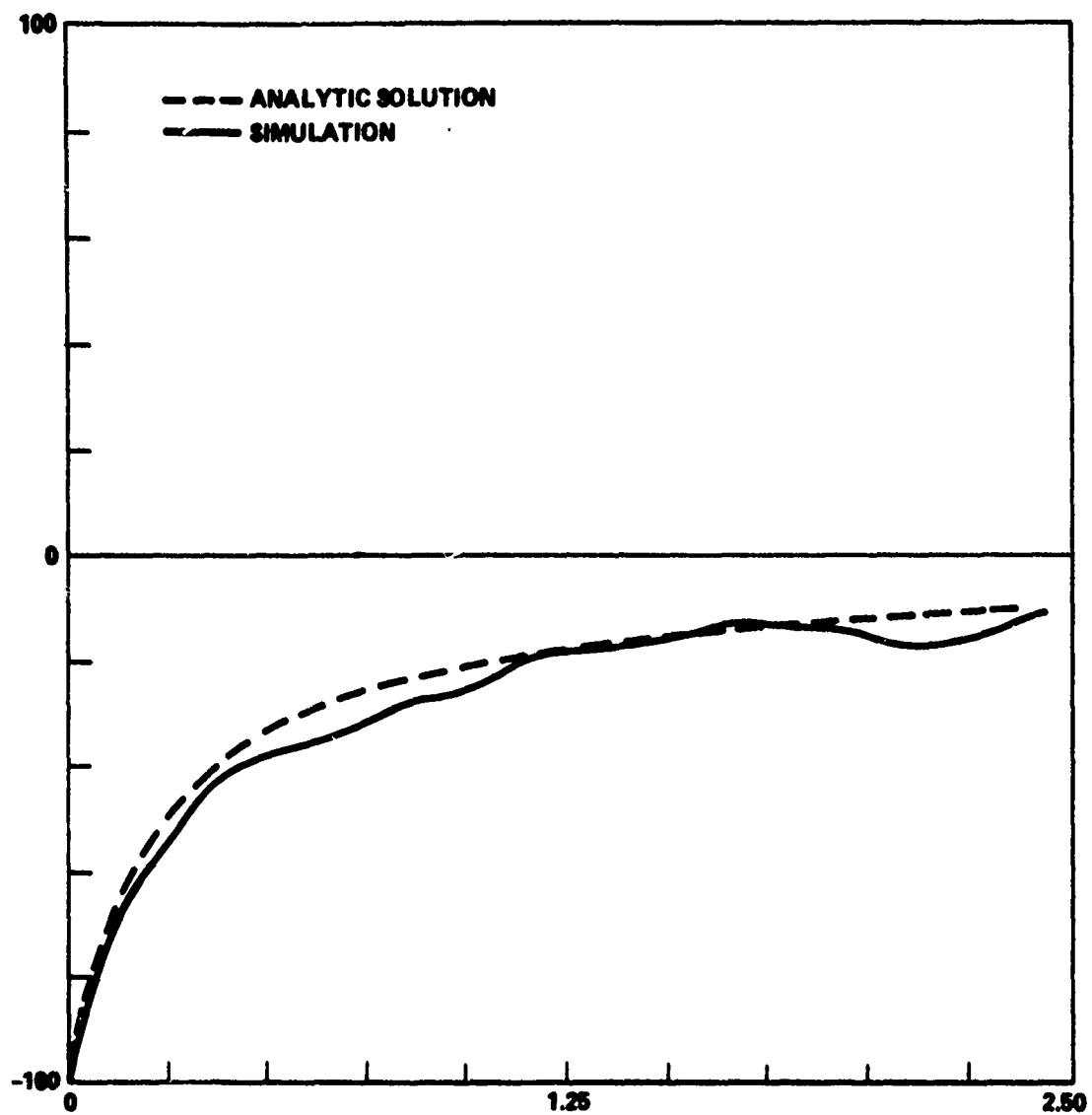Figure 4.36. Crosscovariance of S and ϵ_2, Run 9
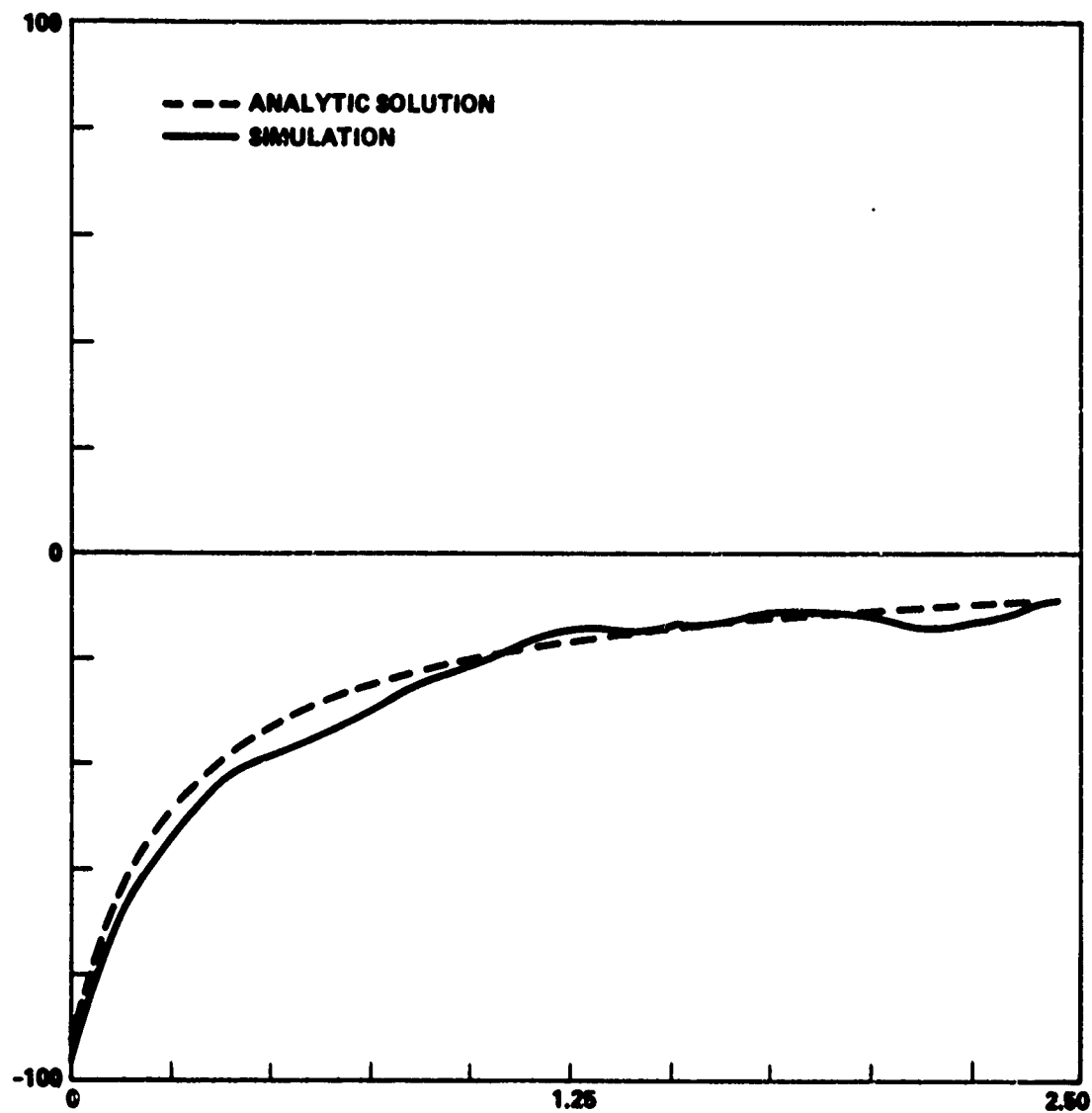
Figure 4.37. Crosscovariance of ϵ_1 and ϵ_2, Run 9

5. SUMMARY, CONCLUSIONS, AND APPLICATIONS

5.1 Summary and Conclusions

The objective of this research has been to develop techniques for the analytic calculations of the statistical characteristics of the EM scattering parameters of airborne radar targets. In Chapter 2, a deterministic model of the EM scattering is developed and applied to an ellipsoidal model of a target drone. In Chapter 3, techniques are derived to compute the conditional statistical characteristics of the scattering parameters. These statistical characteristics are conditional on the target flight path since the mean aspect angles are dependent only on the flight path with respect to the radar. Chapter 4 compares the analytically computed statistical characteristics at three sample points on a flight path with results of a Monte Carlo simulation. At each sample point three sets of Euler angle statistics were applied to investigate the sensitivity of the statistics of the scattering parameters to the statistics of the aspect angles. The results indicate the validity of the approximations used, at least for the selected target and flight path.

The prime objective of developing techniques for analytic calculation of the statistical characteristics of the EM scattering parameters has been accomplished. The ability to examine the statistical relationships among the scattering parameters will be of great value in designing tracking filters and evaluating system performance against

102

other than ideal targets. Furthermore, the deterministic model of the scattering parameters may aid in the understanding of the scattering phenomena and their effects on radar systems.

The secondary objective of identifying areas where existing data or theory does not support the general application of the primary objective has also been accomplished. The number of problem areas exceeded expectations. The ability to model the EM scattering from relatively simple geometrical shapes is limited. Most aircraft are made up of large numbers of not so simple geometrical shapes which cannot in general be accurately modeled by quadratic surfaces, circular cylinders or flat plates. It is essential that key reentrant structures such as the engine ducts be modeled since these represent primary scattering centers in certain regions of aspect angles, in fact, for many aircraft they are the largest backscattering elements in the entire sector within 45 degrees of nose-on. The inclusion of bistatic angles and the effects of polarization will add additional complexities to an already complex problem.

The almost total lack of measured data on random aircraft flight characteristics is one of the most surprising facts encountered. These data are necessary to improve the accuracy of the results.

Measured glint data are extremely limited and do not exist on targets of interest for air defense systems. Therefore, an evaluation of the general accuracy of the calculated glint data is limited to empirical judgment.

5.2 Applications and Recommendations

The results of this research have several applications in radar tracking of aircraft. Two of these applications are:

(1) The statistics of the radar scattering characteristics may be used in radar system simulations and evaluations. Present simulations and analyses either ignore the target induced errors or assume that they are independent additive processes. It is shown here, however, that the target induced errors are not independent, but that they are correlated with the RCS and each other. More accurate simulations may result from more accurate modeling of the target induced effects and the correlations among them. In order to further simplify the application of the results to radar simulations, additional work should be directed toward the development of dynamical models of stochastic processes having the desired statistics. Haddad [65] presents an approach for dynamical modeling of separable Markov processes, however, this may not be sufficient for some of the targets. More complicated techniques can be based on the works of Doob [66], Frost [67], Faurre [68], Kailath and Frost [69], and Haddad and Valisalo [70].

(2) The error statistics may be applied to the design of optimum tracking systems. The usual approach to the design and analysis of tracking filters is to assume that the measured errors are due only to additive white noise. Typical examples of such analyses include the works of Mosca [71], Sharenson [72], and Urkowitz [73]. With statistical models of the target induced errors it will be possible to generalize these works to more realistic conditions, including non-gaussian, trajectory-dependent, correlated noise.

Other applications include the investigation of the statistical relationships of the scattering parameters for different polarizations and different frequencies. Basalov and Ostrovityanov [32] and Ewell, Alexander, and Tomberlin [74] have investigated the effects of polarization on the radar scattering characteristics of a target and the effects on angle tracking. More accurate statistical models would be useful in this area to evaluate the possibility of using polarization agility to aid in reducing tracking errors. The analytic model developed in Chapter 2 can be generalized to include the effects of polarization by us'ng the works of Uslenghi and Lee [55], Moll and Seecamp [48], and Pierson and Clay [56]. Sims and Graf [34, 35] have investigated the use of frequency agility to reduce rms tracking errors due to target induced errors. Finally, a statistical analysis of the frequency sensitivity of target scattering, using techniques developed here, may be used to extend the work in this area.

5.3 Additional Efforts and Future Plans

This research is a portion of an ongoing task in the area of airborne radar target signatures. Three tasks have been planned to help fill the gaps in data and theory as applied to this problem. Other tasks are under development but require coordination and concurrence of other agencies for actual implementation.

A contract effort is in progress at the University of Illinois to develop solutions to the EM scattering theory for selected geometrical bodies. These will be used first to develop a more accurate model of the scattering from the BQM-34A target drone. Later these solutions and others can be used to model the radar scattering from other airborne targets of interest.

Two radar scattering measurements programs are in progress which will provide data to aid in validation and improvement of the analytic solutions to the scattering problem. One measurement program is at RATSCAT, Holloman Air Force Base, New Mexico. These measurements include glint, monostatically and bistatically, in addition to the more conventional RCS measurements on the BQM-34A and BQM-34F target drones. The second measurements program is being done by General Dynamics, Convair Aerospace Division, Fort Worth, Texas on the same target drones. This program will use short pulse technology and sophisticated data processing to identify the location and provide information on individual scattering centers. It is expected that these two measurements programs will aid greatly in the development of more accurate analytic modeling techniques.

The data desired on aircraft flight characteristics are essential to the statistical modeling effort. However, any program to make the necessary measurements will require the assistance of the Air Force or the Navy, or both. Development of actual data requirements has not been initiated due to lack of time.

The work reported here is of interest to all services. Closer coordination is planned in the future due to the overlapping interests and the expense involved in this type of research.

REFERENCES

1. Barton, D. K., _Radar System Analysis_, Prentice-Hall, 1964.

2. Barton, D. K., and Ward, H. R., _Handbook of Radar Measurement_, Prentice-Hall, Inc., 1969.

3. Skolnik, M. I., _Introduction to Radar Systems_, McGraw-Hill, 1962.

4. Peters, L., Jr., and Weimer, F. C., "Tracking Radars for Complex Targets', _Proc IEE (GB)_, 110, pp. 2149-216?, December 1963.

5. Berkowitz, R. S., _Modern Radar: Analysis, Evaluation, and System Design_, John Wiley and Sons, 1965.

6. Brown, W. M., and Palermo, C. J., _Random Proces...s, Communications and Radar_, McGraw-Hill, 1969.

7. Nathanson, F. E., _Radar Design Principles; Signal Processing and the Environment_, McGraw-Hill, 1969.

8. Wheeler, G. J., _Radar Fundamentals_, Prentice-Hall, 1967.

9. Marcum, J. I., _A Statistical Theory of Target Detection by a Pulsed Radar_, The Rand Corporation, Santa Monica, California, Report No. RM-754, 1 December 1947.

10. Swerling, P., _Probability of Detection for Fluctuating Targets_, The Rand Corporation, Santa Barbara, California, Rand Memo-1217, 17 March 1954.

11. Swerling, P., "Detection of Fluctuating Pulsed Signals in the Presence of Noise", _IRE Trans on IT_, 3, pp. 175-178, September 1957.

12. Swerling, P., _Probability of Detection of Some Additional Fluctuating Target Cases_, Aerospace Corporation, El Segundo, California, Report No. TOR 669(9990)-14, March 1966.

13. Heidbreder, G. R., and Mitchell, R. L., _Detection Probabilities for Log-Normally Distributed Signals_, Aerospace Corporation, El Segundo, California, Report No. TR-699(9990)-6, April 1965.

14. Sponsler, G. C., "First Order Markov Process Representation of Binary Radar Data Sequences," _IRE Trans on IT_, 3, pp. 56-64, March 1967.

15. Weinstock, W. W., _Target Cross Section Models for Radar Systems Analysis_, University of Pennsylvania, Ph.D. Dissertation, Electrical Engineering, 1964.

16. Delano, R. H., A Theory of Target Glint or Angular Scintillation in Radar Tracking, _Proc of IRE_, 41, pp. 1778-1784, December 1953.

17. Delano, R. H., "Further Reply to Comments by L. Peters and F. C. Weimer", _IRE Trans on AP_, 9, pp. 227-228, March 1961.

18. Muchmore, R. B., "Aircraft Scintillation Spectra" _IRE Trans on AP_, 8, pp. 201-212, March 1960.

19. Muchmore, R. B., "Reply to Comments by Leon Peters, Jr., and F. C. Weimer", _IRE Trans on AP_, 9, pp. 112-113, January 1961.

20. Peters, L., Jr., and Weimer, F. C., "Reply by Comments by R. H. Delano", _IRE Trans on AP_, 9, pp. 228, March 1961.

21. Peters, L., Jr., and Weimer, F. C., "Reply to Comments by R. P. Muchmore", _IRE Trans on AP_, 9, pp. 229, March 1961.

22. Peters, L., Jr., and Weimer, F. C., "Concerning the Assumption of Random Distribution of Scatterers as a Model of an Aircraft for Tracking Radars", _IRE Trans on AP_, 9, pp. 110-111, January 1961.

23. Meade, J. E., "Target Considerations", _Guidance_, by A. S. Locke, et al, D. Van Nostrand Company, Inc., Ch. 11, pp. 420-442, 1955.

24. Ostrovityanov, R. V., "Angular Noise", _Radioteckhnika i Elektronika_, 4, pp. 592, 1966. (Radio Engineering and Election Physics, pp. 507-515, 1966).

25. Howard, D. D., "Radar Target Angular Scintillation in Tracking and Guidance Systems Based on Echo Signal Phase - Front Distortion", _Proc of NEC_, 15, pp. 840-849, 1959.

26. Gubonin, N. S., "Fluctuations of the Phase Front of a Wave Reflected from a Complex Target", _Radiotekhnika i Electronika_, 10, p. 844, May 1965.

27. Lindsay, J. E., "Angular Glint and the Moving, Rotating, Complex Radar Target", _IEEE Trans on AES_, 4, pp. 164-173, March 1968.

28. Dunn, J. H., and Howard, D. D., "Radar Target Amplitude, Angle and Doppler Scintillation from Analysis of the Echo Signal Propagating in Space", _IEEE Trans on MTT_, 16, pp. 715-728, September 1968.

29. Crispin, J. W., Jr., and Maffett, A. L., "The Practical Problem of of Radar Cross Section Analysis," _IEEE Trans. on AES (Correspondence)_, March 1971.

108

30. Borison, S. L., **Biased Velocity Estimated Due to Phase Center Motion**, Lincoln Laboratory, Massachusetts Institute of Technology, Tech. Note 1967-35, September 1967.

31. Edrington, T. S., "The Amplitude Statistics of Aircraft Radar Echoes," **Trans. on Military Electronics**, MIL-9, January 1965.

32. Basalov, F. A., and Ostrovityanov, R. V., "Effect of Signal Polarization on Angular Noise Characteristics," **Radiotekhnika i Elektronika (USSR)**, 12, 2221-23, December 1967.

33. Dunn, J. H., Howard, D. D., and King, A. M., "Phenomena of Scintillation Noise in Radar Tracking Systems", **Proc of IRE**, 47, pp. 855-863, May 1959.

34. Sims, R. J., and Graf, E. R., "The Reduction of Radar Glint by Diversity Techniques," **IEEE Trans. on Antennas and Propagation**, AP-19, July 1971.

35. Sims, R. J., and Graf, E. R., **The Determination of Glint for a Complex Radar Target**, Auburn University, Engineering Experiment Station, Final Report Vol II, July 1969.

36. Corriher, H. A., Jr., and Pyron, B. O., A Bibliography of Articles on Radar Reflectivity and Related Subjects: 1957-1964, **Proc of IEEE**, 53, pp. 1025-1064, August 1965.

37. Corriher, H. A., Jr., **Radar Reflecitvity of Aircraft**, Georgia Insittute of Technology, Final Report, Project A-1025, Contract N00014-67-A-0159-003, 19 January 1970.

38. Mie, G., "Beitrage zur Optik truber Medien, speziell Kollidaler Metallosungen," **Ann. Phys.**, 25, p. 377, 1968.

39. Crispin, J. W., and Maffett, A. L., "Radar Cross Section Estimation for Complex Shapes", **Proc of IEEE**, 53, pp. 372-382, August 1965.

40. Bowman, J. J., Senior, T. B. A., and Uslengi, P. L. E. (Editors), **Electromagnetic and Acoustic Scattering by Simple Shapes**, North-Holland Publishing Company, Amsterdam, 1969. (Also available through DDC AD 699 859.).

41. Crispin, J. W., Jr., and Siegel, K. M., **Methods of Radar Cross Section Analysis**, Academic Press, 1968.

42. Ruck, G. T., Barrick, D. E., Stuart, W. D., and Krichbaum, C. K., **Radar Cross Section Handbook**, Vols 1 & 2, Plenum Press, 1970.

43. Ross, R. A., "Radar Cross Section of Rectangular Flat Plates as a Function of Aspect Angle", **IEEE Trans. on AP**, 14, pp. 329-335, May 1966.

44. Ross, R. A., and Bechtel, M. E., "Scattering-Center Theory and Radar Glint Analysis", _IEEE Trans on AES_, 4, pp. 756-762, September 1968.

45. Oshiro, F. K., Mitzner, K. M., Louis, S., Coleman, J. R., and Heath, H. C., _Calculation of Radar Cross Section, Part II, Analytical Report_, Northrop Corporation, Norair Div, Hawthorne, California, Report No. NOR-69-173-PT-2, April 1970.

46. Oshiro, F. K., Mitzner, F. M., Louis, S., Colemen, J. R., and Heath, H. C., _Calculation of Radar Cross Section, Part III, Users Manual_, Northrop Corporation, Norair Div, Hawthorne, California, Report No. NOR 69-173-PT-3, April 1970.

47. Oshiro, F. K. et al., _Calculation of Radar Cross Section_, Technical Report AFAL-TR-71-50, May 1971, Northrop Corporation, Hawthorne, California.

48. Moll, J. W., and Seecamp, R. G., "Calculation of Radar Reflecting Properties of Jet Engine Intakes Using a Waveguide Model," _IEEE Trans. on Aerospace and Electronic Systems_, AES-6, September 1970.

49. Ryan, C. E., Jr., _A Computer Program for Backscatter by Smoothly Joined, Second Degree Surfaces of Revolution_, Ohio State University, Electro-Sciences Laboratory, Report No. 2430-6, April 1968.

50. Ryan, C. E., _A Geometrical Theory of Diffraction Analysis of the Radar Cross Section of Sectionally Continuous Second-Degree Surface of Revolution_, Ohio State University, Electro-Sciences Laboratory, Report No. 2430-7, March 1968.

51. Keller, J. B., "A Geometrical Theory of Diffraction", _Proceedings of Symposia in Applied Math_, Vol VIII, 1958, McGraw-Hill.

52. Keller, J. B., "Backscatter from a Finite Cone", _IRE Trans on AP_, 8, pp. 175-182, March 1960.

53. Keller, J. B., "Geometrical Theory of Diffraction," _Journal of the Optical Society of America_, 52, pp. 116-130, February 1962.

54. Bechtel, M. E., _Computation of Transient Responses of Radar Targets_, Cornell Aeronautical Laboratory, CAL No. UF-2457-E-2, September 1968.

55. Uslenghi, P. L. E., and Lee, S. W., _High Frequency Backscattering from an Elliptical Metal Plate_, Antenna Laboratory, University of Illinois, Antenna Laboratory Report No. 72-6, 1972.

56. Pierson, W. A., and Clay, R. W., (General Dynamics), _T-33 Radar Cross Section Measurements and Scintillation Analysis_, Final Technical Report, Nr. RADC-TR-72-30, February 1972, Rome Air Development Center, Griffiss Air Force Base, New York.

110

57. Thomas, J. B., *An Introduction to Statistical Communication Theory*, John Wiley and Sons, 1969.

58. Wragg, A., and Dowson, D. C., "Fitting Continuous Probability Density Functions Over [0, ∞) Using Information Theory Ideas," *IEEE Trans. on Information Theory*, Correspondence, IT-16, March 1970.

59. Kolk, R. W., *Modern Flight Dynamics*, Prentice-Hall Inc., 1961.

60. Viterbi, A. J., *Principles of Coherent Communication*, McGraw-Hill, 1966.

61. Cochran, W. T.; Cooley, J. W.; Favin, D. L.; Helms, H. D.; Raenel, R. A.; Lang, W. W.; Maling, G. C., Jr.; Nelson, D. E.; Rader, C. M.; and Welch, P. D; "What is the Fast Fourier Transform?" *Proceedings of the IEEE*, Vol 55, No. 10, October 1967, pp. 1664-1674.

62. Cooley, J. W., Lewis, P. A. W., and Welch, P. D., "The Fast Fourier Transform and its Applications", *IEEE Trans Education*, 12, No. 1, March 1969, pp. 27-34.

63. Cooley, J. W., Lewis, P. A. W., and Welch, P. D., "Application of the Fast Fourier Transform to Computation of Fourier Integrals, Fourier Series and Convolution Integrals," *IEEE Trans. On Audio and Electroacoustics*," Vol AU-15, pp. 79-84, June 1967.

64. Bendat, J. S., and Piersol, A. G., *Random Data: Analysis and Measurement Procedures*, Wiley-Interscience, N. Y., 1971.

65. Haddad, A. H., "Dynamical Representation of Markov Processes of the Separable Class," *IEEE Trans. on Information Theory*, IT-16, September 1970.

66. Doob, J. L., *Stochastic Processes*, John Wiley and Sons, Inc., 1953.

67. Frost, Paul A., *A New Form of Representation of Stochastic Integrals and Equations* by R. L. Stratonovich, translated and introduced by Frost. Technical Report No. 7050-9, Systems Theory Laboratory, Stanford Electronics Laboratory, Stanford University, August 1966.

68. Faurre, P. L., *Representation of Stochastic Processes*, Doctoral Dissertation, Electrical Engineering Department, Stanford University, February 1967.

69. Kailath, Thomas and Frost, Paul A., *Mathematical Modeling of Stochastic Processes*, presented at the 1968 Joint Automatic Control Conference, University of Michigan, Ann Arbor, Michigan, June 26, 1968.

70. Haddad, A. H., and Valisalo, P. E., "Generation of Random Time-Series Through Hybrid Computation," Proceedings of Conference on Hybrid Computation, Sixth International Analogue Computation Meetings, Munich, Germany, 31 August - 4 September, 1970.

71. Mosca, E., "Angle Estimation in Amplitude Comparison Monopulse Systems," IEEE Trans. on Aerospace and Electronic Systems, AES-5, March 1969.

72. Sharenson, S., "Angle Estimation Accuracy with a Monopulse Radar in the Search Mode", IRE Trans on ANE, 9, pp. 175-179, September 1962.

73. Urkowitz, H., "The Accuracy of Maximum Likelihood Estimates in Radar and Sonar", IEEE Trans on MIL, 8, pp. 39-45, January 1964.

74. Ewell, G. W., Alexander, N. T., and Tomberlin, E. L., Investigation of the Effects of Polarization Agility on Monopulse Radar Angle Tracking, Final Technical Report, Vol. I., Engineering Experiment Station, Georgia Institute of Technology, June 1971.

APPENDIX A. FAR-FIELD M-BODY ELECTROMAGNETIC SCATTERING EQUATIONS

A.1 General

The following derivation assumes that the target is composed of M point scatterers and is illuminated by a linearly polarized incident plane wave moving along the line of sight in the direction of the target.

The Poynting vector for an electromagnetic field is given by

$$\vec{P} = \text{Re } (E \times H*) \tag{A.1}$$

where

P = Poynting vector

$$E = \left(E_x \vec{I} + E_y \vec{J} + E_z \vec{K} \right) e^{j\omega t}$$

$$H = \left(H_x \vec{I} + H_y \vec{J} + H_z \vec{K} \right) e^{j\omega t}$$

ω = angular frequency.

Figure A.1 depicts the target oriented coordinate systems (polar and Cartesian) and Equations (A.2) and (A.3) define the transformations between these two coordinate systems.

$$\begin{bmatrix} \vec{u}_r \\ \vec{u}_\theta \\ \vec{u}_\varphi \end{bmatrix} = \begin{bmatrix} D \end{bmatrix} \begin{bmatrix} \vec{I} \\ \vec{J} \\ \vec{K} \end{bmatrix}$$

$$\begin{bmatrix} \vec{I} \\ \vec{J} \\ \vec{K} \end{bmatrix} = \begin{bmatrix} D^{-1} \end{bmatrix} \begin{bmatrix} \vec{u}_r \\ \vec{u}_\theta \\ \vec{u}_\varphi \end{bmatrix} \tag{A.2}$$
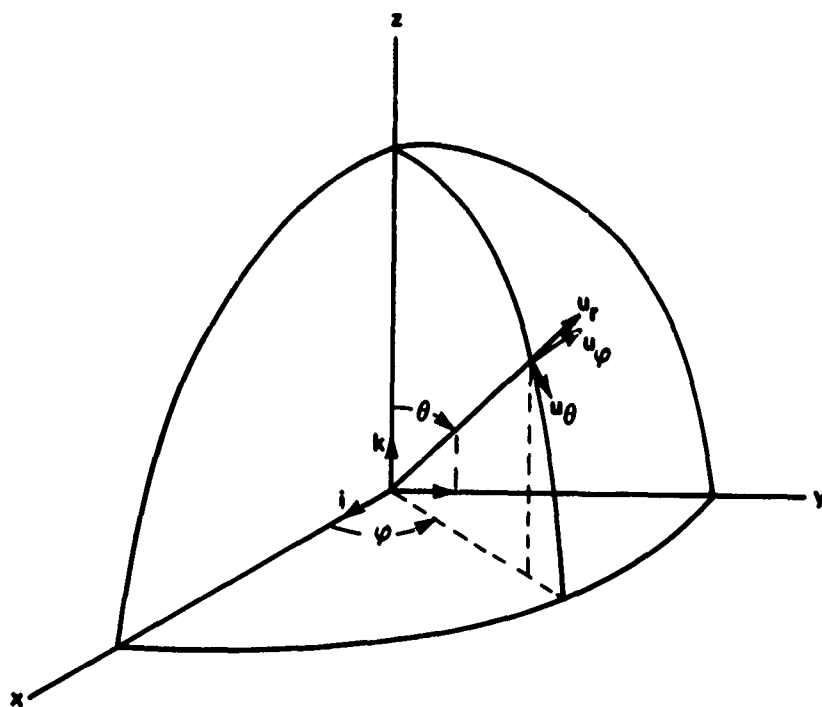
Figure A.1. Target Centered Coordinate Systems

where

$$d_{11} = \sin \theta \cos \varphi$$

$$d_{12} = \sin \theta \sin \varphi$$

$$d_{13} = \cos \theta$$

$$d_{21} = \cos \theta \cos \varphi$$

$$d_{22} = \cos \theta \sin \varphi$$

$$d_{23} = - \sin \theta$$

$$d_{31} = - \sin \varphi$$

$$d_{32} = \cos \varphi$$

$$d_{33} = 0 \tag{A.3}$$

The incident wave has electric and magnetic components given by

$$\vec{E}_{inc} = \left(E_{\theta \ inc} \ \vec{u}_\theta + E_{\varphi \ inc} \ \vec{u}_\varphi \right) e^{j\omega t} \tag{A.4}$$

and

$$\vec{H}_{inc} = \left(H_{\theta \ inc} \ \vec{u}_\theta + H_{\varphi \ inc} \ \vec{u}_\varphi \right) e^{j\omega t} \tag{A.5}$$

where

$$\vec{P}_{inc} = Re \left(\vec{E}_{inc} \times \vec{H}_{inc}^* \right) \qquad .$$

The components of the electromagnetic wave scattered from the i-th element, having cross section S_i, are expressed as

$$\vec{E}_{ref} = - \sqrt{S_i} \ \vec{E}_{inc} \tag{A.6}$$

116

$$\vec{H}_{ref} = -\sqrt{S_i} \ \vec{H}_{inc} \qquad\qquad (A.7)$$

where

$$\vec{P}_{ref} = -S_i \ \vec{P}_{inc} \qquad\qquad .$$

The units of P_{ref} are watts and those of P_{inc} are watts/m^2.

A.2 Geometrical Computations

Let the source and observation point Q be located at (x, y, z) or
(R, θ, φ) and the i-th scatterer be located at (x_i, y_i, z_i) with
respect to the target centered coordinate system. Then the observation
point is at $(x - x_i, y - y_i, z - z_i)$ or $(R_i, \theta_i, \varphi_i)$ with respect to
the shifted coordinate systems centered at the i-th element, and has
unit vectors $\vec{u}_{ri}$, $\vec{u}_{\theta i}$, $\vec{u}_{\varphi i}$, in the local polar coordinate system
centered at the i-th element. The relations between the coordinates
are given by

$$R_i = \left[\left(x - x_i \right)^2 + \left(y - y_i \right)^2 + \left(z - z_i \right)^2 \right]^{\frac{1}{2}} \qquad (A.8)$$

$$\varphi_i = \arctan\left(\frac{y - y_i}{x - x_i} \right) \qquad\qquad (A.9)$$

and

$$\theta_i = \arccos\left(\frac{z - z_i}{R_i} \right) \qquad\qquad . \qquad (A.10)$$

The Cartesian unit vectors $\vec{i}$, $\vec{j}$, $\vec{k}$ are related to the polar unit
vectors $\vec{u}_{ri}$, $\vec{u}_{\theta i}$, $\vec{u}_{\varphi i}$ at the observation point by the transformation

$$\begin{bmatrix} \vec{i} \\ \vec{j} \\ \vec{k} \end{bmatrix} = \begin{bmatrix} D_i^{-1} \end{bmatrix} \begin{bmatrix} \vec{u}_{ri} \\ \vec{u}_{\theta i} \\ \vec{u}_{\varphi i} \end{bmatrix} \qquad\qquad (A.11)$$

where D_i is obtained by substituting θ_i and φ_i for θ and φ in D.

The reflected E field from the i-th element may be written as

$$\vec{E}_i = E_{\theta i} \, \vec{u}_{\theta i} + E_{\varphi i} \, \vec{u}_{\varphi i}$$

where the radial dependence is neglected. Hence, the transformations (A.2) and (A.11) result in the following expressions for the components of the reflected field in the original system are given by

$$
\begin{bmatrix}
E'_{ri} & \vec{u}_r \\
E'_{\theta i} & \vec{u}_\theta \\
E'_{\varphi i} & \vec{u}_\varphi
\end{bmatrix}
=
\begin{bmatrix} D \end{bmatrix}
\begin{bmatrix} D_i^{-1} \end{bmatrix}
\begin{bmatrix}
0 & \\
E_{\theta i} & \vec{u}_{\theta i} \\
E_{\varphi i} & \vec{u}_{\varphi i}
\end{bmatrix}
\qquad (A.12)
$$

If it is assumed that $R \gg \sqrt{x_i^2 + y_i^2 + z_i^2}$, then $\theta_i \approx \theta$, $\varphi_i \approx \varphi$, and $R_i \approx R$, then the components of the E field in (A.12) become approximately

$$E'_{ri} \approx E_{\theta i} \left(-x_i \cos\theta \cos\varphi - y_i \cos\theta \sin\varphi - z_i \sin\theta \right)$$

$$+ E_{\varphi i} \left(-x_i \sin\varphi + y_i \cos\varphi \right)$$

$$E'_{\theta i} \approx E_{\theta i}$$

$$E'_{\varphi i} \approx E_{\varphi i} \qquad . \qquad (A.13)$$

The relative phase difference between the reflected electromagnetic waves of two scatterers is given by

$$\alpha = \frac{4\pi}{\lambda} \Delta R \qquad (A.14)$$

where ΔR is the difference in range. The phase shift for each scatterer must be computed so that the vector fields can be properly summed. If the target center is used as the reference point, then for

the i-th scatterer $\Delta R_i = R - R_i \approx - x_i \sin \theta \cos \varphi - y_i \sin \theta \sin \varphi - z_i \cos \theta$ so that the fields observed at point Q from the i-th element have a time dependence of $e^{j(\omega t + \alpha_i)}$.

A.3 Total Field Summation

Let

$$\vec{P} = P \, \vec{u}_r = \text{Re} \, (\vec{E} \times \vec{H}*) \, \vec{u}_r \tag{A.15}$$

be the incident power on the target array where

$$\vec{E} = E \left(\cos \delta \, \vec{u}_\theta + \sin \delta \, \vec{u}_\varphi \right)$$

$$\vec{H} = H \left(- \sin \delta \, \vec{u}_\theta + \cos \delta \, \vec{u}_\varphi \right)$$

and δ is the polarization angle of the E field referenced to the $-u_\theta$ vector. Then the electromagnetic fields reflected from the i-th element and observed at Q are given from (A.13) by

$$E_{\text{rec } i} = \frac{E}{R} \sqrt{S_i} \left[\left(\frac{\cos \delta}{R} f_{1i} + \frac{\sin \delta}{R} f_{2i} \right) \vec{u}_r \right.$$
$$\left. + \cos \delta \, \vec{u}_\theta + \sin \delta \, \vec{u}_\varphi \right] \tag{A.16}$$

$$H_{\text{rec } i} = \frac{H}{R} \sqrt{S_i} \left[\left(- \frac{\sin \delta}{R} f_{1i} + \frac{\cos \delta}{R} f_{2i} \right) \vec{u}_r \right.$$
$$\left. - \sin \delta \, u_\theta + \cos \delta \, \vec{u}_\varphi \right] \tag{A.17}$$

where

$$f_{1i} = - x_i \cos \theta \cos \varphi - y_i \cos \theta \sin \varphi - z_i \sin \theta \quad ,$$

and

$$f_{2i} = - x_i \sin \varphi + y_i \cos \varphi \quad .$$

Hence, the total fields at Q due to the entire target array are given by:

$$E_{rec} = \frac{E}{R} \sum_{i=1}^{M} \sqrt{S_i} \left[\left(\frac{\cos \delta}{R} f_{1i} + \frac{\sin \delta}{R} f_{2i} \right) \vec{u}_r + \cos \delta \, \vec{u}_\theta \right.$$
$$\left. + \sin \delta \, \vec{u}_\varphi \right] e^{j(\omega t + \alpha_i + \pi)} \qquad \text{(A.18)}$$

$$H_{rec} = \frac{H}{R} \sum_{i=1}^{M} \sqrt{S_i} \left[\left(-\frac{\sin \delta}{R} f_{1i} + \frac{\cos \delta}{R} f_{2i} \right) \vec{u}_r - \cos \delta \, \vec{u}_\theta \right.$$
$$\left. + \cos \delta \, \vec{u}_\varphi \right] e^{j(\omega t + \alpha_i)} \qquad . \qquad \text{(A.19)}$$

The components of power received at Q are found from (A.1). Thus, the $\vec{u}_r$ component of received power is given by

$$P_{r\ rec} = \text{Re} \left(E_{\theta\ rec}\, H^*_{\varphi\ rec} - E_{\varphi\ rec}\, H^*_{\theta\ rec} \right) =$$
$$= \frac{P}{R^2} \sum_{i=1}^{M} \sum_{j=1}^{M} \sqrt{S_i S_j} \, \cos \left(\alpha_i - \alpha_j \right) \qquad . \qquad \text{(A.20)}$$

Similarly the $\vec{u}_\theta$ and $\vec{u}_\varphi$ components of received power are expressed, respectively, by

$$P_{\varphi\ rec} = \text{Re} \left(E_{r\ rec}\, H^*_{\theta\ rec} - E_{\theta\ rec}\, H^*_{r\ rec} \right)$$
$$= \frac{P}{R^3} \sum_{i=1}^{M} \sum_{j=1}^{M} \sqrt{S_i S_j} \, f_{2i} \cos \left(\alpha_i - \alpha_j \right) \qquad \text{(A.21)}$$

and

$$P_{\theta\ rec} = \text{Re} \left(E_{\varphi\ rec}\, H^*_{r\ rec} - E_{r\ rec}\, H^*_{\varphi\ rec} \right)$$
$$= \frac{P}{R^3} \sum_{i=1}^{M} \sum_{j=1}^{M} \sqrt{S_i S_j} \, f_{1i} \cos \left(\alpha_i - \alpha_j \right) \qquad . \qquad \text{(A.22)}$$

120

A.4 The Scattering Parameters

The RCS, S, is defined by

$$S = \left| \frac{P_{ref}}{P_{inc}} \right| \tag{A.23}$$

with both P_{inc} and P_{ref} being referred to the target, that is with the radial dependence of power removed. P_{inc} has units of watts/m^2 and P_{ref} has units of watts. In this case,

$$S = \frac{R^2}{P} \left| P_{r\,rec} \right| = \sum_{i=1}^{M} \sum_{j=1}^{M} \sqrt{S_i S_j} \; \cos\left(\alpha_i - \alpha_j\right) \; . \tag{A.24}$$

The u_φ error, ϵ_φ, in linear units at the target, is given by

$$\epsilon_\varphi = \frac{R\,P_{\varphi\,rec}}{P_{r\,rec}} = \frac{1}{S} \sum_{i=1}^{M} \sum_{j=1}^{M} \sqrt{S_i S_j} \; f_{2i} \; \cos\left(\alpha_i - \alpha_j\right) \; . \tag{A.25}$$

The u_θ error, ϵ_θ, measured in linear units at the target, is given by

$$\epsilon_\theta = \frac{R\,P_{\theta\,rec}}{P_{r\,rec}} = \frac{1}{S} \sum_{i=1}^{M} \sum_{j=1}^{M} \sqrt{S_i S_j} \; f_{1i} \; \cos\left(\alpha_i - \alpha_j\right) \; . \tag{A.26}$$

The target phase, referenced to the target center, is given by

$$PHAS = \arctan\left(\frac{\sum_{i=1}^{M} \sqrt{S_i} \; \sin \alpha_i}{\sum_{i=1}^{M} \sqrt{S_i} \; \cos \alpha_i} \right) \; . \tag{A.27}$$

These equations are used in Chapter 2 in the analytic modeling of the scattering parameters from a target.

APPENDIX B.   STATISTICS OF THE ASPECT ANGLES

Let $(R_0, \theta_0, \varphi_0)$ be the polar coordinates of the target in the ground fixed coordinate system, and (R, θ, φ) be the coordinates of the origin of the ground fixed coordinate system in the target fixed coordinate system.   Since $R_0 = R$, only the aspect angles need to be considered in the analysis.   From (2.1) and (3.3)

$$
\begin{bmatrix} \sin\theta \cos\varphi \\ \sin\theta \sin\varphi \\ \cos\theta \end{bmatrix} = [T\alpha] \begin{bmatrix} T_{\beta\gamma} \end{bmatrix} \begin{bmatrix} -\sin\theta_0 \cos\varphi_0 \\ -\sin\theta_0 \sin\varphi_0 \\ -\cos\theta_0 \end{bmatrix} \qquad (B.1)
$$

$$
\begin{bmatrix} \sin\theta \cos\tilde{\varphi} \\ \sin\theta \sin\tilde{\varphi} \\ \cos\theta \end{bmatrix} = \begin{bmatrix} T_{\beta\gamma} \end{bmatrix} \begin{bmatrix} -\sin\theta_0 \cos\varphi_0 \\ -\sin\theta_0 \sin\varphi_0 \\ -\cos\theta_0 \end{bmatrix} \qquad (B.2)
$$

where $\tilde{\varphi} = \varphi - \alpha$.   The angles θ_0 and φ_0 are dependent on the flight path only and therefore they can be considered as deterministic for the calculation of the conditional joint density of θ and φ.   Therefore, (B.1) and (B.2) may be considered as functions of the random variables α, β, and γ, and β and γ respectively.   It is possible to solve (B.2) for β and γ as functions of θ and $\tilde{\varphi}$ as follows.

Let

$$
r_0 = \sqrt{\sin^2\theta_0 \cos^2\varphi_0 + \cos\theta_0}
$$

$$r_0 \cos \beta_0 = \sin \theta_0 \cos \varphi_0$$

$$r_0 \sin \beta_0 = \cos \theta_0 \qquad , \qquad \text{(B.3)}$$

then

$$\sin \theta \cos \tilde{\varphi} = - r_0 \cos \beta_0 \cos \beta - r_0 \sin \beta_0 \sin \beta$$

$$= - r_0 \cos \left(\beta - \beta_0 \right) \qquad . \qquad \text{(B.4)}$$

Let

$$r = \sqrt{\sin^2 \theta \sin^2 \tilde{\varphi} + \cos^2 \theta}$$

$$r \cos \gamma_0 = \sin \theta \sin \tilde{\varphi}$$

$$r \sin \gamma_0 = \cos \theta \qquad , \qquad \text{(B.5)}$$

then

$$\sin \theta_0 \sin \varphi_0 = - r \cos \gamma_0 \cos \gamma + r \sin \gamma_0 \sin \gamma$$

$$= - r \cos \left(\gamma + \gamma_0 \right) \qquad . \qquad \text{(B.6)}$$

Therefore, from (B.4) and (B.6),

$$\cos \left(\beta - \beta_0 \right) = - \frac{\sin \theta \cos \tilde{\varphi}}{r_0} \qquad \text{(B.7)}$$

$$\cos \left(\gamma + \gamma_0 \right) = - \frac{\sin \theta_0 \sin \varphi_0}{r} \qquad \text{(B.8)}$$

$$\tan \beta_0 = \frac{\cos \theta_0}{\sin \theta_0 \cos \varphi_0} \qquad \text{(B.9)}$$

$$\tan \gamma_0 = \frac{\cos \theta}{\sin \theta \sin \tilde{\varphi}} \qquad . \qquad \text{(B.10)}$$

Hence, β and γ can be written explicitly as

$$r_0 \cos \beta_0 = \sin \theta_0 \cos \varphi_0$$

$$r_0 \sin \beta_0 = \cos \theta_0 \qquad , \qquad (B.3)$$

then

$$\sin \theta \cos \tilde{\varphi} = - r_0 \cos \beta_0 \cos \beta - r_0 \sin \beta_0 \sin \beta$$

$$= - r_0 \cos (\beta - \beta_0) \qquad . \qquad (B.4)$$

Let

$$r = \sqrt{\sin^2 \theta \sin^2 \tilde{\varphi} + \cos^2 \theta}$$

$$r \cos \gamma_0 = \sin \theta \sin \tilde{\varphi}$$

$$r \sin \gamma_0 = \cos \theta \qquad , \qquad (B.5)$$

then

$$\sin \theta_0 \sin \varphi_0 = - r \cos \gamma_0 \cos \gamma + r \sin \gamma_0 \sin \gamma$$

$$= - r \cos (\gamma + \gamma_0) \qquad . \qquad (B.6)$$

Therefore, from (B.4) and (B.6),

$$\cos (\beta - \beta_0) = - \frac{\sin \theta \cos \tilde{\varphi}}{r_0} \qquad (B.7)$$

$$\cos (\gamma + \gamma_0) = - \frac{\sin \theta_0 \sin \varphi_0}{r} \qquad (B.8)$$

$$\tan \beta_0 = \frac{\cos \theta_0}{\sin \theta_0 \cos \varphi_0} \qquad (B.9)$$

$$\tan \gamma_0 = \frac{\cos \theta}{\sin \theta \sin \tilde{\varphi}} \qquad . \qquad (B.10)$$

Hence, β and γ can be written explicitly as

$$\beta = \text{arccos}\left(-\frac{\sin\theta\,\cos\tilde{\varphi}}{r_0}\right) + \text{arctan}\left(\frac{\cos\theta_0}{\sin\theta_0\,\cos\varphi_0}\right) \quad \text{(B.11)}$$

$$\gamma = \text{arccos}\left(-\frac{\sin\theta_0\,\sin\varphi_0}{r}\right) - \text{arctan}\left(\frac{\cos\theta}{\sin\theta\,\sin\tilde{\varphi}}\right) \quad \text{(B.12)}$$

where r_0 and r are defined in (B.3) and (B.5).

The joint probability density function of θ and $\tilde{\varphi}$ is found by the transformation

$$f_{\theta,\tilde{\varphi}}(\theta,\tilde{\varphi}) = \frac{f_\beta(\beta)\,f_\gamma(\gamma)}{|J|}.$$

where β and γ are expressed as in (B.11) and (B.12), and J is the Jacobian of the transformation. Since α is an additive factor to φ, the joint probability density function for θ and φ is found by convolving the joint density function for θ and $\tilde{\varphi}$ with the density function for α in the φ variable only.

The magnitude of the Jacobian of the transformation is given by

$$|J| = \left| \frac{\partial\theta}{\partial\beta}\frac{\partial\varphi}{\partial\gamma} - \frac{\partial\varphi}{\partial\beta}\frac{\partial\theta}{\partial\gamma} \right|$$

where the partial derivatives are found by implicit differentiation to be

$$\frac{\partial\theta}{\partial\beta} = \cos\gamma\,\cos\tilde{\varphi}$$

$$\frac{\partial\theta}{\partial\gamma} = \sin\tilde{\varphi}$$

$$\frac{\partial\varphi}{\partial\beta} = -\sin\gamma - \cot\theta\,\cos\gamma\,\sin\tilde{\varphi}$$

$$\frac{\partial\tilde{\varphi}}{\partial\gamma} = \cot\theta\,\cos\tilde{\varphi}$$

124

resulting in the expression

$$|J| = \sqrt{\frac{1 - \sin^2 \theta_0 \sin^2 \varphi_0}{\sin^2 \theta} - \cos^2 \tilde{\varphi}} \quad .$$

The transformation from β-γ space to θ-$\tilde{\varphi}$ space is one-to-one only if β and γ are restricted to the region $0 \leq \beta \leq \pi$, and $0 \leq \gamma \leq 2\pi$. The quadrant for β_0 and γ_0 can be found by considering the signs of the numerator and denominator in (B.9) and (B.10). The quadrant for $(\gamma + \gamma_0)$ and $(\beta - \beta_0)$ are found by considering (B.17) as well as (B.8) and (B.11).

Figures B.1 and B.2 depict the joint probability density functions for θ and $\tilde{\varphi}$, and θ and φ for $\bar{\theta} = 1.6497$ and $\bar{\tilde{\varphi}} = -0.20186$, i.e., at sample point 1 as defined in Chapter 4. Table B.1 compares the moments calculated by numerical integration of the joint probability density function for θ and φ, and the moments calculated from the linear approximations of (3.19) and (3.20).
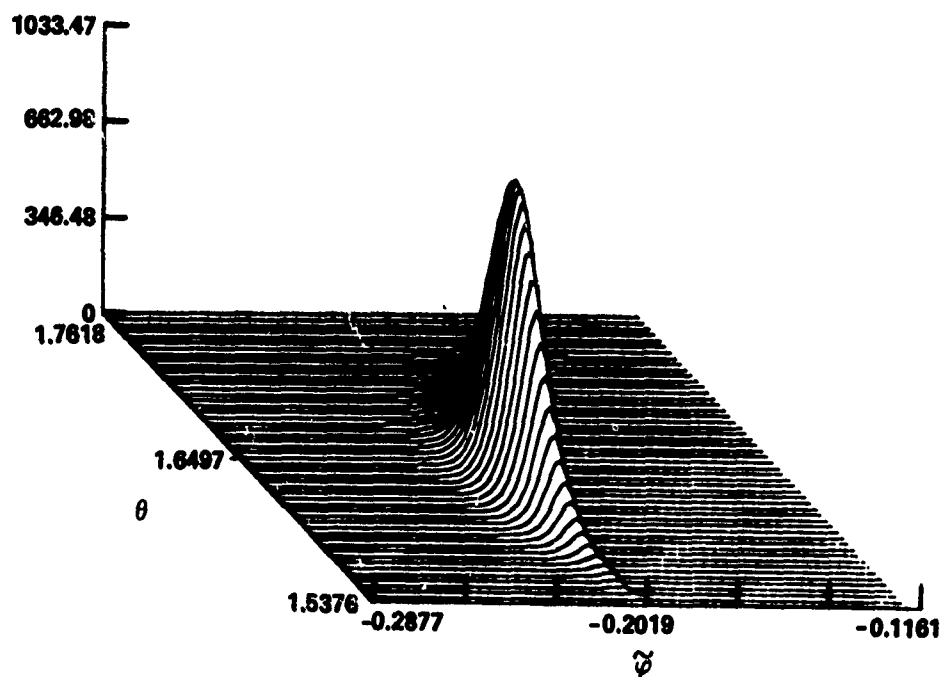
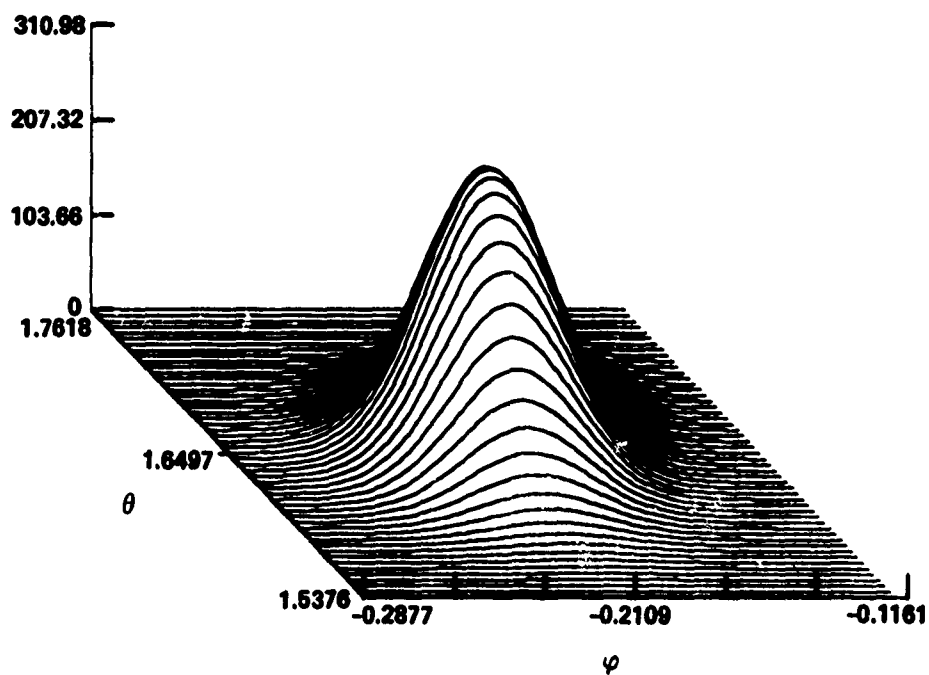Figure B.1.   Joint Probability Density Function of θ and $\tilde{\varphi}$

Figure B.2.   Joint Probability Density Function of θ and φ

Table B.1

Comparison of Aspect Angle Statistics for Exact Solutions
and Linear Approximations

Parameter	Linear Approximation	Exact Solution
$\overline{\theta}$	1.6497	1.6493
$\overline{\phi}$	- 0.20186	- 0.20163
σ_θ	0.02803	0.02796
σ_ϕ	0.02145	0.021571
$\rho_{\theta,\phi}$	0.2479	0.2785

APPENDIX C.   ERROR ANALYSIS

C.1   General

It was pointed out in Chapter 3 that the process described for computing the statistical characteristics introduces errors due to the assumptions made. In the computation of the four moments by numerical integration there are errors introduced at two points. In the computation of the covariance functions using the characteristic function method, there are errors introduced at three points. This Appendix estimates these errors or their level of significance.

C.2   Computation of the Moments Using Numerical Integration

There are two sources of errors in the computation of the moments by numerical integration as described in Chapter 3. One error is due to truncation of the data and the probability denisty function. The other error is due to the use of the rectangular (Euler) technique for numerical integration. Let x and y be normal random variables with joint probability density function $f(x,y)$ and let $g(x,y)$ be a function whose moments are to be calculated. Both functions are truncated at -4σ and $+4\sigma$ from the means in each dimension and then sampled at N points in each dimension. The moments of $g(x,y)$ are computed by

$$E\left\{g^r(x,y)\right\} = \sum_{n=1}^{N} \sum_{m=1}^{N} g^r(n\Delta x, m\Delta y)\ f(n\Delta x, m\Delta y)\ \Delta x \Delta y$$

$$(C.1)$$

where the origin is shifted to the $(-4\sigma, -4\sigma)$ point and Δx and Δy are the sample intervals. If N is sufficiently large, and $g(x,y)$ is a

128

relatively smooth function, then the accuracy obtained by (C.1) is adequate. The error is computing the expectation of a constant function over the region described using 128 data points in each dimension is about 0.013 percent.

The first two moments computed this way have been compared to the results using (3.37) and (3.39) with excellent results. As was demonstrated in Chapter 4, excellent agreement with the results of simulations was also obtained.

C.3 Computation of the Covariance Functions

The computation of the covariance functions using a discretized version of the characteristic function method introduces errors at three points. The one-dimensional case will be considered first. The errors in computing the expectation of a function g(x) are introduced due to the following assumptions:

(1) The replacement of the actual function g(x) by a periodic function $g_T(x)$.

(2) The use of the Fast Fourier Transform (FFT) to estimate the Fourier series coefficients for the periodic function $g_T(x)$.

(3) The use of a finite number of the Fourier series coefficients in the summation of the expectation of $g_T(x)$.

The actual function, g(x), is replaced by a periodic function, $g_T(x)$, such that

$$g_T(x) = g(x)$$

for

$$-\frac{T}{2} \le x \le \frac{T}{2}$$

$$g_T(x) = g_T(x + kT)$$

where the period T is defined to be 2Mσ where σ is the standard deviation of the probability density function f(x) which is assumed to have zero mean.

The first error in computing the expectation (3.39) is introduced by the approximation

$$E\left\{g(x)\right\} \cong E\left\{g_T(x)\right\} \qquad . \qquad (C.2)$$

This error may be bounded as

$$E_1 = \left| E\left\{g(x) - g_T(x)\right\}\right| \leq \int_{-\infty}^{\frac{T}{2}} \left| g(x) - g_T(x)\right| f(x)\, dx$$

$$+ \int_{\frac{T}{2}}^{\infty} \left| g(x) - g_T(x)\right| f(x)\, dx \leq 4 \sup\left| g(x)\right| \operatorname{erfc}\left(\frac{T}{2\sigma}\right) \quad . \quad (C.3)$$

For

$$\frac{T}{2} = 4\sigma \quad , \quad \operatorname{erfc}\left(\frac{T}{2\sigma}\right) \approx 3 \times 10^{-5} \quad ,$$

so that

$$E_1 \leq 1.2 \times 10^{-4} \sup\left| g(x)\right| \qquad (C.4)$$

The periodic function $g_T(x)$ may be represented by its Fourier series

$$g_T(x) = \sum_{m=-\infty}^{\infty} A_m \exp\left(j\frac{2\pi mx}{T}\right) \qquad (C.5)$$

so that its expectation is given by

$$E\left\{g_T(x)\right\} = E\left\{\sum_{m=-\infty}^{\infty} A_m \exp\left(j\frac{2\pi mx}{T}\right)\right\} = \sum_{m=-\infty}^{\infty} A_m \Phi_x\left(\frac{2\pi m}{T}\right) \qquad (C.6)$$

where $\Phi_x(v)$ is the characteristic function of the random variable x.

The second error encountered in computing the expectation is in estimating the Fourier series coefficients A_n by using the FFT. From (3.40), the estimate of the n-th coefficient is given by

$$\hat{A}_n = \frac{1}{N} \sum_{k=0}^{N-1} g_T(k \triangle x) \exp\left(-j \frac{2\pi \, kn \, \triangle x}{T}\right) \qquad (C.7)$$

which with (C.5) results in

$$\hat{A}_n = \frac{1}{N} \sum_{k=0}^{N-1} \sum_{m=-\infty}^{\infty} A_m \exp\left(j \frac{2\pi \, km \, \triangle x}{T}\right) \quad \exp\left(-j \frac{2\pi \, kn \, \triangle x}{T}\right)$$

$$= \frac{1}{N} \sum_{m=-\infty}^{\infty} A_m \frac{1 - \exp\left[-j \, 2\pi(m-n)\right]}{1 - \exp\left[\frac{-j \, 2\pi \, (m-n)}{N}\right]}$$

$$= \sum_{m=-\infty}^{\infty} A_m \exp\left[j(m-n)\left(\frac{N-1}{N}\right)\pi\right] \frac{\sin(m-n)\pi}{N \sin(m-n)\frac{\pi}{N}}$$

$$= \sum_{i=-\infty}^{\infty} A_{n+iN} , -\frac{N}{2} \le n < \frac{N}{2} \qquad \qquad (C.8)$$

The resulting error is due to aliasing caused by failure to meet the Nyquist sampling criterion. Furthermore, it only yields a finite number of coefficients.

The third source of error is in taking only a finite number of terms in the summation (C.6) namely,

$$E\left\{g_T(x)\right\} \cong \sum_{n=-k}^{k} A_n \tilde{\phi}(n) \qquad (C.9)$$

where

$$\tilde{\phi}(n) = \phi_x\left(\frac{2\pi n}{T}\right) = \exp\left[-\frac{1}{2}\left(\frac{\pi n}{M}\right)^2\right] . \qquad (C.10)$$

A bound on the resulting error may be obtained as

$$E_2 = \left| \sum_{|n|>k} A_n \tilde{\phi}_x(n) \right| \le 2 \sup_{n>k} \left| A_n \right| \sum_{n=k+1}^{\infty} \tilde{\phi}(n)$$

$$\le 2 \sup_{n>k} \left| A_n \right| \frac{\exp\left[-\frac{1}{2}\left(\frac{\pi(k+1)}{M} \right)^2 \right]}{1 - \exp\left(-\frac{\pi(k+1)}{M} \right)} \qquad . \quad (C.11)$$

For $M = 4$ and $k = 8$ the resulting bound is equal to

$$E_2 \le 3.10^{-11} \sup_{n>k} \left| A_n \right| \qquad . \qquad (C.12)$$

The above analysis for the third error source does not apply to a joint characteristic function of strongly correlated random variables. The normalized two-dimensional characteristic function for two jointly Gaussian, random variables is given by

$$\tilde{\phi}(u,v) = \exp\left[-\frac{1}{2}\left(u^2 + 2ruv + v^2 \right) \right]$$

where r is the correlation coefficient of x and y. When $r = 1$,

$$\tilde{\phi}(u,-u) = 1$$

so that the argument for limiting the sum as in the one-dimensional case does not hold. However, when $|u + rv| > 8$, the characteristic function is less than 2×10^{-9}. Therefore, only about 8 terms on each side of the line $u = -v\,\text{sgn}(r)$ need be taken in the summations.

Now consider the spectrum of the transform of the scattering parameters under study here. It can be shown that 99 percent of the power is contained in about half of the total spectrum. Therefore, it is possible to limit the summations to a narrow band about the

line defined above. In practice, it is possible to obtain excellent results using even fewer components than those containing 99 percent of the power. Similarly the aliasing error represented by (C.8) can be neglected.